Department of Civil and Environmental Engineering

Development and analysis of a dual-permeability model for subsurface stormflow and solute transport in a forested hillslope

Hanne Laine-Kaulio

Aalto University

DOCTORAL DISSERTATIONS

Aalto University publication series
DOCTORAL DISSERTATIONS 71/2011

Development and analysis of a dual-permeability model for subsurface stormflow and solute transport in a forested hillslope

Hanne Laine-Kaulio

Doctoral dissertation for the degree of Doctor of Science in Technology to be presented with due permission of the School of Engineering for public examination and debate in Auditorium R1 at the Aalto University School of Engineering (Espoo, Finland) on the 7th of October 2011 at noon.

Aalto University
School of Engineering
Department of Civil and Environmental Engineering
Water Engineering

Supervisor
Prof. Harri Koivusalo

Instructors
Prof. Emer. Pertti Vakkilainen
Dr. Tuomo Karvonen

Preliminary examiners
Prof. Jan Seibert, University of Zurich, Switzerland
Dr. Ilona Bärlund, Helmholz Centre for Environmental Research, Germany

Opponent
Dr. Docent Ari Laurén, Finnish Forest Research Institute, Finland

Aalto University publication series
DOCTORAL DISSERTATIONS 71/2011

ISBN 978-952-60-4245-9 (pdf)
ISBN 978-952-60-4244-2 (printed)
ISSN-L 1799-4934
ISSN 1799-4942 (pdf)
ISSN 1799-4934 (printed)

Aalto Print
Helsinki 2011

Finland

The dissertation can be read at http://lib.tkk.fi/Diss/

Publication orders (printed book):
hanne.laine@aalto.fi

Author
Hanne Laine-Kaulio

Name of the doctoral dissertation
Development and analysis of a dual-permeability model for subsurface stormflow and solute transport in a forested hillslope

Publisher School of Engineering

Unit Department of Civil and Environmental Engineering

Series Aalto University publication series DOCTORAL DISSERTATIONS 71/2011

Field of research Water Resources Engineering

Manuscript submitted 14 March 2011 **Manuscript revised** 17 June 2011

Date of the defence 7 October 2011 **Language** English

☒ **Monograph** ☐ **Article dissertation (summary + original articles)**

Abstract

Preferential flowpaths related to the soil structure have a decisive influence on subsurface flow and transport processes in forest soils in the boreal region. In dual-permeability models, the soil pore space is divided into a slow flow matrix domain and a preferential flow domain that are connected by a transfer term. The main objective of this study was to develop an advanced, physics-based, three-dimensional dual-permeability model that captures the main mechanisms behind a subsurface stormflow and solute transport event in a forested hillslope. A variety of experimental data were collected to describe the soil properties, flowpaths and processes in Finnish conditions, and to support the model development, parameterisation and analysis. The collected dataset consists of soil analyses, field measurements and tracer experiments.

The model developed was used to simulate tracer migration in the study slope during an artificially generated stormflow event. As many parameters as possible were a priori fixed to reduce problems with equifinality and model identifiability. Parameterisation of the soil matrix was fixed relying on the fact that fast subsurface stormflow is related to the preferential flow routes and is not sensitive to the slow matrix processes. Similarly, water retention properties were a priori fixed in the preferential flow domain. With respect to capturing the dynamics of the tracer plume, the model was sensitive to the remaining parameters, which include the saturated hydraulic conductivity of the preferential flow domain, the fractioning of the total porosity to soil matrix and preferential routes, and the transfer coefficient between the two pore domains. Identification of these parameters was based on the tracer experiment data.

The parameterisation routine used proved to be applicable to the development of the dual-permeability model, and this study emphasized the importance of the tracer dataset for the development and analysis of the model. The parallel and coupled simulation of the soil matrix and the preferential flow domain with the dual-permeability model was found to be essential in reproducing the observed, dynamic changes in the moisture conditions, flow velocities and tracer concentrations during the different stages of the event. The dual-permeability model was able to capture the main features of the observed stormflow and solute transport event. A further development and evaluation of the model call for field data in dry conditions and advances in the measurement and parameterisation of the water retention properties and porosity values.

Keywords forest soil, runoff generation, subsurface stormflow, preferential flow, solute transport, physics-based modelling, dual-permeability model

ISBN (printed) 978-952-60-4244-2 **ISBN (pdf)** 978-952-60-4245-9

ISSN-L 1799-4934 **ISSN (printed)** 1799-4934 **ISSN (pdf)** 1799-4942

Location of publisher Espoo **Location of printing** Helsinki **Year** 2011

Pages 192 **The dissertation can be read at** http://lib.tkk.fi/Diss/

Aalto-yliopisto

Tiivistelmä

Aalto-yliopisto, PL 11000, 00076 Aalto www.aalto.fi

Tekijä
Hanne Laine-Kaulio

Väitöskirjan nimi
Välitöntä valuntaa ja aineiden kulkeutumista metsämaassa kuvaavan, kahden huokoston mallin kehittäminen ja analysointi

Julkaisija Insinööritieteiden korkeakoulu

Yksikkö Yhdyskunta- ja ympäristötekniikan laitos

Sarja Aalto University publication series DOCTORAL DISSERTATIONS 71/2011

Tutkimusala Tekninen vesitalous

Käsikirjoituksen pvm 14.03.2011 **Korjatun käsikirjoituksen pvm** 17.06.2011

Väitöspäivä 07.10.2011 **Kieli** Englanti

☒ **Monografia** ☐ **Yhdistelmäväitöskirja (yhteenveto-osa + erillisartikkelit)**

Tiivistelmä

Maaperän rakenteeseen liittyvillä oikovirtausreiteillä on ratkaiseva vaikutus veden virtaus- ja aineiden kulkeutumisprosesseihin boreaalisen vyöhykkeen metsien maaperässä. Kahden huokoston malleissa maan huokostila jaetaan hitaita virtausprosesseja edustavaan maamatriisiin ja oikovirtausreitteihin, jotka on kytketty toisiinsa vaihtotermin avulla. Tämän työn päätavoite oli kehittää yksityiskohtainen, fysikaalinen, kolmiulotteinen, kahden huokoston malli, joka sisältää keskeisimmät mekanismit välittömän valunnan ja aineiden kulkeutumisen kuvaamiseen metsäisellä rinteellä. Työssä kerättiin kokeellinen aineisto, joka kuvaa monipuolisesti maaperän ominaisuuksia, virtausreittejä ja -prosesseja Suomen olosuhteissa, ja tukee mallin kehittämistä, parametrisointia ja analysointia. Aineisto koostui laboratorioanalyyseistä, kenttämittauksista ja merkkiainekokeista.

Työssä kehitetyllä mallilla simuloitiin merkkiaineen kulkua koerinteellä keinotekoisen valuntatapahtuman aikana. Mahdollisimman suuren parametrijoukon arvot kiinnitettiin mallin identifioituvuusongelmien vähentämiseksi. Maamatriisin parametriarvot kiinnitettiin sillä perusteella, että välitön valunta liittyy maan oikovirtausreitteihin, eikä ole herkkä hitaille, maamatriisissa tapahtuville prosesseille. Oikovirtausreittien vedenpidätysparametrien arvot kiinnitettiin vastaavasti. Merkkiainepulssin dynamiikan kannalta malli oli herkkä muille parametreille, jotka ovat oikovirtausreittien kyllästyneen tilan hydraulinen johtavuus, kokonaishuokostilan jako maamatriisiin ja oikovirtausreitteihin, ja huokostojen välinen vaihtokerroin. Parametrien identifiointi perustui merkkiainekokeen mittausaineistoon.

Parametrisointimenettely osoittautui soveliaaksi kahden huokoston mallin kehittämisen kannalta, ja tämä tutkimus korosti merkkiainekokeen mittausaineiston tärkeyttä mallin kehittämisessä ja analysoinnissa. Maamatriisin ja oikovirtausreittien rinnakkainen ja kytketty simulointi kahden huokoston mallilla oli välttämätöntä dynaamisten maankosteus-, virtausnopeus- ja ainepitoisuusmuutosten simuloinnin kannalta, valuntatapahtuman eri vaiheissa. Kahden huokoston malli pystyi kuvaamaan havaitun valunta- ja aineiden kulkeutumistapahtuman keskeisimmät piirteet. Kuivia olosuhteita edustava mittausaineisto sekä uudet tavat mitata ja parametrisoida vedenpidätys- ja huokoisuusominaisuuksia ovat puolestaan tärkeitä mallin jatkokehityksen kannalta.

Avainsanat metsämaaperä, valunnan muodostuminen, välitön valunta, oikovirtaus, aineiden kulkeutuminen, fysikaalinen mallintaminen, kahden huokoston malli

ISBN (painettu) 978-952-60-4244-2 **ISBN (pdf)** 978-952-60-4245-9

ISSN-L 1799-4934 **ISSN (painettu)** 1799-4934 **ISSN (pdf)** 1799-4942

Julkaisupaikka Espoo **Painopaikka** Helsinki **Vuosi** 2011

Sivumäärä 192 **Luettavissa verkossa osoitteessa** http://lib.tkk.fi/Diss/

Author's contribution

This dissertation is a direct extension of the Licentiate's thesis of the author (Laine-Kaulio 2008). The author is fully responsible for the manuscript and the research work behind it. This includes the planning, implementation and analysis of the experiments presented in Chapters 3 and 4, and the development and analysis of the simulation model presented in Chapter 5. The author is responsible for the site description in Chapter 2, however, the soil analysis contains data measured from a set of disturbed soil samples, collected by an undergraduate student at the University of Oulu, and originally reported in her Master's thesis together with a set of Guelph measurements (Postila 2006). Measurements reported in Postila (2006) were complemented and reanalysed for this study. Considering the experimental part of this study in general (Chapters 2, 3 and 4), contribution of laboratory and field personnel was needed in order to carry out the large number of measurements. The role of the instructors and the supervisor was to comment on the measurement plans, model development and the manuscript.

Acknowledgements

This study was conducted in a dynamic working environment. During the journey of almost seven years, the former Helsinki University of Technology, Helsinki School of Economics, and School of Art and Design have merged together, forming the current Aalto University. Alongside the administrative changes, the research group involved in this work, the Water Resources Research Group has undergone a generational change, and the study was supervised by altogether three professors.

I am grateful to Emeritus Professor Pertti Vakkilainen for the encouragement throughout my studies and for providing me feedback on my work, based on a broad view and expertise in water resources management. Professor Tuomo Karvonen I want to thank for kindly providing me targeted and specialized guidance related to the content of my work, despite transferring to new duties. Professor Harri Koivusalo is acknowledged for taking on the supervision of my work in its final stage and for providing detailed comments on the manuscript.

I also am grateful to several foreign experts who have contributed to the work along the way. Above all, I want to thank Professor Jeffrey J. McDonnell from the Oregon State University for providing invaluable guidance in hillslope hydrology, Professor Jan Seibert from the University of Zurich and Senior Researcher Dr. Ilona Bärlund from the Helmholz Centre for Environmental Research Magdeburg for taking the effort to pre-examine this thesis, and Dr. Docent Ari Laurén from the Finnish Forest Research Institute for accepting the invitation to act as my opponent.

The study would not have been possible without the funding provided by several sources. I wish to thank Timo Maasilta and Maa- ja vesitekniikan tuki ry (the Land and Water Technology Association), the Graduate School RYM-TK/Kirsu, the Academy of Finland, the European Commission and the Environment and Sustainable Development Programme, and the Sven Hallin Research Foundation for the financial support. In addition, I want to acknowledge Oy Celego Ab for donating the dye for the experiments, and

Marketta Ahtiainen for providing hydrometeorological data of the Kangasvaara area.

Related to the experimental work, I greatly appreciate the contribution of Soile Backnäs and Heini Postila from the University of Oulu, Sirpa Piirainen and Leena Finér from the Finnish Forest Research Institute, Raimo Nevalainen, Satu Putkinen and Hannu Pelkonen from the Geological Survey of Finland, and Aino Peltola and Jyrki Nurminen from our own research group at the Aalto University. From the Water Research Research Group, I also owe thanks to Jarkko Koskela for making the effort to comment on the manuscript.

At the end, I want to highlight the collaboration as well as all the rather unofficial gatherings with a number of colleagues from different universities, institutes and companies. Aware of not being able to mention everyone by name, special thanks to Nora, Ulla, Marie, Lassi, Gerald and Pirjo. Family and friends, in particular my husband Tuomas and our baby girl Klara are to thank for lifting the spirits in spare time.

In Espoo on 22 August 2011,

Hanne Laine-Kaulio

Contents

List of Symbols

α	[L^{-1}]	Parameter of the van Genuchten water retention curve
α^*	[L^2T^{-1}]	Diffusion
α_L	[L]	Longitudinal dispersivity
α_T	[L]	Transverse dispersivity
α_w	[$L^{-1}T^{-1}$]	First order water transfer coefficient
α_{wl}	[L^{-2}]	Lumped first order water transfer coefficient
β	[-]	Matrix-macropore geometry factor
β	[-]	Parameter of the van Genuchten water retention curve
γ_w	[-]	Empirical coefficient in the water transfer term
ζ	[-]	Switch term for flow direction
θ	[-]	Volumetric water content
θ_R	[-]	Residual volumetric water content
θ_S	[-]	Saturated volumetric water content
σ	[SL^{-1}]	Electrical conductivity
υ	[L^2T^{-1}]	Kinematic viscosity
Γ_s	[$ML^{-3}T^{-1}$]	Solute transfer term between two pore domains
Γ_w	[T^{-1}]	Water transfer term between two pore domains
A	[L^2]	Area
a	[L]	Distance between a matrix and macropore block
B	[-]	Coefficient of the Piezometer method
b	[L]	Aquifer thickness
C	[ML^{-3}]	Concentration
C^d	[L^{-1}]	Differential water capacity
C_r	[-]	Courant number
D	[L^2T^{-1}]	Dispersion coefficient
d	[-]	Flow direction switch in advective solute transfer
d	[L]	Pore diameter
H	[L]	Hydraulic head

h	[L]	Pressure head
K	[LT^{-1}]	Hydraulic conductivity
K_a	[LT^{-1}]	Hydraulic conductivity at matrix-macropore interface
K_R	[-]	Relative hydraulic conductivity
K_S	[LT^{-1}]	Saturated hydraulic conductivity
L	[L]	Length, distance
n	[-]	Porosity
n	[T]	Time step
Pe	[-]	Peclet number
Q	[L^3T^{-1}]	Discharge
q	[LT^{-1}]	Darcy flux
R	[LT^{-1}]	Infiltration velocity
Re	[-]	Reynolds number
r	[L]	Radius
S	[T^{-1}]	Sink / source term
S	[-]	Storage coefficient, specific yield
S_e	[-]	Degree of saturation
T	[T]	Total (calculation) time
T	[L^2T^{-1}]	Transmissivity
t	[T]	Time point, duration
V	[L^3]	Volume
v	[LT^{-1}]	Flow velocity, pore velocity
W	[L]	Water level
X	[-]	Coefficient for the Guelph permeameter
x	[L]	Distance in the x direction, x-coordinate
y	[L]	Distance in the y direction, y-coordinate
z	[L]	Distance in the z direction, elevation head, z-coordinate

List of Figures

List of Tables

1 Introduction

1.1 Background

1.1.1 Runoff generation theories

The history of runoff generation theories dates back to centuries before Common Era. Based on the empirical knowledge of the old cultures of the Orient and Egyptians, the Greek natural philosophers developed hypotheses of flow in soil and streamflow generation (e.g. Dyck and Peschke 1995). They believed that, in addition to rainfall, river flow consists of water that has flown uphill from the sea inside the ground, and has risen back to soil surface in upland areas. Their theories also included a mechanism of underground air changing into water, which could flow uphill to feed upper reaches. These conceptions were disproved after the Middle Ages, and in the 17th century, the French hydrologist Pierre Perrault showed quantitatively that rainfall alone can produce the flow in rivers (e.g. Dyck and Peschke 1995). Since Perrault, a great number of studies of the modern era have contributed to our current understanding on runoff generation in nature.

In the 18th century, development of water related sciences was highest in hydraulics, fluid mechanics and mathematics (Hubbart 2007). Soil and groundwater hydrology started to grow as its own discipline in the 19th century. The most significant advancement of that time was the publication of Darcy's law in 1856 that describes flow in saturated porous media. The law is named after the French engineer Henry Darcy, who was occupied with water supply and hydraulics, but made significant contributions to groundwater hydrology as well. Some 75 years later, Richards (1931) proved that Darcy's law is also apt for describing water movement in unsaturated soil, as he applied the continuity requirement of Buckingham (1907) to Darcy's law. Thus, the resulting Richards' equation for describing subsurface flow – that is still used today – was already set early in the 20th century.

Most of the concepts underlying our current understanding of runoff generation processes in soil can also be found in studies of the first decades of the 20th century (Beven 2006). In 1933, Horton published one of the most

significant studies of that time introducing *infiltration excess overland flow*, also known as *Hortonian overland flow* as the main runoff producing mechanism. According to the study, streamflow is the difference between rainfall and infiltration capacity of soil, when the rainfall exceeds the capacity. Hortonian overland flow became the mainstream hydrological theory for decades, even though in the same period results were also reported from catchments that were not dominated by surface runoff (Beven 2006).

In contrast to Horton's theory, Hoover and Hursh (1943) concluded that elevation influences runoff generation in forest land, as higher areas have steeper and thinner slopes with smaller water storage capacity than the lower ones. They also referred to *subsurface stormflow* or *preferential flow* as a runoff producing mechanism by noting that outflow from a nearly saturated talus-fill in their catchment occurred at rapid rates because of steep slopes and large voids in the fill material. In addition to the competing theories of the Hortonian overland flow, Beven (2004) shows that Horton's model for runoff generation was not strictly valid even in Horton's own experimental catchment. Nevertheless, infiltration excess overland flow is generated on soils with very low permeability.

Although both surface and subsurface flow were discussed in the early studies of the 20th century, it was not until the 1960s when detailed field studies for understanding the physical processes of runoff generation began to emerge (Hubbart 2007). The sixties also saw the advent of computer applications in hydrological studies. Summarizing the benchmark papers collected by Beven (2006), many studies of the sixties revolved around the concept of *partial contributing area* or *variable source area*. In general, peak discharge in a stream was found to originate from a relatively small area of a watershed. Processes by which water enters streams, and also the role of *subsurface stormflow* or *translatory flow* from steeper areas farther off the river in mobilising old water in soil near the stream (Hewlett and Hibbert 1967), remained more disputable. Dunne and Black (1970) ended the decade by presenting the process of *saturation excess overland flow*, also known as *Dunne overland flow* and *return flow*. They concluded from their watershed that overland flow from a small, oversaturated area produced the peak discharge, whereas subsurface flow played a minor role in the peak.

Studies of Whipkey (1965, 1967) and Weyman (1970) belong to the first actual hillslope studies that elaborately explore subsurface flow along a hillside. Their studies were based on measuring throughflow in the field at different soil depths. Whipkey (1965) found that in coarse-textured upper soil layers, water infiltrates downwards in vertical direction until it reaches saturation that

prevails in the denser, fine-textured subsoil. The amount of lateral flow in the dense subsoil was relatively small and constant. As storm depths increase, saturation reaches the upper layers resulting in remarkably higher lateral flow rates. Thus, most of the lateral outflow came from the transition area at about 90 cm depth, located between the subsoil with low permeability and the coarser topsoil, corresponding to the depth of the root zone in the slope. Whipkey also demonstrated how the response of the slope to irrigation was different for dry and wet antecedent conditions. Nonetheless, the flow pattern was similar in all cases. In a later study, Whipkey (1967) diagnosed the subsurface stormflow in the coarse upper soil layers as non-Darcian flow (Beven 2006), flow that does not follow Darcy's law.

Whereas Whipkey studied subsurface flow in response to artificial irrigation, Weyman reported similar results during natural rainfall events. According to Weyman (1970), storm flow originated from the illuvial horizon at a depth of 10-45 cm in his site and base flow from a depth of 45-75 cm. Storm flow was found to be controlled by the upslope extent of saturated conditions and base flow was found to be supplied by slow unsaturated flow from the whole soil mass to a small constant zone of saturation. Weyman (1970) expanded his analysis to stream hydrographs, and noted that the outflow rates from soil plots were of same form as the stream hydrographs. Thus, he concluded that the quick response of stream discharge to rainfall is a result of rapid increases in throughflow output as saturated conditions extend upslope.

Following the Benchmark Papers Anthology by McDonnell (year unknown, see the References Chapter for other details) from Weyman (1970) on, more and more hillslope studies continued to build up on each other, utilizing the most versatile experimental methods including soil analyses, trenches, troughs, well screens, lysimeters, and tracers from ions and isotopes to dyes. Harr (1975), for instance, presented calculations for water fluxes in a steep forested slope, based on soil analysis, tensiometer, piezometer, and precipitation data. According to his study, unsaturated flow predominated in soil during moderate size winter storms, but discontinuous and intermittent saturation of upslope subsoil was also found. In addition, Harr (1975) reported an abrupt decrease in the water flux to the lower part of the slope some 10 hours after the end of rain, which he interpreted as a result of nearly complete draining of large pores.

Sklash and Farvolden (1979), for their part, utilized basin-scale isotope experiments and discharge data in showing that groundwater dominates the runoff hydrographs most of the time in a number of watersheds. This groundwater ridging into streams was to originate from the almost

instantaneous conversion of capillary fringe into phreatic water table after the onset of rain. Sklash and Farvolden (1979) conjectured these processes to be independent of the upland area response.

The series of studies related to the steep and thin slopes of the Maimai watershed in New Zealand was started by Mosley in the late seventies. According to Mosley (1979), flow in macropores and in seepage zones in soil was the predominant mechanism in producing channel storm flow, and all parts of the watershed contributed to the stormflow even during very small storms. In contrast to Mosley's theory, Pierce et al. (1986) reported a study from the Maimai area where they proved that only a minor proportion of the storm runoff in the stream was new rainwater. The emerging contradiction between lateral preferential flow and storm hydrographs composing of old water was resolved in the Maimai area by McDonnell (1990). He showed that preferential flow can result in old water displacement by translatory flow. Thus, both the previous studies, the one of Mosley's (1979) and the one of Pierce et al. (1986) were partly correct. New studies related to runoff generation in the Maimai catchment are still published today (e.g. Graham et al. 2010a, b).

The Maimai area has also been subject to modelling studies that aim to provide more insight into the hillslope processes and characteristics – studies often referred to as *virtual experiments*. Using the Maimai area as an example, Dunn et al. (2007) studied the factors influencing the residence time of catchment waters with virtual experiments that were created with a semi-distributed, conceptual hydrological model. Another catchment where modelling has recently been used to study the subsurface runoff processes is the Panola hillslope in Georgia, Unites states (see Chapter. 1.1.2). For instance Weiler and McDonnell (2004) created a series of virtual experiments with a model that was based on conceptualizing the water balance within the saturated and unsaturated zone, in relation to soil physical properties in a spatially explicit manner on the hillslope scale. They examined the interaction between water flowpaths, source and mixing of water on the hillslope scale for the Panola slope.

The development and use of advanced and detailed, physics-based models have recently gained more attention in describing hillslope behaviour, and applications have also become available for the Panola slope (e.g. Hopp and McDonnell 2009, James et al. 2010). In addition to the different types of model-based studies on flow processes in hillslopes, several studies relying on dye tracer visualisation of flowpaths in soil have become available during the

past decade (e.g. Weiler 2001, Flury and Wai 2003, Flury and Flühler 2004, Shipitalo et al. 2004, Weiler and Flühler 2004).

Although different mechanisms dominate the runoff generation in different geographic locations and climatic conditions, several mechanisms can concurrently occur at different locations of a hillslope, or at different times at the same locations of the slope as well (Beven 2006). On the catchment scale, hydrological response to a rainfall event is the result of numerous, complex interactions both among the hydrometeorological inputs and the landscape properties, and the multitude of interactions make it difficult to identify the dominant controls on the catchment response (Woods and Sivapalan 1999). Soil properties, land use, and climatic conditions affect runoff generation and cause variability across regions. Thus, saturation and infiltration excess overland flow, different types of preferential flow, translatory flow and subsurface storm flow, groundwater ridging, as well as the concept of variable source area, all formulate our perception of the runoff generation phenomenon.

According to Uhlenbrook et al. (2001), future research should bring more insight into the spatial and temporal distribution of different processes on catchment scale, into the runoff generation processes on hillslope scale, and into the interaction between macropores and soil matrix on plot scale. Hillslopes can be regarded as the basic elements of catchments (cf. Troch et al. 2003). Therefore, new measurement methods to directly determine hillslope inputs and outputs are searched for (e.g. Beven 2006). Research focus is also suggested to be moved beyond the complexity of all runoff generation mechanisms and landscape heterogeneities more into classifying hillslope responses and exploring organizing principles that underlie the complexities (McDonnell et al. 2007).

Considering the global research needs and trends, and taking into account studies currently available on Fennoscandian conditions, more plot and hillslope scale studies of flow processes, routes, and velocities in forest soils are needed. Compared to agricultural soils, descriptions of solute transport in upland soils on scales smaller than catchments are in general scarce (Stutter et al. 2005). Nordic studies (e.g. Koivusalo et al. 2000, Laudon et al. 2004 and 2007, Mäkitalo 2009, Ilvesniemi et al. 2010) have also concentrated on catchment scale with observations of discharge and quality variables at the catchment outlet, supplemented with point scale soil analyses and meteorological data. New studies should further bridge the gap between current point and catchment scale knowledge by providing new insight into the main mechanisms governing flow in Fennoscandian forest soils and into

the parameters describing hydraulic properties of the soils. The following aspects characterise Fennoscandia.

In Fennoscandia, land use is dominated by forests and the area belongs to the cool to temperate, coniferous and mixed forest zones in the Köppen-Geiger climate classification (Peel et al. 2007). Topography in the forested regions is mostly characterised by gently sloping hills. In regard to soil type, glacial tills are the main surface deposits, similarly to other boreal environments in the northern hemisphere (Beldring 2002). Characteristics of the Fennoscandian tills that have the greatest influence on the hydrogeological properties are porosity, pore size distribution, macropores, heterogeneity and anisotropy. These properties are controlled by the grain-size distribution, spatial distribution and orientation of the particles, structural properties, and the degree of compaction of the till (Haldorsen and Krüger 1990). In tills, the soil structure has the strongest influence on the hydraulic conductivity, which decreases rapidly with depth (Lind and Lundin 1990). Together with soil formation processes, biological features of forested areas, such as litter layers, high organic contents and extensive root systems, as well as diverse micro- and macrofauna, create soils with high macroporosity, low bulk density and high saturated hydraulic conductivity and infiltration rates (Neary et al. 2009).

Jenssen (1990) notes that there are no ideal methods for measuring the saturated hydraulic conductivity of till soils. Studies comparing and evaluating different methods for till are few, and comparative studies should be carried out in order to facilitate selection of appropriate methods. Jenssen (1990) also points out that measurement of hydraulic conductivity is scale dependent. Several studies have shown the scale dependency of hydraulic conductivity (e.g. Lind and Lundin 1990, Buttle and House 1997). The main uncertainties in laboratory measurements are connected with the representativeness of the sample size, density and structure, and possible interfacial flow along the cylinder-soil interface. Jenssen (1990) considers field methods more reliable since they represent a larger soil volume. The main uncertainty regarding the field methods is connected to the equation used in calculating the saturated hydraulic conductivity values from the measurements (Jenssen 1990).

Surface runoff is rare in forest environments, and most rainfall moves to streams by subsurface flow pathways (Neary et al. 2009). As a conclusion of the review of Beldring (2002) for the boreal forest environments with shallow till deposits, groundwater is found to be the major determinant of runoff generation. As Rodhe (1989) concludes on the basis of isotopic hydrograph separation in 10 Swedish basins, stream stormflow is usually dominated by pre-event water. Lepistö (1994) collected a dataset on oxygen isotope

concentrations in rain water, groundwater and in the stream of the study catchment of Rudbäck in southern Finland, when studying the hydrological processes that contribute to nitrogen leaching. According to Lepistö's (1994) results, 10-20 % of annual runoff originated from event water and 80-90 % originated from pre-event water, so that the fraction of event water may constitute as much as 50-70 % of the total runoff on the rainfall event time scale (Lepistö et al. 1994, Koivusalo et al. 2000).

Together with Lepistö's (1994) results, analysis of long term soil moisture data on Finnish forest soils reveals that translatory flow and old water displacement are the main mechanisms of stream flow generation, since the majority of subsurface flow has been found to occur in pores larger than 30 μm (Hänninen et al. 2010). Macropores consisting of decayed and live roots, subsurface erosion, surface bedrock fractures, and animal burrows, form a pore network for lateral preferential flow in steep forested slopes underlain by bedrock or till (Sidle et al. 2001). Preferential flowpaths enable the formation of subsurface stormflow with a varying fraction of old water and during the melting season or heavy rainfall events, when the soil moisture prior to the event is high. The study of Laudon et al. (2007) demonstrated the role of preferential flow during snow melt events, as the soil water isotopic composition in a forested Swedish catchment revealed a clear connection between recent snow melt water and soil water, despite the large pre-event fraction in the stream. Thus, the majority of melt water infiltrates in soil, raises the groundwater level and results in a mobilization of pre-event water stored in the hillslope (Laudon et al. 2007).

1.1.2 Modelling of subsurface flow and transport processes

Physics-based modelling of flow and solute transport in soil usually relies on Darcy's law (1856) and Richards' equation (1931, cf. Chapter 1.1.1). The use of these equations has proven to be challenging both in terms of parameterisation and suitability of the models to describe the phenomenon. Weiler et al. (2003) note that the insufficient knowledge of lateral preferential flow and the lacking process description of it may constitute the largest impediment to moving forward in catchment modelling. Preferential flow generally refers to all mechanisms where transport of water is primarily associated with a fraction of the total pore network, and may either accelerate or delay the movement of dissolved matter depending upon the position of the matter compared to the position of the preferential flowpaths (Allaire et al. 2009).

Several studies report the inadequacy of the traditional Darcy-Richards approach to describing flow, in particular fast, subsurface stormflow in hillslopes (e.g. James et al. 2010, Jansson 2005, Schwartz et al. 2000, Espeby 1989). Means to measure water fluxes in soil are considered important, as mentioned above for the runoff phenomenon (cf. Chapter 1.1.1), in developing model representations for hillslope responses to rainfall and snow melt events. Confrontation between the complex, real-world phenomena and the limited data available on them has been largely avoided by resorting to model calibration, even though parameterisation is only one of the problems in model development (Beven 2006). Still, narrowing the range of variation of model parameters with new measurements and *soft data* or *fuzzy data* on the phenomenon (cf. Seibert and McDonnell 2002, McDonnell 2003), current model structures can be assessed further and new process descriptions can be developed.

Despite the limitations referred to above, and despite alternative approaches such as the *TOPMODEL* (Beven and Kirkby 1978, Beven 1997, Beven and Freer 2001), the Mulungu et al. (2005) model, and *Distres* (Spaaks et al. 2009), Richards' equation seems to hold so far its position as the fundamental formula in the physics-based models. The latest model structures take into account preferential flow by dividing soil into two, or even more pore domains (e.g. Jarvis 1991, Gerke and van Genuchten 1993a, 1993b, 1996, Ray et al. 1997, Vogel et al. 2000, Simunek et al. 2003, Vogel 2004, Ray et al. 2004, Larsbo et al. 2005, Gerke 2006, Gerke et al. 2007). Depending on the model, Richards' equation is used as the governing equation for water flow in each pore domain, or in some of the modelled domains. Models where no flow inside the soil matrix is allowed and water flows only in large pores and between the pore domains, are usually called *dual porosity* models, whereas models, where flow is allowed within each domain and between them, are referred to as *dual* or *multi permeability* models. As a general term for all the models, the *multi pore domain* model is used in this study.

In two pore domain models, soil matrix and macropores are connected to each other by an exchange term. Water exchange between the domains is usually defined analogously to flow inside each domain. Depending on the application, flow velocity between the domains is dependent upon the pressure head difference and average hydraulic conductivity, or relies on the moisture conditions of either one or both of the domains. Solute exchange between the domains is based on the water exchange, and usually consists of advective and dispersive exchange. The method of quantification used for water and solute exchange depends on the features of the modelled phenomenon. For instance,

to ensure fast exchange between the domains, arithmetic mean of the hydraulic conductivity of the domains may be used instead of geometric mean (Gerke and van Genuchten 1993b), and exchange may depend on the moisture conditions of the more dynamic preferential flow domain (Ray et al. 2004).

Dual-permeability models enable the consideration of heterogeneity in pore sizes, which results into slow matrix flow and fast preferential flow. As parameterisation is seen problematic already for one pore domain models, the situation is even more troublesome for the multi-domain case. Soil properties, i.e. water retention and conductivity parameters, need to be defined for both domains, and in addition, coefficients governing the exchange of water and solutes between the domains need to be defined. No direct measurement methods are available for determining the coefficient related to the exchange. Thus, the overall performance of the dual Richards approaches and their derivates can only be tested through advances in parameterisation and measurements related to different conditions and scales. Development of measurement methods and advances in the usability of measurements in reducing model and parameter uncertainty are considered to be crucial for model development (McDonnell and Tanaka 2001).

Even though several studies advocate the use of advanced and complex, Richards' equation-based, dual-permeability flow and solute transport models, no earlier studies have applied versatile hillslope datasets of forest areas to develop and test the models and evaluate the parameterisations in detail. So far, such studies are only available for more traditional, single pore domain models of forest areas (e.g. James et al. 2010). The most advanced dual-permeability models have been applied to agricultural soils (e.g. Gärdenäs et al. 2006). In general, the number of model applications is limited in relation to the models available, as the majority of studies have concentrated on investigating the parameterisation of a single model rather than on investigating different model structures or entirely different models for specific sites (Buytaert et al. 2008).

Among the most analysed sites is a forested, experimental hillslope in the Panola Mountain State Conservation Park in Georgia, United States. Over the last 25 years, a unique dataset has been collected to characterize the hydrologic behaviour of the Panola hillslope and to provide a framework for the development and testing of process-based models (James et al. 2010). The Panola data include rainfall-runoff measurements at the slope, soil moisture and water table observations, information on the soil physical and hydraulic properties, and data on water quality variables and tracers (for more information see e.g. Tromp-van Meerveld et al. 2008, McIntosh et al. 1999,

Peters et al. 1998). The most advanced model applications of the Panola slope include three-dimensional simulations of transient moisture status and flow along the slope with a one pore domain, Richards' equation-based HYDRUS model (Hopp and McDonnell 2009) and TOUGH2 model (James et al. 2010). Applications of two pore domain models for Panola are not yet available.

For Fennoscandian forest soils, Koivusalo et al. (e.g. 2003, 2000) used the tracer dataset of Lepistö (1996, see Chapter 1.1.1) in assessing the performance of a quasi-three-dimensional, one pore domain, Richards' equation-based model that was developed for predicting rainfall runoff processes in a small (18 ha), forested catchment of Rudbäck. Since the simulated fraction of the pre-event water in the stream was less than a half of the measured fraction, Koivusalo et al. (2000) called for improved incorporation of tracer study results in physics-based flow models in future studies. Kareinen and Ilvesniemi (2002) simulated water fluxes in macro-, intermediate meso- and micropores in different horizons of a till podzol of Hyytiälä in southern Finland with the ACIDIC-3 model, using tensiometer data and lysimeter data on the ion composition of the soil water. According to their simulations, the fraction of macropore flow decreased, and the fraction of micropore flow clearly increased with depth, but most of the flow occurred in mesopores at all depths, when the model was applied in natural weather conditions.

Other modelling studies that include preferential flow in the Fennoscandian forested till soils include the study of Espeby (1989) with a set of soil analyses, isotope studies and modelling, as well as the detailed modelling study of Jansson et al. (2005). Espeby's application of the SOIL model (Jansson and Halldin 1979) contained a simple bypass routine, and the simulations indicated that a pure Darcian approach cannot fully explain flow in heterogeneous soil such as forested till. The study of Jansson et al. (2005) was based on TDR (time domain reflectometry) measurements at the same slope as Espeby's (1989) measurements. Jansson et al. (2005) used the COUP model (Jansson and Karlberg 2001), and concluded that a one pore domain, one dimensional flow model was able to describe better the general behaviour of the slope throughout the melting season, but the two domain approach was needed in modelling the instant infiltration and runoff peak following immediately after rainfall.

Together with the classification approaches mentioned above, detailed experimental research combined with physics- and process-based modelling can be considered one of the key strategies in moving forward in hillslope hydrology. As Beven (2006) notes, the field and the modelling communities worked almost separately for a long time because of the incompatibility

between available modelling approaches and the complex real-world processes. In addition, hydrological networks are mostly designed for operational rather than scientific purposes (Kirchner 2006). Successful interplay between modelling and experimenting is an iterative process (Figure 1) that helps validate both the models and the measurement methods. Measurement methods, methods to analyse data, and modelling approaches can all be advanced by elaborating linkages between them (Kirchner 2006).

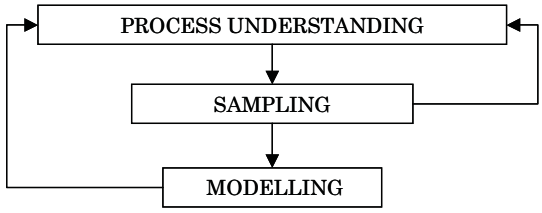

Figure 1. Iterative model development process (cf. Grayson and Blöschl 2000).

Modelling studies combined with experimental work can be considered investigative modelling approaches. When predictive applications aim to find answers to more practical problems such as flood control issues, investigative applications help in improving our understanding of hydrological processes behind the flow and solute transport phenomena, and allow more insight into the system behaviour (Blöschl and Sivapalan 1995). Investigative applications can also be set up to assess the governing equations and the parameterisation behind the model itself. Thus, even though complex and detailed 3D models are seldom operationally applicable in large-scale environmental assessments and predictions, they increase our understanding of geohydrological phenomena, aid in testing hypotheses and evaluating data, provide ideas for new experiments and measurement campaigns, and facilitate the development of simpler models for operational use (Loague and VanderKwaak 2004). The study of Bronstert (1999) showed that detailed hydrological models can be successfully applied to hillslopes, if comprehensive data are available and the model used comprises all relevant processes.

The goodness of fit of model applications and uncertainties related to the applications are usually evaluated following general testing procedures (presented by, e.g., Klemeš 1986, Refsgaard 2000) and likelihood methods (e.g., the *General Likelyhood Uncertainty Estimation* method, GLUE by Beven and Binley 1992). When a model is used for investigative purposes, optimization of the different performance criteria related to the testing is usually of less importance than in testing a model for operational work. When a model is used for operational work in prevailing conditions, it is often

enough that the model gives the right answers even for the wrong reasons, as long as an acceptably high goodness of fit is reached, but if the model is applied to new conditions in the future, it is important that the model also works for the right reasons, even with a lower goodness of fit (Kirchner 2006, Gupta et al. 2008).

When the focus of a model evaluation is in investigating how adequate the model structure is, how well the main mechanisms and processes related to modelled phenomenon are presented in the model, and how well the experimental data available supports the model development, usability of the general testing procedures and procedures to analyse the uncertainties is often limited. Kirchner (2006) notes that, for instance, a split sample test may not be informative, if the adequacy of a model structure is assessed by overlaying the model predictions onto the observations, and the datasets used for calibration and validation represent similar conditions. Kirchner (2006) reminds that the model's fit to the data may reflect other mechanisms than those controlling the response to the forcing of interest. Overparameterisation and tuning of the parameter values makes the model behaviour less dependent on its structure.

Overparameterisation is also linked with the concept of *equifinality*, referring to more than one parameter set proving equally good representations of the observed phenomenon, and to the concept of *identifiability*, referring to a set of parameters that all meaningfully contribute to the solution and that is unequivocal (Ebel and Loague 2006). Related to the uncertainty issues, the use of formal likelihood methods is restricted to cases where the models used are considered adequate representations of the system (Beven 2008), which poses a problem for the task of assessing the model structure itself. Other presuppositions of formal likelihood methods are that an error model can be found to define a likelihood function, and the error structure is stationary in calibration and in predictions, which is often not the case with epistemic, knowledge-based uncertainties related to real applications (Beven 2008).

Challenges related to overparameterisation and insufficiency of the theories behind models create a need for developing models that are parametrically more efficient and a need for developing model testing regimes that compare models against data more comprehensively, given the intrinsic limitations of the available data (Kirchner 2006). While simpler models are called for to reduce problems with equifinality and parameter efficiency, some systems are not simple enough to justify simple models (Ebel and Loague 2006). Thus, another way to increase the parameter efficiency related to the already existing models is to collect data, specifically based on the requirements of the model

in question. If optimal measurement methods do not exist, data should be collected with a variety of methods and the use of the different measurements in model parameterisation and testing should be assessed.

To assess the model parameterisations as well as the model structure, chemical and isotopic data provide powerful means to test whether a model is giving the right answers for the right reasons, but especially high-frequency chemical data on runoff generation are still rather rare and not yet been widely used for model evaluation (Kirchner 2006). Manipulation experiments can provide particularly incisive tests of hydrological theory, because controlled experiments can isolate individual mechanisms, thus providing a more precisely defined target for the theory to hit (Kirchner 2006). Structurally different model versions, run against chemical data and parameterised with different measurements, can be considered hypotheses of how a hydrological system works. Each model structure with each parameterisation represents a hypothesis that can be tested (Beven 2008).

1.2 Objectives and outline of the study

To conclude from the Background (Chapter 1.1), new hillslope scale studies of the hydraulic properties, runoff generation mechanisms and flow pathways in forested areas are called for. Although the concepts of base flow, groundwater flow and translatory flow broadly describe runoff generation in Fennoscandian, forested till soils, preferential flow and subsurface stormflow contribute to the runoff generation, and yet, only scattered data are available on it. Studies that closely couple a variety of specifically designed measurements and manipulation experiments containing chemical data to model development and testing, have a crucial role in further understanding hillslope behaviour, adequacy of the experimental data and the models. Detailed hillslope hydrological models can be used as research tools, if comprehensive data are available and the model used comprises all relevant processes. Full three-dimensional, Richards' equation-based, two pore domain models for flow and solute transport have not been developed and tested with versatile datasets for specific, forested hillslopes, even though many studies advocate the use of physics-based models in analysing and simulating the runoff generation processes.

This study operates on soil core to hillslope section scale and aims to provide new information on the hydraulic properties, flow paths and runoff generation processes, in particular on preferential flow and subsurface stormflow in a

Fennoscandian, forested hillslope with a shallow till cover above impermeable bedrock. The study focuses on collecting and analysing a versatile dataset from the hillslope, consisting of soil analyses and tracer experiments, and on systematically utilising the data in developing a full three-dimensional, Richards' equation-based, dual-permeability flow and solute transport model for the study slope. The main objective is to capture a subsurface stormflow event in a tracer dataset, to assess the adequacy of the dual-permeability model to describe the observed event, and to ultimately find a suitable model representation for subsurface stormflow and conservative solute transport in the study slope. Thus, the study pioneers the development of an adaptable and advanced dual-permeability model for a forested hillslope, using a dataset that is specifically collected to exhibit preferential flow and subsurface stormflow in the slope, and to consistently parameterise, develop and analyse the model.

Parametrically and structurally different model versions are considered alternative hypotheses of how to capture the observed stormflow event with the model. The model applications are rather investigative than predictive, as they focus on assessing the parameterisation and structural properties of the model versions, in relation to the observed phenomenon and available data. By contributing simultaneously to the experimental work and modelling, the study aims to bring the experimental data closer to model development. The study is carried out in a site that represents typical, Finnish landscape in terms of land use, vegetation, topography, and soil type. Chapters of the study build up on each other and the following objectives and hypotheses are defined for the different chapters.

Soil analysis (Chapter 2) aims to i) classify the soil physical and hydraulic properties in a common way, ii) capture the heterogeneity, variation and depth distribution of the soil properties by utilizing a variety of laboratory and field methods, and for analysing the results of the tracer experiments and model applications, iii) provide data for the model parameterisation, and provide the basis for assessing the reliability, representativeness and usability of the different soil parameters in modelling. The soil parameters are compared and analysed with each other and with the reference values available from the literature. The study hypothesizes that analyses made from disturbed, screened soil samples can be used as estimates for the soil properties of the matrix domain, and that properties of the preferential flow domain can be derived from undisturbed soil samples and with the help of tracer data and inverse modelling that represent larger scales. The soil structure is presumed to be the key factor behind the hydraulic properties.

Dye tracer studies (Chapter 3) aim to i) provide visual information on flow pathways and patterns in unsaturated and saturated soil, ii) elucidate the features of the soil structure together with the soil analysis, and iii) demonstrate the infiltration into variably unsaturated soil and the lateral stormflow above the phreatic water table in saturated soil. Based on a qualitative analysis of vertical and horizontal cross-cuts of three, stained soil plots, the dye tracer studies are expected to visualize the runoff generation processes that are captured quantitatively in the ion tracer experiment (Chapter 4). Together with the soil analysis, the dye tracer studies are to support the analysing of the results of the ion tracer experiment and the conceptualisation of the runoff generation phenomena at the study slope.

Ion tracer experiments (Chapter 4) aim to provide quantitative data on the initiation, steady-state and recession period of a subsurface stormflow and conservative solute transport event, for i) interpreting the runoff generation mechanisms in the study slope, and ii) developing and analysing the advanced physics-based flow and solute transport model for the slope. The ion tracer experiment also aims to iii) provide data for inverse modelling of hillslope scale saturated hydraulic conductivity. Together with the data from the soil analysis, estimates obtained for the saturated hydraulic conductivity by inverse modelling are hypothesized to serve as a basis for the model parameterisation so that only one model parameter is entirely unknown: the transfer coefficient between two pore domains in a dual-permeability model. The ion tracer experiment is expected to contribute to the model parameterisation also by providing targeted, chemical data for the model development that reduces problems with equifinality and model identifiability. Changes in the tracer concentrations along the slope in varying moisture conditions are expected to demonstrate the exchange of water and solute between the soil matrix and the preferential flowroutes so that a dual-permeability model can be identified.

The model development (Chapter 5) aims to i) provide an assessment of the suitability of the different model versions to describe the recorded subsurface stormflow and solute transport event, ii) capture the main mechanisms behind the event, iii) contribute to assessing further the usability of the data available for the parameterisation and the simulations, and iv) conceptualise further the features of the event. From the structural point of view, the main hypothesis is that preferential flow dominates the subsurface flow and transport processes to such an extent that a traditional, one pore domain model cannot reproduce the observed tracer plume with any parameterisation. A two pore domain approach is expected to be needed for an adequate simulation of the recorded event. In terms of the parameterisation, the main hypothesis is that the

exchange coefficient governing the transfer of water and solute between the pore domains can be estimated, when the majority of the model parameters are *a priori* fixed and a small number of parameters are adjusted or calibrated based on initial estimates and soft data. The model development relies on the concentration data of the tracer experiment, and the study thereby aims to demonstrate the usability and importance of the tracer data for the model development.

2 Site description

2.1 Overview and set up of the experimental field

Kangaslampi area in eastern Finland has been subject to several studies in forestry and catchment hydrology (e.g. Piirainen et al. 2007, Lauren et al. 2005, Mannerkoski et al. 2005, Piirainen 2002, Kämäri et al. 1998, Finér et al. 1997). The woodland area belongs to the middle boreal forest zone and the coniferous forests of the area are dominated by Norway spruce, with scattered Scots pines and white birches (Finér et al. 1997). The area is classified as *Vaccinium-Myrtillus* type according to the Finnish forest site type classification (Cajander 1949, Mikola 1982). Soils are thin, haplic podzols with sandy till as the parent material (FAO 1988), representing the most common soil type in Finland. The underlying bedrock is formed of gneiss granite and granodiorite (Finér et al. 1997). Topography is characterized by gently sloping hills that are surrounded by riparian areas, ponds and small lakes (Figure 2b). The long-term (1971-2000) mean annual air temperature is +1.9 °C and the mean annual precipitation is 564 mm of which approximately 200 mm falls as snow (Piirainen et al. 2007). About half of the annual precipitation generates runoff.

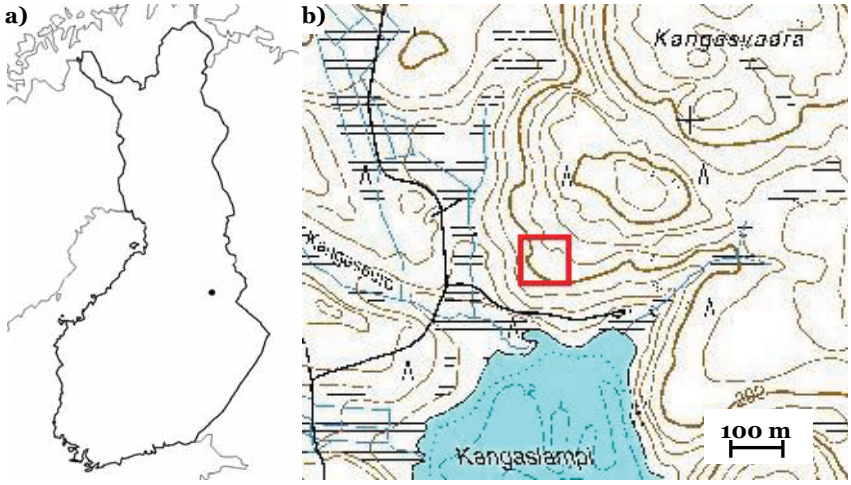

Figure 2. Location of the Kangaslampi area in eastern Finland (a), and location of the experimental site in Kangaslampi area (b) (National Land Survey of Finland).

Experiments of this study were performed in the red square area shown in Figure 2b. The area belongs to the midslope part of the hill (cf. portions of a slope, Miyazaki 2006). The study area was bounded with the help of a ground penetrating radar, so that the bedrock underneath is impervious with minor fractures, the bedrock slopes to the same direction as the soil surface, and the thickness of the soil profile above bedrock varies moderately around 1 m. The soil profile thickness is both up- and downslope from the study area remarkably thinner, varying around 0.5 m. Average slope within the study area was about 15 %. Upslope from the study area, the slope increases and is greater than 20 % near the top of the hill. Downslope from the study area the slope reduces slowly towards the Kangaslampi pond to an average of 7 %. The average soil type within the study area is sandy till with a high stone content (for a more detailed soil analysis see Chapter 2.2), whereas both up- and downslope the soil type is different with smaller stone content and softer soil material. However, the soil type around the whole area is generally classified as sandy till.

Figure 3. View on the Kangaslampi study area prior to the experiments in June 2005.

The area was in natural state prior to the experiments (Figure 3). The mineral soil column had not been treated in any way. The tree stand had regularly been thinned during the past, but clear cutting, stem only harvesting, soil harrowing and new planting had only taken place further on the top and on the side of the

hill, from 1996 to 1999 (e.g. Piirainen et al. 2007). The mixed, coniferous forest in the study area was approximately 70 years old, composing of Norway spruce (*Picea abies Karsten*, 55 %), Scots pine (*Pinus sylvestris L.*, 28 %) and white birch (*Betula pubescens Ehrh.*, 17 %). Based on a relascope sample plot, the mean tree height was 20 m and the mean volume 273 m^3/ha. The field layer vegetation on the study area consisted of dwarf shrubs (*Vaccinium vitis-idaea L.*, *V. myrtillus L.* and *Empetrum nigrum*). Feather mosses (*Pleurozium schreberi*) dominated the bottom layer. The forest floor consisted of a litter and mor humus layer.

Positioning of the different measurements and experiments is shown in Figure 4. The 2 m^3 pit on the left top corner of the area was dug for soil sampling, and the 12 m long trench at the bottom for soil sampling and dye tracer experiments. The majority of the study area were reserved for the observation wells needed for the ion tracer experiment. All measurements and experiments were scheduled for a one week intensive period in September 2005, June 2006 and June 2007. Soil sampling was carried out in 2005, and supplemented in 2007, ion tracer experiments were performed 2005, and dye tracer experiments in 2006.

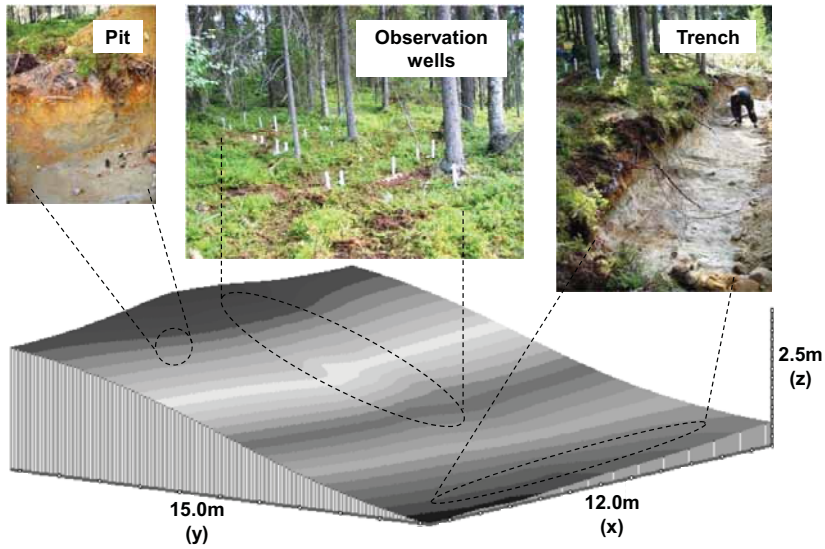

Figure 4. Location of the observation wells for ion tracer studies, and location of the pit and trench for soil analyses and dye tracer experiments in the midslope part of the Kangaslampi slope.

2.2 Soil physical properties

2.2.1 Characteristics of the soil profile

The trench face shows that soil in the Kangaslampi study slope is clearly podzolised, composing of an *eluvial horizon* E, *illuvial horizon* B, *transitional zone* BC, and *subsoil horizon* C (Figure 5). The mineral soil profile is overlain by a *mor humus layer* O. Acronyms O, E, B, BC and C are used in the following for the different soil horizons. In the context of preferential flow, lower index *m* is used for the soil matrix and lower index *p* for preferential flow domain in the acronyms of the soil horizons. Based on measurements in the trench, pit and drill holes made for the observation wells (Figure 4), thickness of the soil profile varies from 69 cm to 116 cm within the study area. According to the trench and pit measurements, average thicknesses of the different soil horizons are 9 cm (5-14 cm) in the E horizon, 14 cm (8-20 cm) in the B horizon, and 17 cm (8-30 cm) in the BC horizon, and the remaining thickness of the varying soil profile falls into the C horizon. Thickness of the O layer is 7 cm (5-10 cm).

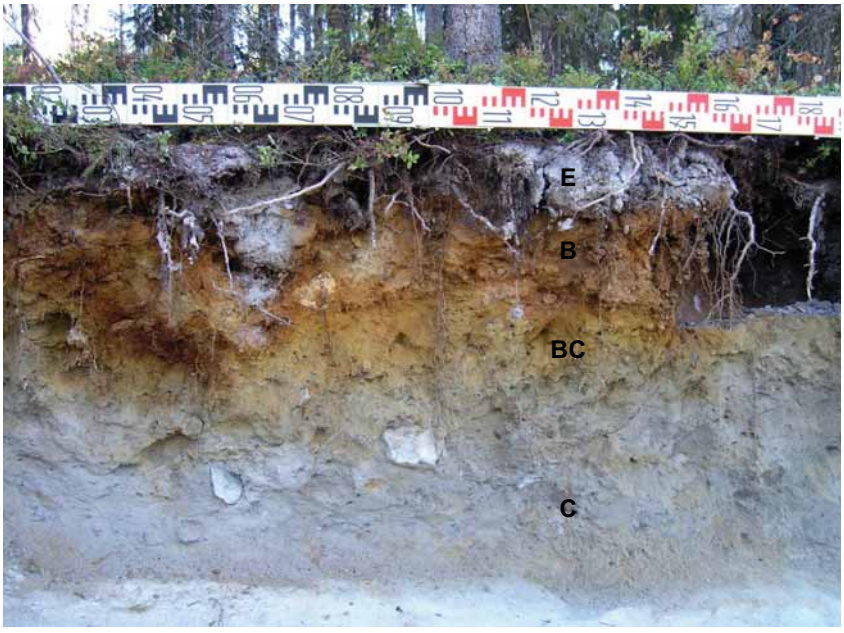

Figure 5. Vertical crosscut of the Kangaslampi podzol profile. E denotes the *eluvial*, B the *illuvial*, BC the *transitional*, and C the *subsoil horizon*.

Stone content of the Kangaslampi soil is high. In the E horizon and in the upper half of the B horizon stones cover as much as 20-48 % of the soil

volume. As a result of about ten thousand years of post-glacial podsolisation, solutes have flown and accumulated below the stones, forming areas with thick E, B and BC horizons: The average total thickness of these three, uppermost horizons is 40 cm. In the Kangaslampi slope, the podzol profile represents the thickest E and B horizons in Finland, since the thickness of these three horizons is reported to be 35 cm at the most (Hyyppä et al. 1992). The amount of stones reduces rapidly in the BC zone, and the stoniness of the C horizon is 5-12 %. Average stone contents are 34, 30, 17 and 9 % for the E, B, BC and C horizons, respectively. In addition to stones, the illuviated sesquioxides and organic matter have formed a strongly cemented B horizon (Ortstein) with a very low permeability. Cemented soil fragments are found in areas where the total soil thickness is at its highest (Figure 6).

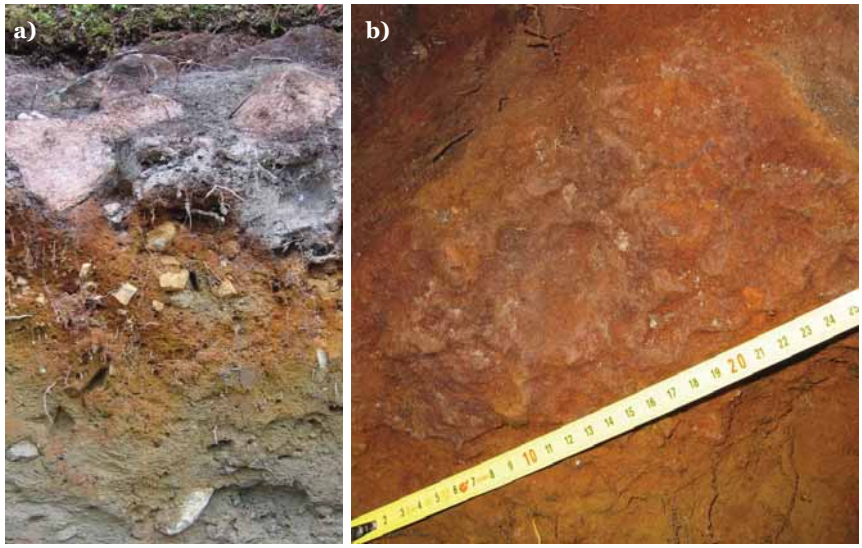

Figure 6. Stone content in the E and B horizons is more than a third of the soil volume in Kangaslampi, but diminishes clearly in the BC zone (a). In areas, where the podzol profile is at its thickest the B horizon is strongly cemented (b).

2.2.2 Grain size distribution, content of organic matter, and bulk density

Grain size distributions, based on dry and wet screening as well as hydrometer analysis, are shown in Figure 7. The soil type in all of the soil horizons within the study area is sandy till. Granularity data however show considerable heterogeneity in the texture of the Kangaslampi till and the soil material varies remarkably even on a small scale, especially within the two uppermost soil horizons. In the E horizon, sandy till varies from silty to gravelly, in the B and BC horizons it is mainly gravelly, and in the C horizon merely sandy.

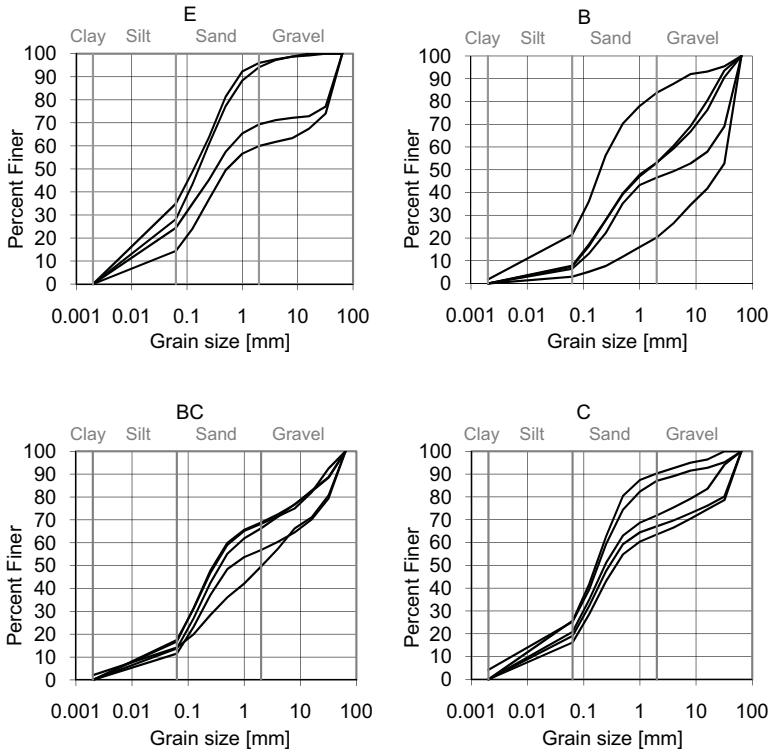

Figure 7. Grain size distribution of the Kangaslampi soil, based on 4-5 samples for each soil horizon E, B, BC and C.

The average grain size distribution of the E and C horizons are overlapping in Figure 8. The texture of the E horizon differs, however, from the texture of the C horizon because of the higher stone content and a higher variation in the grain size data. The coarsest and the most heterogeneous material are found in the B horizon, where the cemented soil fragments are also found (cf. Figure 6).

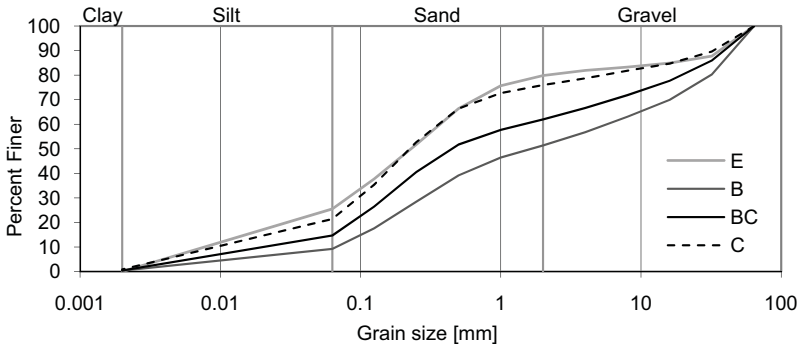

Figure 8. Average granularities of the Kangaslampi soil horizons.

Content of organic matter, based on drying soil samples for 16 hours in 105 °C and then igniting a fraction of the dried soil samples for an additional two hours in 800 °C, is highest in the B horizon, varying from 5.0 to 12.2 mass-%. Both in the E and BC horizons the content varies between 1.0 and 3.3 mass-%. In the C horizon the content is less than 1.0 mass-%, ranging from only 0.6 to 0.8 mass-%. Bulk densities, based on determining the soil volume with air pressure volumeter, steel cylinder or by water volume, and combined with drying and weighing the samples, are 1203 kg/m^3 for the E, 1580 kg/m^3 for the B, 1468 kg/m^3, for the BC and 1560 kg/m^3 for the C horizons. The bulk densities correspond to values obtained for a vast number of samples representing similar forest soils in Finland (Jauhiainen 2004).

2.3 Soil hydraulic properties

2.3.1 Sampling

Data on the soil hydraulic properties create the foundation for the parameterisation of a Richards' equation-based flow and solute transport model. Samples for analyzing the soil hydraulic properties, i.e., the water retention curves and the saturated hydraulic conductivity, were first collected at four points around the pit and the trench (Figure 4) in June 2005. Small soil samples for water retention analysis were also collected from the boreholes that were needed in the measurement of saturated hydraulic conductivity in the field with a permeameter. The analyses were made from disturbed samples that were sieved into a grain size smaller than one fifth of the sample diameter, i.e., 2 mm for the water retention samples, and 1.6 mm for the samples of the saturated hydraulic conductivity. The samples were recompressed to the natural density based on bulk density data.

Sieving of the samples destroys the natural soil structure. The structure loss has the most notable effect on the results of saturated hydraulic conductivity in the uppermost soil horizons, because the volume of macropores is high near the soil surface, and macropores strongly increase the hydraulic conductivity of soil (Chapter 1.1.1). However, analyses made from disturbed samples give an indication of the saturated hydraulic conductivity of the soil matrix, because the matrix properties are strongly controlled by the soil texture (e.g. Jarvis 2007). To be able to better estimate the effect of preferential flowpaths on the hydraulic properties, the water retention and porosity data were supplemented with a small set of undisturbed samples in June 2007, and the results obtained

both from the disturbed samples and the undisturbed samples were analysed together. Estimates of the saturated hydraulic conductivity obtained from the disturbed soil samples were supplemented with measurements with a permeameter in the field, and by means of inverse modelling, data from the ion tracer experiments of this study provided further estimates on the saturated hydraulic conductivity (Chapter 4).

2.3.2 Water retention properties

The water retention data, determined with a pressure plate apparatus, are shown in Figure 9. Each curve represents the results of one soil sample.

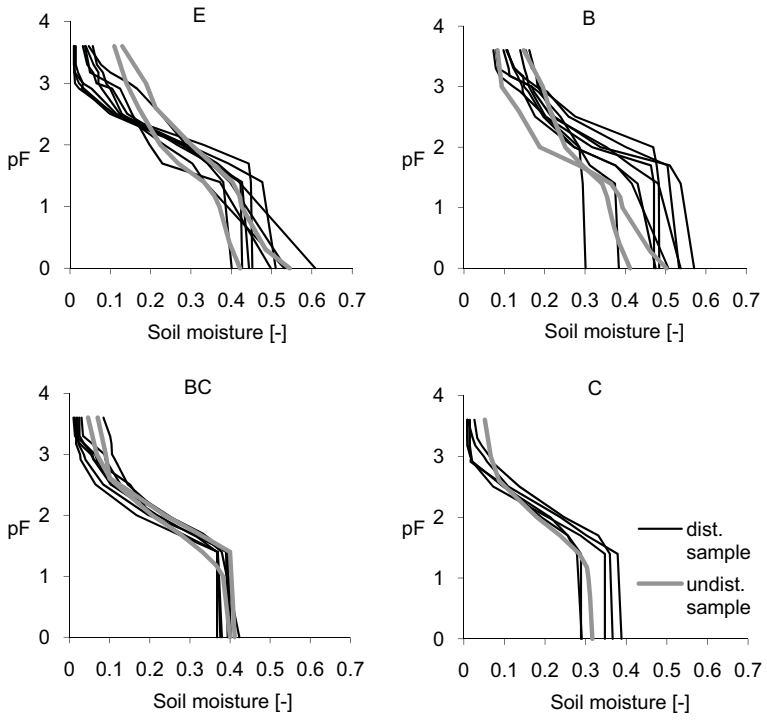

Figure 9. Water retention curves for each soil horizon E, B, BC and C of the Kangaslampi till. The black curves represent the data on the disturbed soil samples and the grey curves the data on the undisturbed soil samples.

The curves determined from the undisturbed soil samples exhibit a similar form than the curves determined from the disturbed samples. This indicates that the loss of the natural soil structure in sieving the first set of samples does not entirely change the results. Considering the shapes of the curves in the E and B horizons in greater detail, about half of the curves of the disturbed samples differ clearly from the curves of the undisturbed samples, whereas

half of the curves correspond to the curves of the undisturbed samples, in particular near saturation. Thus, the data on the undisturbed soil samples and half of the data on the disturbed soil samples represent more the water retention properties resulting from the soil structure and the total pore size distribution of the soil, whereas the other half of the data on the disturbed samples represents more the water retention properties resulting from the soil texture and the pores of the soil matrix. Variation in the soil physical properties is clearly reflected on the water retention data. Variation is highest in the E and B horizons, and it reduces with depth, similarly to granularity (Chapter 2.2.2). Most water retention curves of the E and B horizons slope more moderately near saturation than the curves of the BC and C horizons. Thus, the average pore sizes and the amount of macropores are clearly higher in the two uppermost horizons, and the soil density increases clearly below the B horizon.

In determining the water retention data for the undisturbed soil samples, pressure head, i.e. suction, was increased in smaller steps near saturation than for the disturbed samples to gain the most reliable data related to the water retention properties of the large soil pores near saturation. Below field capacity, i.e. after reaching a pressure head of -100 cm, the suction was increased in bigger steps for the undisturbed samples as compared to the disturbed samples. The disturbed samples were also kept longer in the pressure plate apparatus in each pressure step. The representativeness of the results of the disturbed samples was expected to be adequate with low moisture contents, since the effect of large pores on the water retention properties is minor with high suction values. Thus, the data on the undisturbed samples is more accurate and more representative for the natural soil structure with macropores near saturation than the data on the disturbed samples, whereas below the field capacity, the data on the disturbed soil samples is more accurate and representative for the soil matrix than the data on the undisturbed samples.

Reference water retention data are available from the nearby Kangasvaara catchment (Figure 2 b), determined by Möttönen (2000). Soil and land use in Kangasvaara area are similar to Kangaslampi. Each soil horizon can be classified as sandy till on average in both areas, and heterogeneity in the granularity shows a similar decrease with depth. However, the amount of fines and coarse material in soil are different for all soil horizons. In the E horizon, both the fine fraction and the fraction of coarse particles are higher in Kangasvaara than in Kangaslampi. In the B horizon, the amount of fines is higher in Kangasvaara than for any horizon in Kangaslampi. Also in the BC

zone, soil in Kangasvaara is more fine-grained. The coarsest material in Kangasvaara is found in the C horizon, whereas the coarsest material is found in the B horizon in Kangaslampi. With respect to the stone content, both the soil in Kangasvaara and Kangaslampi can be considered very stony. A comparison of the water retention data of this study to the data presented in Möttönen (2000) is given in Figure 10.

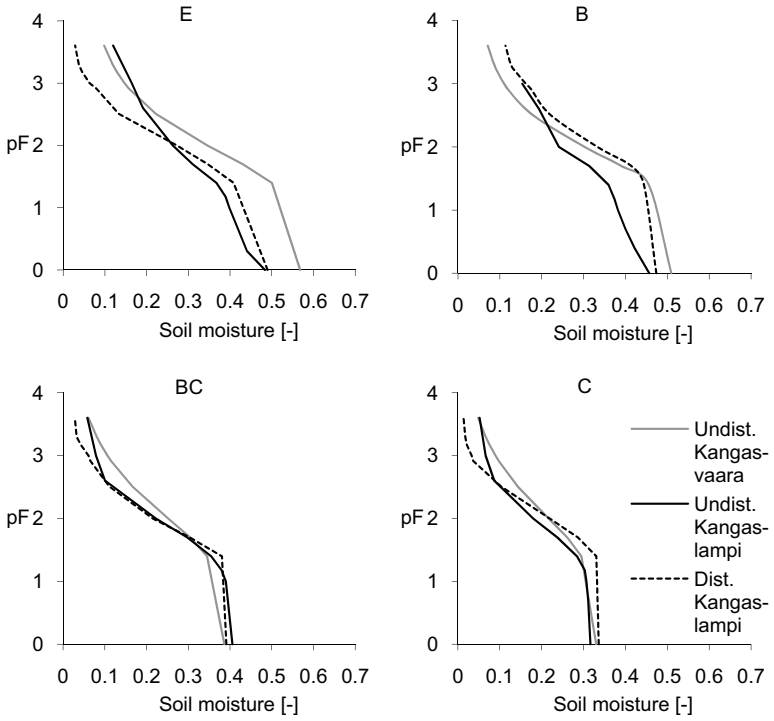

Figure 10. Average, measured water retention data of the Kangaslampi (black lines) and Kangasvaara (grey lines, Möttönen 2000) soil horizons E, B, BC and C. Continuous lines represent the undisturbed samples, and the dashed lines the disturbed samples.

In all soil horizons, the curves of Kangaslampi and Kangasvaara are similar compared to each other. Curves related to the undisturbed samples in both areas show a higher water release near saturation, illustrating the effect of the natural soil structure to the hydraulic properties of forest soil. The residual water contents are smaller for the disturbed curves of Kangaslampi, due to the longer measurement period for each pressure step. In addition, the comparison with the Kangasvaara data indicates that the screening and recompressing of the samples may influence the water retention properties also near residual water content, not only near saturation. Nonetheless, disturbed soil samples can provide representative estimates of the water

retention properties as well, since half of the curves of the screened and recompressed samples express a form similar to the curves of the undisturbed samples.

The van Genuchten model (1980) for relating soil moisture to the hydraulic pressure is:

$$\theta = \theta_R + \frac{\theta_S - \theta_R}{\left[1 + \left(\alpha|h|\right)^{\beta}\right]^{\left(1-\frac{1}{\beta}\right)}} \quad , \qquad (1)$$

where θ [-] is the soil moisture and h [L] is the corresponding pressure head, θ_R [-] is the residual water content, θ_S [-] is the saturated water content, and α [L^{-1}] and β [-] are the model parameters. The parameters were optimised with the method of least squares, by setting a lower limit of zero for the parameter values. Considering the accuracy issues discussed above, the model was forced to fit more accurately against the measured values near saturation than near residual water content. For the first two pressure heads, a deviation of only half a percentage unit was allowed between the measured and modelled moisture contents. Average measured curves and the van Genuchten fits to the average data are shown in Figure 11, and the fitted parameter values are summarized in Table 1.

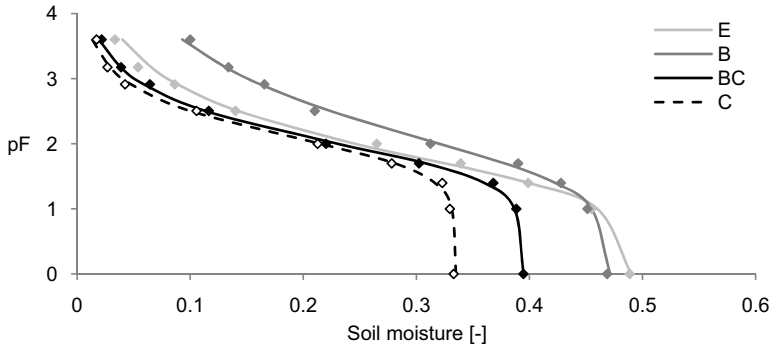

Figure 11. Average water retention data (dots) and their van Genuchten fits (lines) for the soil horizons of the Kangaslampi till.

Stones and boulders (Chapter 2.2.1) affect porosity and water content on a larger scale. To adjust the water retention parameters to the hillslope scale, saturated moisture content and residual moisture content are given in Table 1 with and without stones. Jauhiainen (2004) presents a large variation for the van Genuchten parameter values that are fitted to water retention measurements from a vast number of soil samples, representing similar

Finnish forest soils than in this study. The parameter values obtained in this study (Table 1) correspond to the values presented by Jauhiainen (2004).

Table 1. van Genuchten parameters for the average water retention curves (Figure 11). * denotes values where the stone content is taken into account.

Soil horizon	*α [cm^{-1}]*	*β [-]*	*θ_R=θ_R* [-]*	*θ_S [-]*	*θ_S* [-]*
E	0.036	1.504	0.000	0.491	0.324
B	0.025	1.353	0.001	0.473	0.331
BC	0.018	1.708	0.000	0.395	0.328
C	0.013	1.813	0.000	0.335	0.305

As discussed above, two groups of water retention data can be distinguished from the dataset: curves that slope sharply and curves that slope gently near saturation. In the sharp curves, the difference between the moisture content at saturation and moisture content at the first measured pressure head, pF 1, is below 0.01 (Figure 12). If the sharpest curves are considered to represent the water retention capacity of the soil matrix, and if larger pores are assumed to dominate the water retention capacity related to the gently sloping curves, the sharp curves can be appointed to the soil matrix and the gently sloping ones to the preferential flow domain in the dual-permeability model.

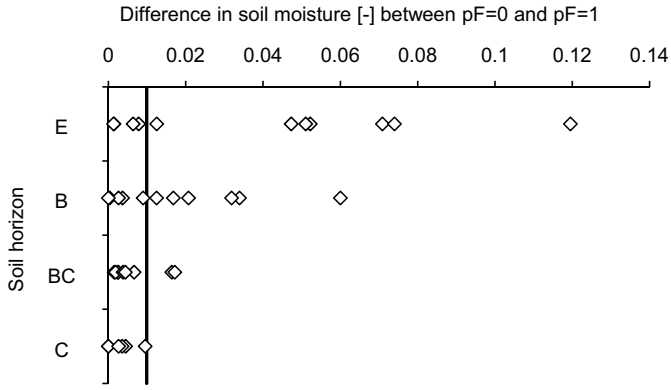

Figure 12. Difference in soil moisture [-] at pF 0 and pF 1 in the Kangaslampi water retention samples. The results are split in two parts at a boundary moisture difference of 0.01.

Grouping of the water retention data as presented in Figure 12 leads to the average water retention curves parameterised in Table 2 and presented in Figure 13.

Table 2. Average van Genuchten parameters of the data appointed to the soil matrix *m* and to the prefential flow domain *p*.

Soil horizon	α [cm^{-1}]	β [-]	θ_R [-]	θ_S [-]
E_m	0.013	1.861	0.000	0.447
B_m	0.008	1.600	0.030	0.435
BC_m	0.012	1.990	0.010	0.390
C_m	0.012	1.898	0.000	0.339
E_p	0.080	1.380	0.000	0.524
B_p	0.039	1.375	0.000	0.499
BC_p	0.032	1.440	0.000	0.412
C_p	0.025	1.544	0.001	0.319

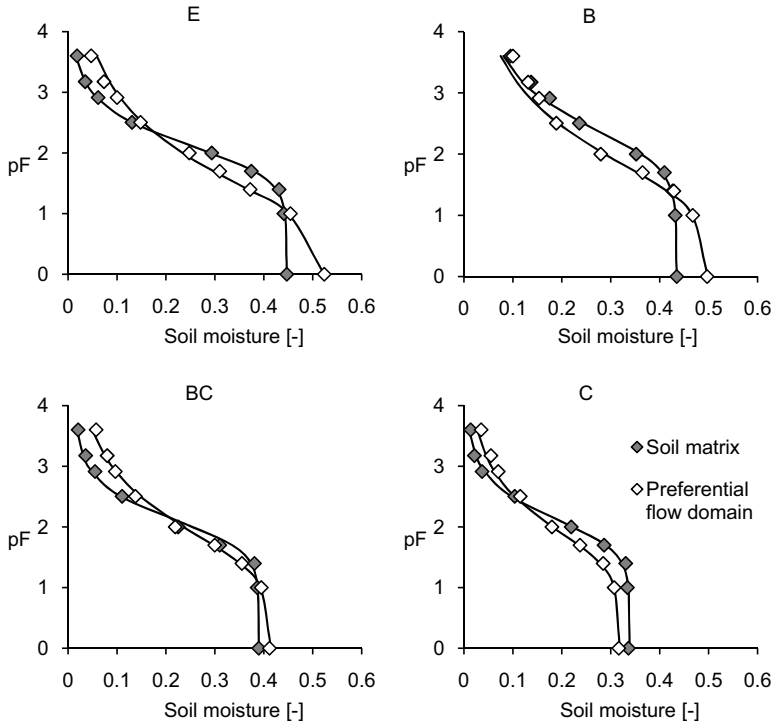

Figure 13. Average, measured water retention curves (dots) and their van Genuchten fits (lines) for the soil matrix and for the preferential flow domain of each soil horizon E, B, BC and C of the Kangaslampi till.

As noted earlier, to describe the water retention properties on a larger scale, the stone content need to be reduced from the water content values. The data also need to be scaled so that the sum of the maximum water content in the soil matrix and in the preferential routes does not exceed the total porosity of the soil. The scaling factor for the moisture values in each pore domain

depends on the definition used for a macropore. Porosity estimates are discussed in Chapter 2.3.4 and suitable fractioning into the two pore domains is further discussed in Chapter 5 in the context of model development. An example of a possible split is presented in Figure 14, using a limiting diameter of 100 µm for a macropore (cf. Chapter 2.3.4).

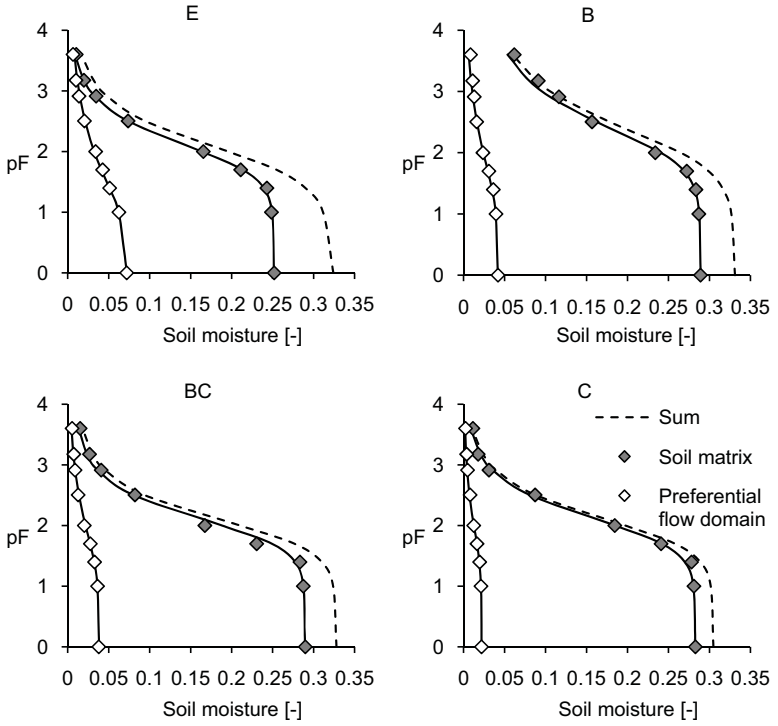

Figure 14. Scaled, average water retention data (dots) and their van Genuchten fits (lines) for the soil matrix, the prefential flow domain, and the original curves summing up both the domains for each soil horizon E, B, BC and C of the Kangaslampi till. Stone content is reduced from the water contents.

The scaling does not change the values of the parameters α and β, because the form of the curves does not change. Thus, the scaling only affects the values of the residual and saturated water contents. Scaled values, where stone contents are taken into account, are presented in Table 3 for the curves presented in Figure 14. Considering the modelling of flow and solute transport (Chapter 5), the average, gentle and sharp sloping van Genuchten curves can be used as such in the model parameterisation, when scaling and stone contents are taken into account in the parameter values.

Table 3. Scaled, average van Genuchten parameters of the data appointed to the soil matrix *m* and to the prefential flow domain *p* (Figure 14). In scaling, a definition of 100 µm is used for a macropore, and the total porosity of each soil horizon that sums up the saturated water content of the soil matrix and the preferential flowroutes, corresponds to the average, measured porosity of each soil horizon, corrected with the stone content data.

Soil horizon	α [cm^{-1}]	β [-]	θ_R [-]	θ_S [-]
E_m	0.013	1.861	0.000	0.252
B_m	0.008	1.600	0.020	0.289
BC_m	0.012	1.990	0.007	0.290
C_m	0.012	1.898	0.000	0.283
E_p	0.080	1.380	0.000	0.072
B_p	0.039	1.375	0.000	0.042
BC_p	0.032	1.440	0.000	0.038
C_p	0.025	1.544	0.000	0.022

2.3.3 Saturated hydraulic conductivity

Estimates for the saturated hydraulic conductivity determined in the laboratory with the constant head method, using a constant cell device, are clearly smaller than those determined in the field with the *Guelph* permeameter (model 2800 K1, Soilmoisture Equipment Corp 1991) (Figure 15).

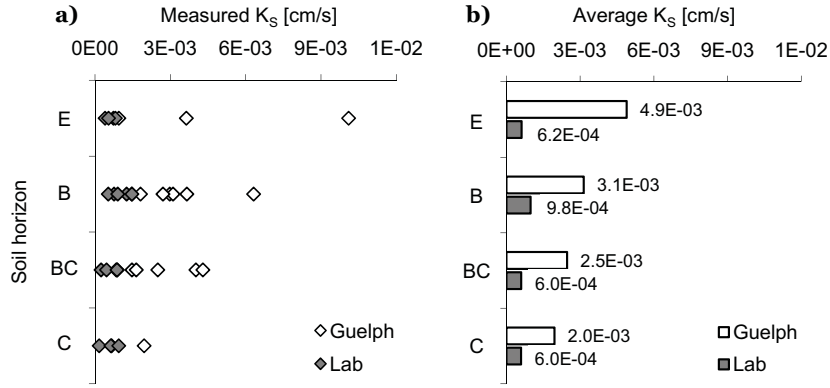

Figure 15. Measured saturated hydraulic conductivity K_S (a), and average of the measured saturated hydraulic conductivity (b) for each soil horizon E, B, BC and C in Kangaslampi, determined from soil core samples in the laboratory (Lab) and with the Guelph permeameter in the field (Guelph).

As noted in Chapter 2.3.1, the laboratory measurements were carried out from screened and recompressed (disturbed) samples, and the original soil

structure of the samples was lost. Therefore, the Guelph measurements in the field represent more the conductivity of undisturbed, natural soil. In addition, the Guelph-measurements represent a wider spatial scale than the laboratory samples. Due to the lower disturbance and the bigger spatial scale of the Guelph-measurements, the Guelph-results include more the effect of preferential flowpaths on the hydraulic conductivity, which is related to the natural pore structure of forest soil.

Average saturated hydraulic conductivity measured in the laboratory has the highest value in the B horizon (Figure 15 b). The B horizon consists of the coarsest soil material (Chapter 2.2.2), which may cause higher conductivity values compared to the other, more fine-grained soil horizons. Also, variation in the laboratory results is highest in the B horizon (Figure 15 a). In contrast to the laboratory results, conductivity values obtained with Guelph in the field decrease non-linearly with depth (Figure 15 a and b). Also the variation in the conductivity values determined with Guelph decrease with depth.

The laboratory values are of the same magnitude as compared to the values available in the Finnish literature for tills. According to Airaksinen (1978), the saturated hydraulic conductivity in sandy tills varies from 1E-6 to 1E-4 cm/s, and the total variation in soils ranging from sandy till with fractions of silt to sandy till with fractions of gravel varies from 1E-7 to 1E-3 cm/s. The computational assessments of Hänninen et al. (2000), based on about 6000 point values from Finnish soil maps and the equation of Sauerbrei (Vukovic and Soro 1992), produced results in the same magnitude as given in Airaksinen (1978). Hänninen et al. (2000) report an average conductivity of ca. 5E-5 cm/s, with the total variation from about 3E-7 cm/s in soils with a high fine fraction to nearly 3E-1 cm/s in coarse-grained soils. Reflected against the areal analysis of Hänninen et al. (2000), Kangaslampi area falls within a regionally low-permeable zone with a conductivity of less than 1E-4 cm/s.

Compared with values determined from undisturbed soil samples in the nearby area of Kangasvaara (Möttönen 2000), the saturated hydraulic conductivity of the BC and the C horizon are of the same magnitude as the laboratory results of disturbed samples from Kangaslampi (Figure 16). The correspondence of the values indicates that screening and recompressing of the samples does not remarkably affect the conductivity estimates in the lower soil horizons with a minor macropore fraction. In the E and B horizons, where the amount of preferential routes is high, the laboratory results of Kangaslampi are clearly lower than in Kangasvaara. Instead, the Kangasvaara results correspond closer to the Guelph results of Kangaslampi in the upper two soil horizons.

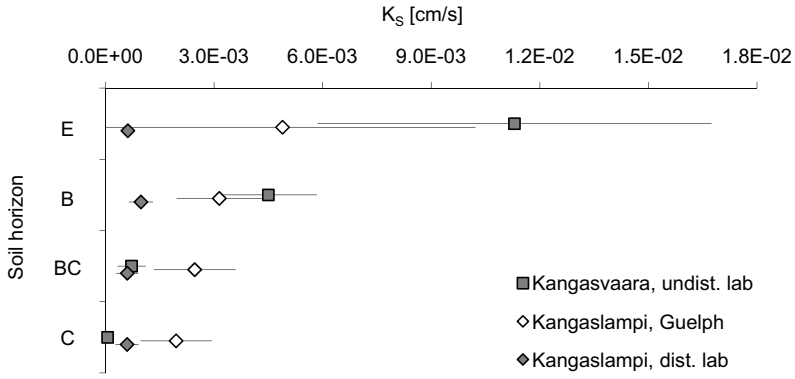

Figure 16. Average saturated hydraulic conductivity K_S for Kangaslampi and for the reference area Kangasvaara with 95 % confidence intervals.

Hydraulic properties of the soil matrix are strongly controlled by the soil texture (e.g. Jarvis 2007). The results obtained from the disturbed soil samples in this study corresponded to the texture-related literature values (Airaksinen 1978, Hänninen 2000) that represent mainly the conductivity of subsoil with a very low fraction of preferential flow routes. Therefore, the conductivity values determined in the laboratory were used in estimating the conductivity of the soil matrix to parameterise the flow model of this study (Chapter 5.1.8). The reference dataset from Kangasvaara shows that measurements made from undisturbed samples capture more of the effect of preferential flowpaths and soil structure on the conductivity. Usability of the undisturbed samples and the Guelph results is discussed further in Chapter 3.3.2 in the context of computational estimates for the saturated hydraulic conductivity.

2.3.4 Porosity, effective porosity and porosity of macropores

Estimates for the porosity of the different soil horizons are available from the data related to determining the water retention curves and the saturated hydraulic conductivity in laboratory. In this study, saturated moisture content of soil is considered equal to the total porosity, and the term *porosity* is used as a synonym for the saturated moisture content. Porosity estimates related to the water retention and saturated hydraulic conductivity data are shown in Figure 17. Porosity was calculated from the dry unit weight and water content values as well as from the maximum water content of the soil samples, assuming the samples were fully saturated.

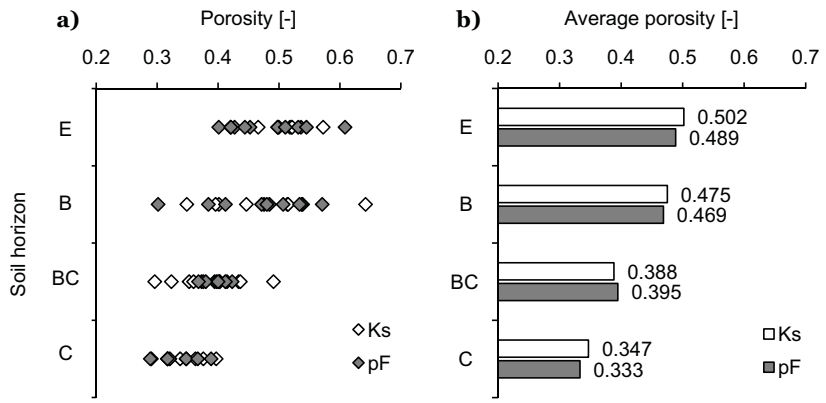

Figure 17. Measured porosity values (a) and average porosity values (b) for Kangaslampi, determined from the water retention samples, denoted with *pF*, and from the samples of the saturated hydraulic conductivity, denoted with K_S.

The variation in the results is very high particularly in the B horizon (Figure 17 a). Average porosity estimates of each horizon are, however, near each other for both of the sample sets (Figure 17 b). Average porosity values obtained from the samples for saturated hydraulic conductivity and water retention curves are 50 % and 49 %, respectively, for the E horizon, 48 % and 47 % for the B horizon, 39 % and 39 % for the BC horizon, and 35 % and 34 % for the C horizon. In addition, a closer look at the water retention data (Figure 10) reveals that average porosity values (i.e. saturated moisture contents) in the disturbed and undisturbed water retention samples fall near each other, within one percentage unit in all soil horizons. Thus, screening and recompressing did not affect the results for the total porosity in this study.

The most severe uncertainty concerning the porosity estimates is related to stones that cover more than a third of the soil volume in the E and B horizons. Estimates are available for the stone contents (Chapter 2.2.1), but no estimates on the void volume surrounding or underlying the stones are available. Even though some of the sample cylinders were pushed close to stones, the small samples cannot fully capture the effect of the void spaces on the larger scale porosity. It is also noteworthy that some air is always trapped in soil, also during saturation. Therefore, the saturated moisture content does not correspond to the total porosity in soil. However, from the point of view of subsurface flow, the part of the pore volume that contributes to flow, i.e., the pore space containing water at saturation, is actually preferred to the total pore volume. The problem of air in soil is rather related to differences in saturation of laboratory samples and soil material in the field: Saturation prevailing in the samples in the laboratory does not necessarily correspond to

the degree of saturation that is possible to obtain in the field. The modelling study (Chapter 5) may give more insight into the correspondence of the saturated moisture content of the soil samples and the soil in the field.

Average porosity values determined in this study (Figure 17 b) are in line with the estimates available in the literature. Airaksinen (1978) gives a range of 45-55 % for the primary porosity of tills. Salonen et al. (2002) give an estimate of 30-60 % for the porosity of mineral soils, but claim the porosity of till to be only 17 % at the highest. Reference values are available for the nearby area of Kangasvaara, based on 16 undisturbed soil samples for each soil horizon (Möttönen 2000). The soil in Kangasvaara corresponds closely to the soil in Kangaslampi, as noted in Chapter 2.3.2. The total porosity of the E and B horizons is higher in Kangasvaara, being 57 % and 51 %, respectively. Differences in the porosity values can be explained with the differences in granularities. As the fine fraction of the Kangasvaara soil material is higher, higher porosities are to be expected. For the BC and C horizons, Möttönen (2000) reported porosity values of 39 % and 33 %, respectively, which correspond to the porosity values in Kangaslampi. As the average soil profile thickness is higher in Kangasvaara, Möttönen (2000) divided the subsoil into two parts, and reported an additional porosity of 29 % for the lower part of the subsoil.

The water retention data of this study were also used for assessing soil effective porosity and porosity of macropores that can be used to estimate the porosity of the preferential flow domain of the soil. The assessment for the macropore volume was based on the equation between the pressure head h [m] and the threshold diameter for a macropore d [μm], given by, e.g., Vakkilainen (1986):

$$h = \frac{30}{d} \quad . \qquad (2)$$

Porosity of macropores is the deviation between the saturated moisture content and the moisture content that corresponds to the pressure head calculated with Equation 2. Estimates of the macropore volume depend on the definition used for a macropore.

Perret et al. (1999) summarise several definitions for the minimum macropore diameter, ranging from 30 to 3000 μm. When one of the early definitions for a macropore, 30 μm is used, 1.0 m suction prevails in soil according to Equation 2, and the soil is in field capacity (e.g. Vakkilainen 1986). The pressure head of 1.0 m also corresponds to the concept of *effective porosity*. Since most of the recent studies that discuss preferential flow use a higher estimate for the

minimum macropore diameter, and use the 30 µm diameter rather as a definition of a mesopore, the 30 µm diameter and the corresponding 1.0 m suction were used in this study in determining the effective porosity of soil.

Several definitions for the macropore diameter, as listed in Perret et al. (1999), were taken into account when estimating the macporosity of soil in this study, e.g. the pore diameter of 75 µm (denoted as *macrovoid* in Brewer et al. 1964), 100 µm (denoted as *macropore* in Jongerius 1957), 200 µm (denoted as *coarse pore* in Russell 1973), 300 µm (denoted as *superpore* in McIntyre 1974), and 1000 µm (denoted as *superpore* in Luxmoore et al. 1990). These diameter values correspond to pressure heads of 0.40, 0.30, 0.15, 0.10 and 0.03 m, respectively, based on Equation 2. Three estimates for the porosity of macropores and estimates for the effective porosity are presented in Figure 18.

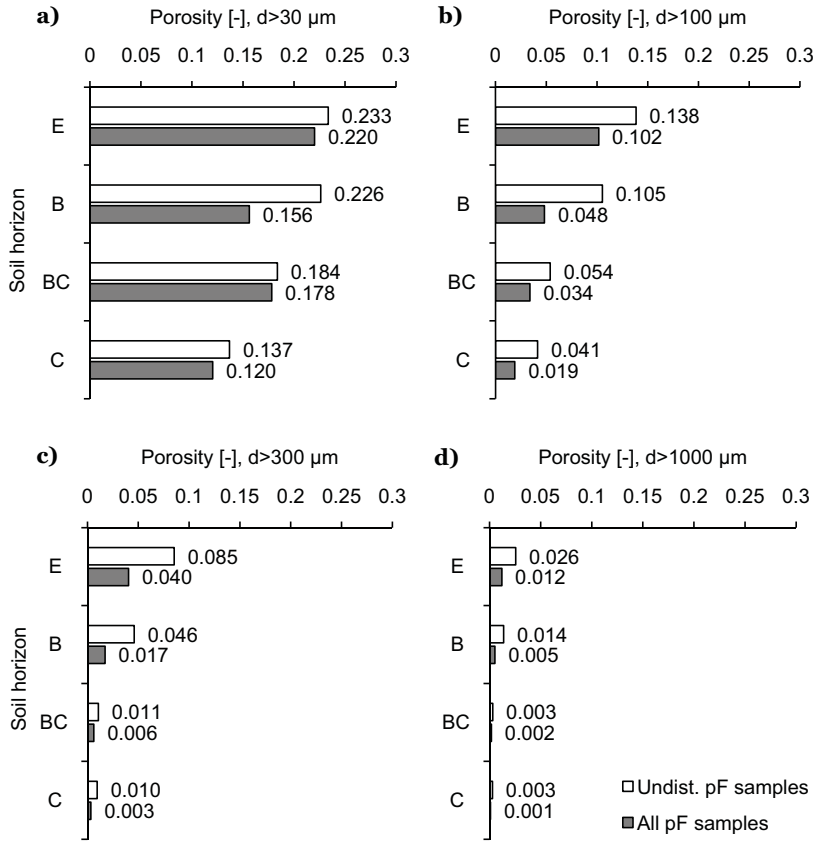

Figure 18. Porosity estimates for Kangaslampi, corresponding to a threshold pore diameter of 30 µm (a), 100 µm (b), 300 µm (c), and 1000 µm (d). Estimates calculated from the average water retention data of all samples are denoted with grey bars, and estimates calculated from the average water retention data of undisturbed soil samples with white bars.

As noted in Chapter 2.3.2 (Figure 9), the form of the curves of the undisturbed samples reflects better the actual water retention near saturation, and give more reliable estimates for the effective pore volume and the macropore volume. Therefore, data related to the undisturbed samples is also presented separately in Figure 18. Effective porosity and macroporosity related to the disturbed and undisturbed samples differ from each other more than the total porosity related to the disturbed and undisturbed samples. Thus, screening of the samples affects the results in terms of estimating the macroporosity.

Stones affect the pore volume of soil remarkably on a larger scale, and corrected porosity values are needed in the flow model that operates on the hillslope scale. Removing the volume of stones and boulders (Chapter 2.2.1) from the porosity results leads to estimates presented in Figure 19.

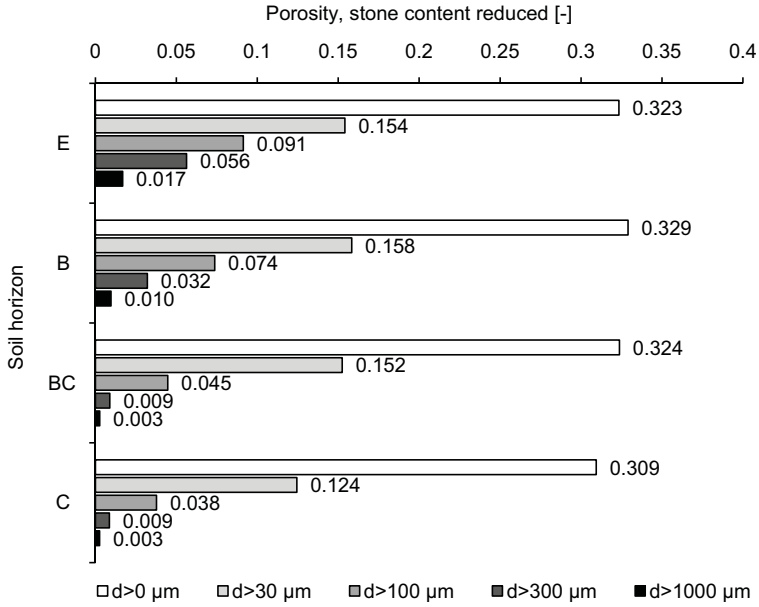

Figure 19. Total porosity (pore diameter *d*>0 µm), effective porosity (*d*>30 µm) and porosity of macropores (*d*>100, *d*>300 and *d*>1000 µm) for Kangaslampi, when stone contents are reduced from the water retention data of the undisturbed soil samples.

Removing the stone contents from the porosity values leads to a total porosity of 31-33 % and to an effective porosity of 12-16 % in the soil profile. After removing the stone contents, estimates of macroporosity are, depending on the definition used for a macropore, 1.7-9.1 % in the E horizon, 1.0-7.4 % in the B horizon, 0.3-4.5 % in the BC horizon, and 0.3-3.8 % in the C horizon. Thus, macropores comprise 5-28 % of the total pore space in the E horizon, 3-23 %

in the B horizon, 1-14 % in the BC horizon and 1-12 % in the C horizon. Effective porosity constitutes 48 % of the total pore space in the E and B horizons, 47 % in the BC horizon and 40 % in the C horizon.

Beven and Germann (1982) note that any experimental technique used to determine soil macroporosity should distinguish between two types of large voids: voids that are hydrologically effective in terms of channeling flow through the soil and those that are not, and, techniques that are based on pore size alone will yield an estimate of total macroporosity that is not necessarily closely related to channeling macroporosity. Instead, Germann and Beven (1981) note that the concept of *air capacity* of soil is closely related to *effective macroporosity*. Therefore, air capacities were determined in this study by saturating the undisturbed soil samples before the water retention measurements, and by measuring the water volume that drains from the samples during 24 hours (cf. Burger 1922 after Germann & Beven 1981 after Beven and Germann 1982). The air capacity is 6.3 % for the E, 3.5 % for the B, 2.3 % for the BC and 1.3 % for the C horizon. These estimates are based on only 1-2 samples, and representativeness of the results is therefore weak.

For macroporosity and effective porosity, only indirect estimates are found for Fennoscandian tills in the literature. For instance Airaksinen (1978) gives an indicative value for the secondary porosity of till, 55-65 %, which is 10 %-units higher than the indicative value for the primary porosity related to the soil matrix. Thus, voids and fissures account for 10 % in till soil after Airaksinen (1978). In several other studies (e.g. Jansson et al. 2005), a general estimate of 4 % is used for the porosity of macropores. Depending on the definition used for a macropore, the porosity of macropores determined in this study increases from 0.5-1.0 % in the C horizon to 4.1-8.5 % in the E horizon, when stones are not taken into account. Effective porosities constitute about a half of the pore volume in each soil horizon, similarly to Dunn et al. (2007).

As no direct estimates for the macroporosity, especially for effective macroporosity (cf. Germann and Beven 1981) can be found, several estimates need to be tested in modelling subsurface flow in Chapter 5. However, the average estimates for the total porosity of soil, corrected with stone content data, can be used as default values in modelling flow and solute transport in the study slope.

3 Dye tracer experiments

3.1 Methods

To visualise flow paths and soil structure, three dye tracer experiments were conducted above the trench (Figure 4) in the Kangaslampi slope in June 2006. The basic idea in the experiments was to douse the soil with dye solution, slice the plots in vertical and horizontal cross profiles, and – while slicing – make visual observations and take photographs of the coloured soil. In the first two experiments (presented in Chapter 3.1.1), dye was poured into unsaturated soil. The volumetric soil moisture prior to the experiments was approximately 12 % in the E, BC and C horizon, and 19 % in the B horizon. The first plot was excavated horizontally, revealing horizons of the podzol one at a time from topsoil down to subsoil, and the second plot was excavated vertically to observe the depth distribution of the colour. When poured into unsaturated soil, the dye exposes infiltration into soil. In the third experiment (presented in Chapter 3.1.2), the dye was poured into wet soil and the plot was excavated in vertical profiles. The purpose of the experiment was to observe the continuity of the colour downslope from its source on a lateral flow plane, which was assumed to form above the saturated zone.

The dye selected for the experiments was *Acid Blue 9*, also known as *Brillant Blue FCF* ($C_{37}H_{34}N_2Na_2O_9S_3$). Acid Blue 9 was selected to this study following the recommendations of similar studies (e.g. Weiler 2001, Weiler and Flühler 2004), and taking into account the toxicological overview available (Flury and Flühler 1994). Acid Blue fulfills the requirements for a good dye for soil studies, since it is not toxic to the environment, and it has good visibility and low retardation in soil at the same time. The blue dye can be seen as blueish or greenish patches in grey to reddish toned till soil. For the experiments, the concentration of the dye solution in relation to the total dye load was tuned using the guidelines given by Flury and Flühler (1994). They suggest a maximum residue of 1 mg/l for the stained study area. Ensuring this limit for the residues on one hand, and taking into account the initial soil moisture and the pore volume of the podzol on the other, 10 litres of 0.5-1 g/l solution was doused into the soil in each of the three experiments. Flury and Flühler (1994) recommend somewhat higher concentrations, 3-5 g/l for ensuring good

visibility in soil, and for instance Weiler and Flühler (2004) used 4 g/l solution. The smaller concentration in this study was however enough to produce a distinct flow profile in soil with the total solution load of 10 litres.

3.1.1 Staining of unsaturated soil

Two plots with an area of 1x1 m² were marked off for examining the dye patterns in unsaturated soil (Figure 20). 10 l of 0.5 g/l dye solution was prepared for each plot, and the solution was poured into the soil slowly and evenly with a sprinkle to a quarter of the plot, to an area of 0.5x0.5 m². Another 3 l of pure water was poured into the soil to wash down the dye that remained in the vegetation and the top organic layer. Then, the solution was left to adsorb in soil. As the average thickness of the podzol within the experimental plots was 80 cm, and the initial soil moisture varied between 14 and 22 %, the thirteen litres of dye solution and pure water corresponded to ca. 25 % of the free pore volume of the soil profile, and 45 % of the pore volume of the three top horizons. In the first experiment, excavations were started two hours after applying the dye, and the second plot was sliced the next day.

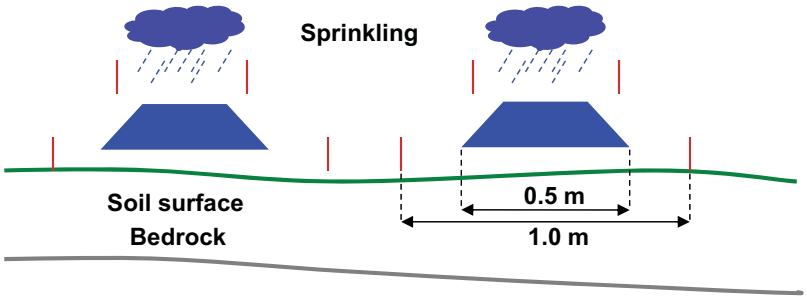

Figure 20. Schematic of the dye tracer experiment in unsaturated soil.

Before starting to slice the plots, the top organic layer was carefully removed. Although the dye was applied to an area of a quarter of a square metre, the excavation was carried out in the whole area of one square metre to track down all the dye that was spread into the soil. Spades, hoes, and brushes of different sizes were used in the excavation and preparation of the soil profiles for photographing. The plots were sliced gradually for following the routes of water as precisely as possible. Visual estimates for the dye coverage on the vertical and horizontal soil profiles were made in situ, and revised later by quantifying dyed squares on a grid that was placed on the crosscut photographs.

3.1.2 Staining of saturated soil

The dye tracer experiment in saturated conditions was carried out inside the upper reach of the ion tracer study area (cf. Figure 4). Selecting this area assured that both numerical and visual information on flow is available from the same spot of the slope. The irrigation tube that was used in the salt tracer experiments (Chapter 4.1) was used in creating the saturated conditions for this experiment. Also, some of the well screens of the salt experiments were used in observing the water levels in the slope, when tuning the water level at a suitable height for the dye experiment. A schematic of the experimental arrangement is shown in Figure 21.

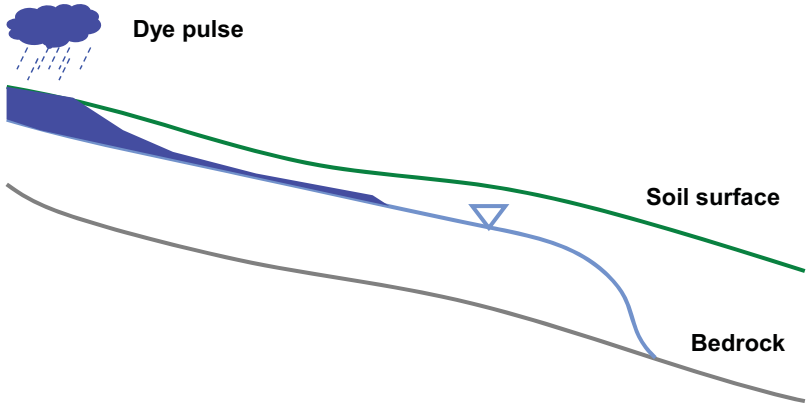

Figure 21. Schematic of the dye tracer experiment in saturated soil.

The experiment was started by setting up the irrigation source for the area. One day before the experiment, the area was irrigated with one cubic metre pure water to increase the initial soil moisture content, and to ensure as uniform moisture pattern as possible for the experiment the next day. To begin the experiment, the area was irrigated through the perforated tube (Chapter 4.1) until the saturated zone was observed to be at least 2.0 m wide and 3.0 m long, and the saturation zone had reached the top organic layer within this area. When these conditions were achieved, the irrigation was stopped and the fall of water levels was observed from five well screens in the area. When the water level had reached the B horizon, the dye pulse was sent downslope near the irrigation tube. The water level was chosen to be tuned to the B horizon based on the flow patterns seen in the unsaturated experiments: The B horizon had proved to contain remarkable amounts of preferential flowpaths, but the dye pattern there was more discontinuous than in the E horizon.

The dye pulse was poured into a shallow hole that had been dug 60 cm downslope from the irrigation tube. The hole was 15 cm long, 100 cm wide and

10 cm deep. Thus, a 100 cm wide pulse was sent downslope from just above the saturation depth. The concentration of the dye pulse was 1 g/l and the total amount of solution poured into the soil was 10 l. To rapidly rinse down the dye to the groundwater table, additional 10 l of pure water was poured into the shallow hole. As the line-type dye pulse was sent downslope, the irrigation was immediately started again to maintain the fast lateral flow in soil. After five minutes the irrigation was stopped, since the water level started to rise in the upper parts of the area. Then, the slope was left to dry overnight, and the soil was sliced into vertical profiles during the next day.

The vertical slicing of the area was started 250 cm downslope from the dye source. As no dye was found, the next profile was dug at a distance of 220 cm. Again, no dye was to be detected. The slicing however revealed interesting features of the soil profile. The bedrock had a wide sag within this area and the thickness of the soil profile was as high as 120 cm on average. Also, the soil mass seemed to be very dense in all depths and the B horizon was strongly mineralized. The slicing was continued in intervals of about 30 cm, and finally, clear traces of the blue dye were found at a distance of 150 cm from the dye source. From this point upslope, the profiles were photographed and carefully investigated.

3.2 Results

3.2.1 Dye coverage and distribution

Infiltration of the dye into the unsaturated soil profile follows the most permeable flow routes in soil that are related to loose soil structure and soil moisture. The depth distribution of the colour (Figure 22 a) follows the thicknesses of the soil horizons (cf. Figure 5) such that where the E and B horizons are thick, dye is found deeper, and vice versa. Within the experimental plots of this study, the colour transport stops in the BC zone, and no colour reaches the C horizon. Also the amount of roots and stones diminishes considerably within the experiment plots when coming to the BC zone. The deepest level in soil where dye was found was around 40 cm from the top of the E horizon, and around 50 cm from the soil surface including the O layer.

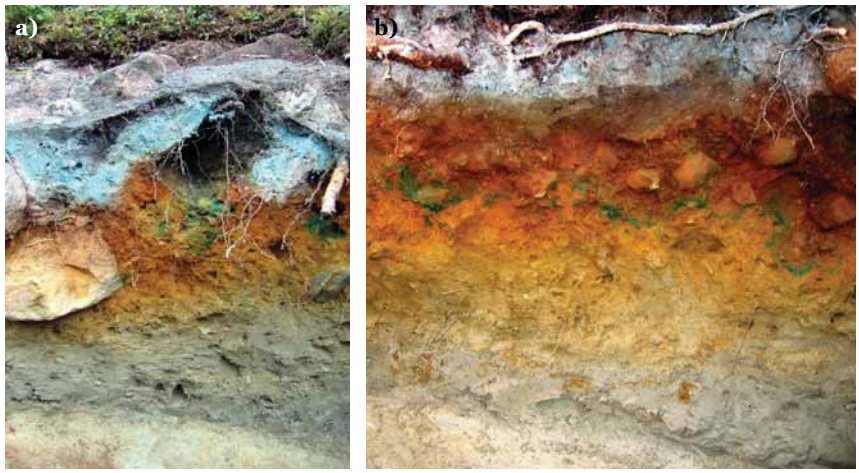

Figure 22. A vertical cross-section of dyed, unsaturated soil (a), and a cross-section of saturated soil, where the dye flows downhill above the water table (b). In (b), the dye pulse is flowing straight out of the picture.

In the uppermost E horizon, the dye is observed in about 90 % of the soil mass on average (Figure 22 a). The top of the horizon is fully coloured and near the B horizon the colouration drops to about 80 %. The colour spreads fairly uniformly in the loose soil mass, as compared to the spreading in the deeper layers. However, there are small areas within the B horizon that are distinctly colourless. The dye was found to accumulate around, and in particular underneath stones: The fourteen stones, that were found in the B horizon and had a minimum diameter of 5 cm, had dark blue hue underneath. Roots were found all over the E horizon, also around the stone surfaces, but no clear colour accumulation especially in the vicinity of live roots was detected.

In the B horizon, the dye covers about 50 % of the soil mass on average. The dye coverage is as high as 80 % in the upper half of the horizon, but the coverage reduces rapidly in the lower half. The coloured patches are clearly defined in the whole horizon. Eleven stones were removed in the horizontal slicing, half of which had dye accumulated below. Some of the stones had even distinct flow stripes on their surfaces. In the horizontal cut, the B horizon had altogether eight coloured patches with a cross-sectional area varying from 1 to 50 cm^2. Patches related to stones were rounder than those related only to roots. Roots were however found especially below the stones, where the dye, as well as water and nutrients accumulate.

In the BC horizon, the darkness of the colour starts to fade more and the boundaries of the coloured patches are blurred. In the upper reaches of the BC horizon the dye covers only about 10 % of the soil mass, and near the C horizon no colour is found anymore. In the horizontal crosscut, the upper reaches of

the BC horizon had six colour patches of size 1 to 10 cm^2. It is to be noted, that the E horizon extended deep inside the BC zone at one coloured point, and this extension brought the dye solution into the BC zone.

In comparison to the patchy dye pattern in the unsaturated soil, the dye leaves behind a continuous plane above saturated zone (Figure 22 b). Since the hydraulic conductivity of pores of all sizes grows as the soil saturates, the more continuous flow line can be created above the phreatic water table. In Figure 22 b, the line-type dye front is flowing straight towards, out from the picture. The unevenness of the line is due to heterogeneity in the grain and pore structure of soil, and due to the small-scale variability in the soil moisture. The vertical cross-section of Figure 22 is located 30 cm downslope from the dye source. The dyed flow plane fades away gradually downhill, and the last traces of the dye were detected at a distance of 150 cm from the source.

Examples of the continuity of the dye above the water table at different distances from the source are shown in Figure 23. As noted in Chapter 3.1.2, no dye was found at a distance of 150 cm or further away from the source, but at a distance of 120 cm (Figure 23 a), thirteen stripes, 2-4 cm wide, were found within the width of the 100 cm wide dye source. At a 60 cm distance (Figure 23 b), half of the 100 cm dye source line was discontinuously coloured. At the zero distance (Figure 23 c) the coloured line covered the full 100 cm width and was continuous. When flowing downhill, the dye did not notably spread beyond the original width of 100 cm. However, the dye plane was very curly due to the heterogeneity of the soil properties and moisture conditions.

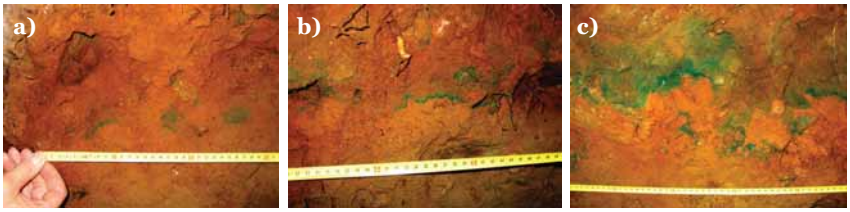

Figure 23. Continuity of the dye pulse at a distance of 120 cm (a), 60 cm (b), and 0 cm (c) from the line-type dye source in saturated soil. In the vertical cross-cut pictures, the dye pulse is flowing straight out of the picture.

Visible amounts of the dye were found in the E horizon as far from the dye source as in the B horizon. At a distance of 90 cm, for instance, as much as 90 % of the E horizon was weakly coloured. Since the depth of saturation was lowered to the B horizon before the dye pulse was sent downslope, dye detected in the E horizon indicates that lateral flow also occurred to some extent in the unsaturated E horizon. However, the E horizon was very wet. Based on the mean soil moisture characteristic data (Chapter 2.3.2), the

degree of saturation was 92 % on average, when the phreatic water table was at the boundary between the E and B horizons at a depth of 10 cm. It is noteworthy that right under the hole where the dye solution was poured, only half of the E horizon was coloured, because the pulse set off converting directly to the lateral direction.

3.2.2 Types of preferential flow paths

Types of preferential flow paths can be visually and qualitatively assessed from the photo material of the dye tracer experiments. In unsaturated conditions, three types of preferential flow paths are identified from the dyed soil profiles. The most distinct ones are stone surfaces (Figure 24). Surfaces of stones of all sizes were coloured in all soil horizons where the dye was found. A closer look at the stone surfaces inside the soil revealed large empty spaces around the stones. As noted in 3.2.1, the colour reaches the same depth as roots and big stones, but also about the same depth as soil frost, which can be estimated to reach a depth of about 50 cm from the soil surface, based on the hydrological yearbook for Finland (e.g. Hyvärinen 1994).

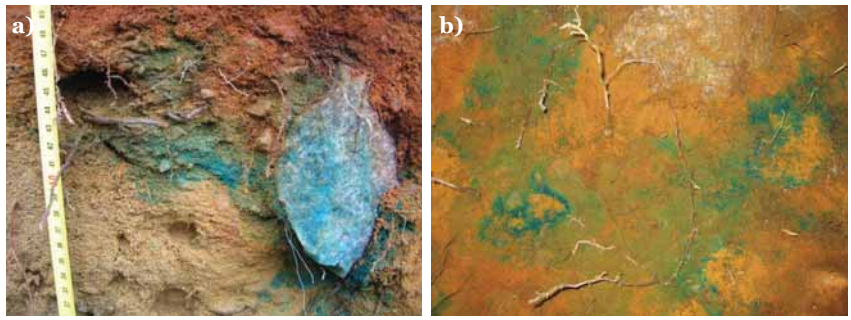

Figure 24. In the B horizon, the colour accumulates especially to stone surfaces (vertical cross section) (a), leaving dark blue circles around them (horizontal cross section) (b).

Together with the stone surfaces, areas with different grain and pore sizes form important flow routes for water and solutes (Figure 25 a). In addition, one larger decayed root hole that had delivered dye solution, was detected in the site (Figure 25 b). This implies to the possibility of empty root holes functioning as preferential flow paths. The role of live roots in preferential flow remains more questionable, since the soil around live roots was not systematically coloured. It is probable that coloured areas related to different grain and pore sizes contain live or decayed roots that are not visible to the naked eye but contribute to the macropore flow. Nonetheless, the only clear connection between the visible roots and the blue dye is that both of them

extend to same depth. The amount of roots and dye also reduce similarly with depth.

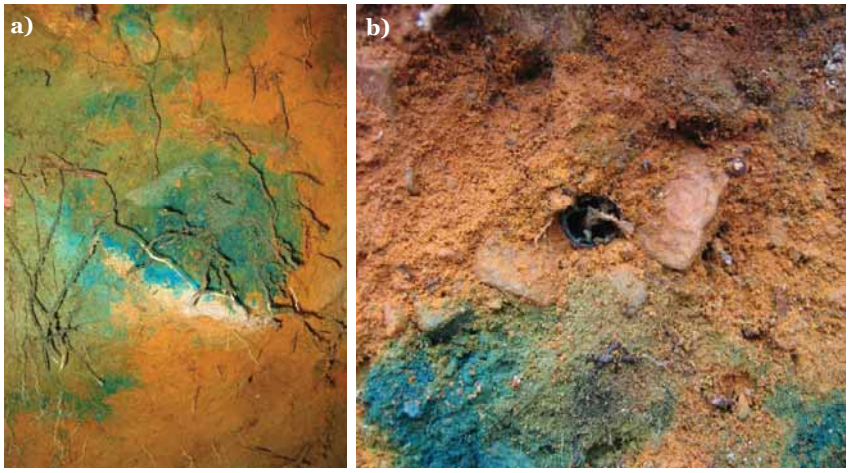

Figure 25. Colour accumulation due to grain and pore size alterations in a vertical cross-section in the B horizon (a), and a 1 cm wide decayed root hole with traces of blue dye inside in the B horizon (b).

3.3 Discussion

Dyes are valuable tracers to visualize flow patterns and pathways in the subsurface (Flury and Wai 2003). In this study, dye tracer experiments were able to visualize the infiltration into unsaturated soil, and to visualize the lateral flow downslope above the phreatic table, and in the capillary fringe zone in saturated conditions. The dye tracer studies were also able to give an indication of the types of the preferential flowroutes and to elaborate the information on the soil physical properties (cf. Chapter 2.2). In general, the dye accumulation was related to changes in granularity, porosity and soil moisture conditions on a small scale, whereas on a larger scale the dye stained the voids around stones and boulders. The visualization of flow patterns and pathways with a dye in the highly heterogeneous forest soil, and in different moisture conditions, gives valuable insight into the complex processes of subsurface runoff generation.

When poured into the variably unsaturated soil, the dye exposed a heterogeneous flow pattern and soil structure with various preferential flowroutes. Due to variation in the vertical extent of the different flowpaths, the lower boundary of the wetted zone is very irregular after pouring the dye solution (Aubertin 1971). In addition to the irrigation intensity, the initial soil moisture content, the duration of the irrigation and the saturated hydraulic

conductivity of the matrix control the occurrence of macropore flow (Jarvis 2007). In this study, the dye spread fairly uniformly in the loose soil material in the E horizon, even though the soil analysis showed a great heterogeneity in grain sizes and water retention properties in the uppermost soil horizons (Chapter 2.2.2, 2.3.2). This indicates that the E horizon contains a well connected macropore network. In the B horizon, the dye pattern was patchy and last traces of dye were found in the BC zone. This indicates that the C horizon does not contain remarkable amounts of preferential routes. This assumption is supported by the water retention data that also indicates a minor macropore fraction for the C horizon (Chapter 2.3.4, Figure 19). Thus, the hydraulic conductivity of the lower half of the dry soil profile is so low that the dye cannot infiltrate beyond the BC horizon.

There are additional factors other than the presence of macropores that prevent the dye from reaching the C horizon in the unsaturated soil. The B horizon adsorbs dye more efficiently than the other soil horizons due to its geochemical properties, and weakening of the colour intensity below the B horizon is partly due to this adsorption, as the dye infiltrates down through the retarding B horizon. Also, coarse textured soils usually wet up fully (Aubertin 1971), suggesting that the dye solution poured into the soil may saturate the soil matrix of the upper soil horizons, and the amount and velocity of the dye solution flowing down into the C horizon is rather small. In general, the dye poured into the unsaturated soil illustrated not just the flowpaths but also the interplay between macro- and micropores in the different soil horizons: the amount of dye detected at each depth gives an indication of how well the macropores are able to moisten the soil in general rather than a direct indication of the amount of the macropores.

In saturated soil, a continuous, dark dye trace was found above the water table in the B horizon as the dye pulse flowed downslope. In addition, most of the E horizon was weakly coloured as far as about 100 cm horizonal distance from the dye source. The dark and clear dye line above the water table visualise how the vast majority of lateral flow occurs near the water table, whereas the faint stains above the water table reveal that fast, lateral flow also occurs in some extent above the water table in soil with a saturation degree of about 90 %. The finding that in the B horizon the infiltration pattern was patchy in unsaturated soil, but rather long and continuous in saturated soil, supports the assumption that macropores have a tendency to self-organize into larger preferential flow systems when the soil saturates, even though individual macropore segments generally are less than 50 cm in length (Sidle et al. 2001). The dye tracer experiments of this study therefore also support the conception that

macropores form the basis of a backbone for lateral preferential flow formation in forested slopes underlain by bedrock or till (Sidle et al. 2001).

Beven and Germann (1982) group macropores on the basis of morphology to pores formed by the soil fauna, pores formed by plant roots, cracks and fissures, and natural soil pipes. Reflected against this grouping, the dye tracer experiments of this study were able to reveal pores formed by plant roots and natural soil pipes in the Kangaslampi soil. Natural soil pipes form because of erosive action of subsurface flows (Zaslavsky and Kasiff 1965 after Beven and Germann 1982) and the voids around, and specifically below the stone surfaces can be considered to be a result of subsurface erosion, in addition to the effect of soil frost on the soil around the stones. The decayed root hole detected in the B horizon, with a visible bark left around the soil pipe, is a clear indication of a pore formed by plant roots. The bark of tree roots sometimes resists decay longer than the xylem, and a hose type of macropore is formed, partially sealed by the bark (Gaiser 1952 and Aubertin 1971 after Beven and Germann 1982). The role of live roots was found uncertain as no systematic dye accumulation was found in the vicinity of live roots. In addition, Beven and Germann (1982) note that the distinction between pores formed by live and decayed root holes may be hard to make, as there is a tendency for new roots to follow the channels of previous roots.

Preferential flowroutes that were considered to be grain and pore size alterations in this study, are probably at least partly related to root channels. Some are related to live roots and some to decayed roots that may not be visible. The physical entrance and expansion of a root in the soil compresses the soil adjacent to it and locally changes the porosity and bulk density (Aubertin 1971). When the root decayes, areas of lower density and higher porosity, or even a clear soil pipe remains in soil. Roots channels form a network of relatively large, continuous, interconnected, open or partially filled channels that serve as pathways for the rapid movement of free water into and through the forest soil profiles. Channels related to decayed root holes may comprise up to at least 35 % of the soil volume, with a rapid decrease with depth (Aubertin 1971). Thus, the preferential flowroutes of the Kangaslampi till are due to roots combined with the soil textural properties and soil formation under soil frost and erosive action.

Even though no visible signs of animal burrows were detected in the dyed soil profiles, the soil fauna may also have an effect on the flowpath formation. Earthworms are the most conspicuous group of animals in most forested soils (Aubertin 1971) and may partly explain the dye accumulation that was linked with grain and pore size alterations in this study. In tile-drained, clay fields

earthworm burrows and cracks have been found crucial for infiltration of water and for formation of drain flow (e.g. Shipitalo et al. 2004). Finally, trunks of trees also form preferential flowpahts for water and solutes (e.g. Johnson and Lehmann 2006). Even though the dye tracer experiments of this study did not reveal the stemflow into soil, as the study plots could not be situated in the vicinity of trees, stemflow and the resulting flow along roots is considered to contribute to preferential flow also in the Kangaslampi slope.

In respect to modelling fast subsurface flow and conservative transport in the slope in this study, the dye tracer experiments emphasize the duality of the soil structure and flow paths as well as the pore size distribution changing with depth. The dye tracer experiments imply that in particular in unsaturated soil and in changing moisture conditions, the soil pore space should be considered two separate storages: preferential flow routes and soil matrix. This is important especially for the uppermost 50 cm of the soil profile. For the subsoil, a one pore domain description can more likely be adequate. The amount, size and conductivity of macropores in the subsoil are at least so low that the dye adsorbs to the soil particles before reaching the subsoil. The dye tracer experiments also imply that the amount of fast flow routes reduces in a non-linear manner with depth, and fast, lateral flow also occurs even though the soil is not fully saturated. Considering the amount of the dye solution poured into to the unsaturated soil and the fact that no dye was detected in the C horizon, the exchange of water and solutes in the upper soil horizons is fast, since the preferential flowroutes also wet up the soil matrix in the upper soil horizons and the water is not just bypassing into the deeper soil horizons.

4 Ion tracer experiment

4.1 Methods

The ion tracer experiment aimed at capturing a subsurface stormflow event in a tracer dataset. The experiment was to demonstrate in particular the lateral preferential flow during the event, and the data were to provide the basis for the development and analysis of a dual-permeability model. The experiment was based on observing the movement of a tracer plume downhill the study slope via observation wells that collect water from the soil profile during the different stages of the event. Sodium chloride was chosen as the tracer due to its affordability, ease of measurement and conservative nature in solute transport in till. Chloride could be detected in observation wells with a portable device for electrical conductivity, which enables an unlimited amount of measurements with arbitrarily controllable, temporal and spatial measurement intervals. Measurement of chloride concentrations in the wells during the experiment is discussed further in Chapter 4.1.1 and 4.1.3.

The chloride concentration of the irrigation solution, 700 mg/l, is of the same magnitude than the concentrations used in reference studies (e.g. Buttle and McDonald 2002, Tsuboyama et al. 1994). Compared to the background concentration in the soil water in the area, the concentration used in this study is 32-fold (cf. Chapter 4.1.1). Chloride is commonly used in studying preferential flow in soils, since it is non-sorbed in soils (e.g. Allaire et al. 2009). Chloride is also not considered to be prone to chemical reactions in sandy mineral soils, making the transport conservative.

Sodium chloride increases, however, the density of water and high concentrations can affect the flow and transport velocity and mechanisms, as compared to natural soil water. A concentration of 3000 mg/l of sodium chloride, corresponding to 1820 mg/l of chloride, is considered a limit for groundwater studies, in order to prevent the flow from becoming density driven (Davis et al. 1980, in Käss 1998). The chloride concentration used in this study is 2.6 smaller than the limit, and the density of the solution is only about 0.1 % higher than the density of the natural soil water. Considering the fast flow processes of a stormflow event, additionally to the small density

difference between the tracer solution and the soil water, the effect of density on flow and solute transport was assumed to be negligible in this study.

4.1.1 Set up of the experimental field

The set up for the experiment consisted of an irrigation source for saturating the soil and sending a chloride pulse downslope, and a set of observation wells for measuring water levels and chloride concentrations along the slope during the different stages of the experiment (Figure 26). A line type irrigation source was chosen instead of irrigating the whole area to be able to study in particular the lateral movement of water and solutes. The irrigation line was created with a perforated plastic tube, which was 3.6 m long and located 20 cm above the soil surface. The tube was connected to a water tank that fed water to the tube by the force of gravity. The irrigation intensity was controlled with a tap that was installed in the connection hose between the irrigation tube and the tank.

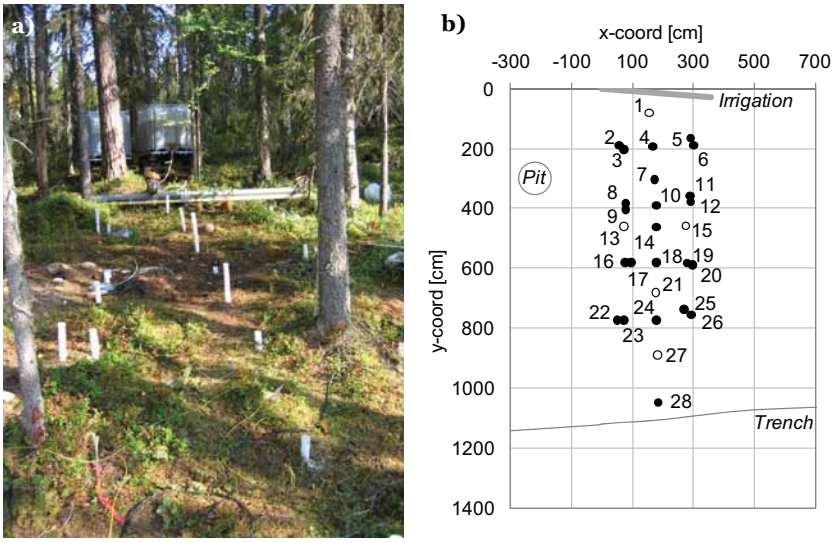

Figure 26. The sodium chloride experimental slope (a). The black dots on the map (b) represent well screens (WS) and the white dots are stand pipes (SP) that collect water only from the soil-bedrock interface.

The observation wells were laid out in a regular formation downhill from the line type irrigation source as shown in Figure 26. In this study, the term *well screen* (WS) is used for an observation well that collects water from the whole soil profile through its perforated walls, and the term *stand pipe* (SP) is used for an observation well that collects water only from the soil bedrock interface. The term *observation well* refers to both the well screens and the stand pipes. Well screens 2 and 3, 5 and 6, 8 and 9, etc. (Figure 26 b) were installed in soil

as pairs, close to each other for observing the small-scale variation in water levels and chloride concentrations that were expected due to the great heterogeneity of the soil properties. One well in each pair was equipped with a pressure sensor that was connected to a data logger recording the water levels in every fifteen seconds. Thus, continuous water level data are available from the regular grid of eight points. In all other wells, water level was measured with a portable device and the results were recorded manually in a data sheet. The measurement interval varied on the basis of observed changes in the water level. A side profile of the soil column with the observation wells along the middle line of the study slope and with the location of the irrigation source is presented in Figure 27.

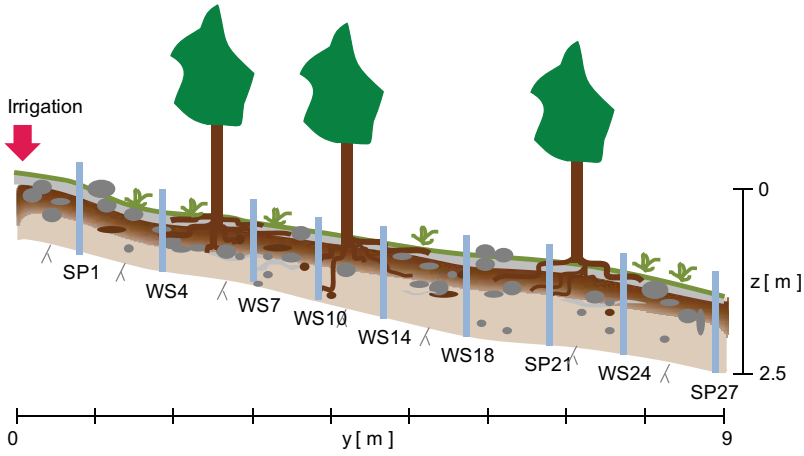

Figure 27. Side profile of the experimental slope, along the middle line of the observation well field that consists of stand pipes (SP) and well screens (WS).

The chloride concentrations were measured with a portable device for electrical conductivity. The sensor of the device was dropped to different depths in the water column in the wells during the experiment. The measurements revealed clear differences in the concentration levels at different depths. Stability of the depth distribution of concentrations in a well, as well as factors controlling the distribution were investigated during the experiment. Stability was tested by stirring the water column in a well with the sensor of the conductivity meter. The water column proved to be hard to mix, as a clear depth distribution prevailed in the wells even after stirring. The concentration values also returned to the same values within few minutes as recorded prior to the stirring. Systematic, density driven stratification with higher concentrations at the bottom of the wells was not observed, since higher concentrations were observed both in the upper and lower half of the water columns in the wells. Measurements at different depths rather indicated

that the depth distribution of the concentrations was affected by different flow conditions at different depths in soil, lateral throughflow and replacement of water in the wells, and mechanisms routing the water from soil into the wells.

As the water columns did not easily mix, electrical conductivity was marked down systematically from two depths. First, the conductivity was measured in the upper half of the water column, and then the sensor was dropped down slowly to the lower half of the column. Concentration values recorded in the lower half of an observation well were considered to correspond roughly to the water flowing in the C horizon, and values recorded in the upper half of an observation well to water flowing mainly in the E, B, and BC horizons, i.e. the horizons that contain considerable amounts of preferential flowpaths (cf. Chapter 2.3.4 and 3.3). The representativeness of the chloride concentrations measured at different depths, as well as the factors behind the depth distributions are further discussed in e.g. Chapters 4.2.1, 4.2.2, 4.3.1, 5.1.8, 5.3.3.

The linear dependence between the chloride concentration and the electrical conductivity (Figure 28) was determined in the laboratory using a set of water samples that were collected from the wells in the field. In the laboratory, the electrical conductivity of the samples was determined first, and thereafter the chloride concentration was determined by titration.

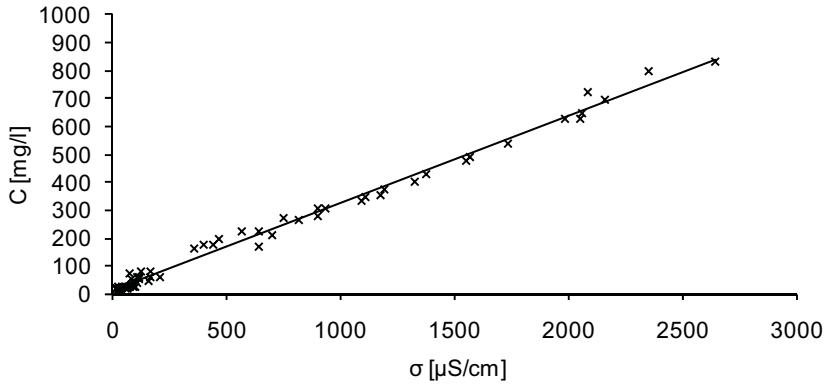

Figure 28. Relation between chloride concentration *C* and electrical conductivity *σ*.

The resulting equation for the electrical conductivity σ [µS/cm] and the chloride concentration C [mg/l] is:

$$C = 0.31\sigma + 13.0 \quad . \qquad (3)$$

The 95 % confidence interval for the slope is 0.306-0.313 and for the constant term 5.86-20.03. The overall accuracy of the equation is very good as the coefficient of determination is as high as 0.99. But as can be seen from the fairly broad confidence interval of the intercept term, the applicability of the equation is lowest near background concentrations. This inaccuracy is due to differences in the ion composition in different water samples, as several ions contribute to the total conductivity of the natural soil water. Thus, the background chloride concentration in the soil water was assessed directly from the titrated water samples, and the equation was used only for higher concentrations. The average and median background chloride concentration values were both 22 mg/l, and the background concentration varied between 17 and 27 mg/l.

As noted above, two types of observation wells were used for measuring water levels and conductivities. The black dots in Figure 26 b represent ordinary well screens with an outside diameter of 40 mm and inside diameter of 31 mm. The screen spacing in the wells was 2 mm and the width of one screen was 0.3 mm. To restrict the accumulation of fine particles to the wells, the wells were covered with a filter fabric from outside. However, lateral flow of water and solutes was observed to occur through the wells. The inside diameter of the screens, 0.3 mm, corresponds for instance to a superpore, defined by McIntyre (1974, in Perret et al. 1999, cf. Chapter 2.3.4).

The five white dots in Figure 26 b are stand pipes that collect water only from the soil-bedrock interface. They were included in the study to observe whether there is a highly conducting soil layer above the bedrock. To check whether salt water was flowing at the interface, water was first removed from the pipe, and then the electrical conductivity of the new water rising to the tube was measured. There was a risk that water would flow into the stand pipes along the outside walls of the pipes from upper soil layers. Thus, the origin of the water rising to the pipes was assessed by comparing the measured conductivity values with the conductivity values of adjacent well screens. The data on the stand pipes were also used in determining the saturated hydraulic conductivity of subsoil with the Piezometer method (Luthin and Kirkham 1949, in Amoozegar 2002). The Piezometer method is presented in Chapter 4.1.4.

All the observation wells were drilled into the soil mechanically. Trees and boulders inside the soil profile controlled the exact spots where the drilling was possible, whereupon slight distortion exists in the grid regularity. Altogether 28 wells were installed in the field and they covered an area of about 3.5x10 m^2. The maximum chloride peak was expected to follow the centre line of the field despite the fact that the bedrock sloped slightly to the

right and the soil surface to the left (Figure 29). Also, the bedrock surface was fairly lumpy, and the thickness of the soil profile and different soil horizons varied within small distances.

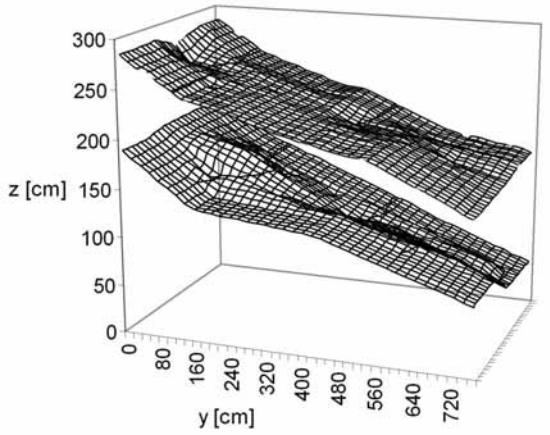

Figure 29. Topography of the soil surface and bedrock within the sodium chloride experimental area.

4.1.2 Initial state

Soil moisture at different depths prior to the experiments was determined from the soil core samples for grain size, bulk density, water retention and saturated hydraulic conductivity analyses (Chapter 2.2 and 2.3). Samples were collected on September 5, 2005 just before beginning the experiments. Based on altogether 25 samples from each soil horizon, the degree of saturation was 25-33 % in the E, 38-45 % in the B, 27-33 % in the BC, and 33-39 % in the C horizon. No water table was present above the bedrock. Uncertainty related to determining the initial moisture conditions was high due to the various methods related to determining the moisture from the different samples and due the large deviation in results.

The lowest estimates for the soil moisture were about about 3 % in the E and C horizons, and about 5 % in the B and BC horizons, whereas the highest estimates approached the total porosity in each horizon. The highest estimates were left out due to the fact that some samples were not packed in a proper manner and had moistened in the rain during transportation and storage. The lowest estimates were left out based on the fact that at various soil moisture stations in forested sandy tills in Finland, moisture values under 5 % have not been recorded (e.g. Hänninen and Penttinen 2006, Hänninen et al. 2003).

Weather and runoff data available from the area (Figure 30 and 31) support the estimates for the initial state of soil moisture and the degree of saturation, even though the values obtained remain uncertain. In general, year 2005 was warm and dry in eastern Finland compared to the long term mean values, and water levels as well as soil moisture values dropped substantially during the summer and autumn (Finnish Environment Institute 2006). The data on the Kangaslampi area one month before the experiments reveal that air temperatures in August rose above 20 °C on eleven days, and 24 °C was exceeded two times, with a maximum temperature of over 28 °C (Figure 30). Even at the beginning of September, just before the experiments, the temperature rose up to 26 °C. Evaporation measurements are not available from the study area. Based on other available weather data (Figure 30 and 31), evaporation as well as water uptake by plants was high compared to the rainfall amounts during the summer of 2005.

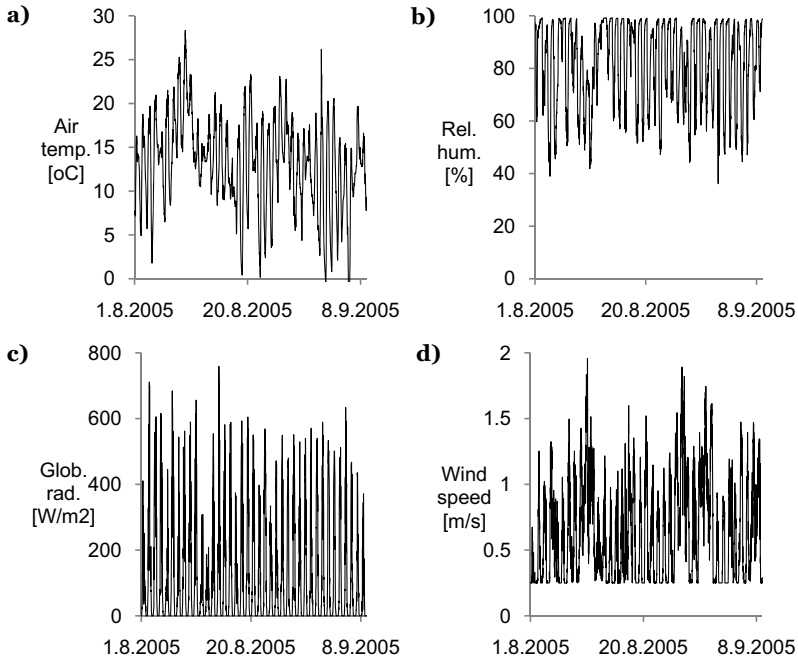

Figure 30. Air temperature (a), relative humidity (b), global radiation (c) and wind speed (d) recorded at the Kangasvaara weather station every 20 minutes in August 2005.

Precipitation in the area was 78 mm in August 2005 and the area had had no rain in four days before the experiments (Figure 31). Intensities of the rainfall events in August had been so low that presumably no water had entered the

mineral soil layers. Prior to the experiments, stream runoff rate in the area was below 1 l/s/km^2. A comparison with long term data reveals that stream runoff rates up to about 195 and 134 l/s/km^2 are recorded in Kangaslampi and Kangasvaara, respectively, during wintertime, and during summertime maximum rates of about 35 and 21 l/s/km^2 are typical (Finér et al. 1997).

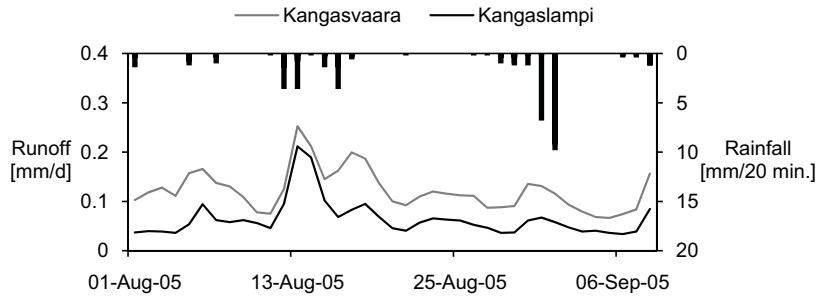

Figure 31. Rainfall and runoff in Kangaslampi and Kangasvaara in August 2005.

4.1.3 Experiment on September 6, 2005

The experiment consisted of two parts. First, one day prior to the sodium chloride experiment on September 5, 2005, an initial irrigation with pure water took place to increase the moisture content of the uppermost section of the experimental slope. Letting the upper section of the slope moisten before the tracer experiment, a sharp moisture gradient was formed in the slope so that the lower section of the slope remained at the initial moisture status (Figure 32). Mechanisms behind the subsurface stormflow event and the preferential flow in the slope would not have become as evident, if the whole slope was at similar moisture conditions in the beginning. This kind of an experiment was expected to reveal more about the fast subsurface flow and water exchange between different pore domains, by proving versatile water table and solute concentration data in the observation wells, as the tracer plume travels downslope first in wet and then in dry soil.

To create saturated conditions in the soil profile during the dry summer season, a large amount of water was needed compared to natural rainfall amounts. During the initial irrigation, soil was doused with 1.5 m^3 of pure water. Water was observed in wells 1, 3, 4, 5, 6 and 7 (Figure 26 b). In wells 1 and 4 water level rose up to the E horizon, in the other wells to the BC or C horizon. If the irrigation were thought to fall onto the nearly 15 m^2 area, where saturation was observed, the irrigation of 1500 l would correspond to a rainfall of ca. 100 mm. The resulting moisture status at the beginning of the

experiment the next day was estimated using observations made during the preliminary irrigation, and water retention data and soil moisture data available from the soil analysis.

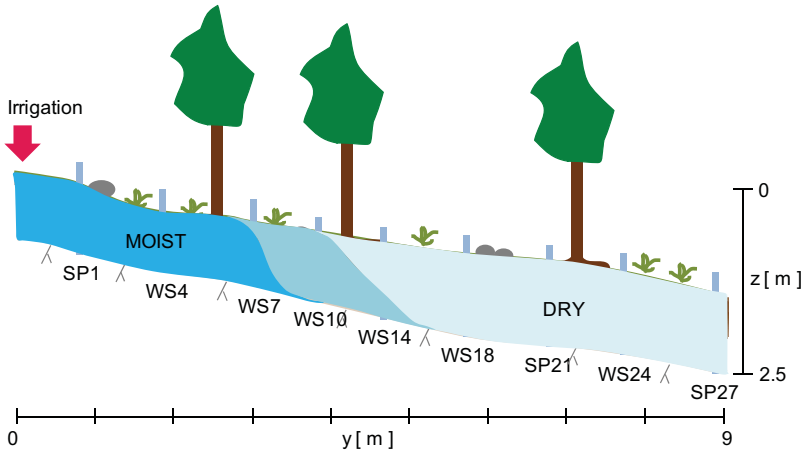

Figure 32. Moisture status of the experimental slope at the beginning of the tracer irrigation. During the initial irrigation with pure water a day before, saturation reached WS7, but not WS10. Therefore, a sharp moisture gradient was estimated to form between WS7 and WS10. At the moist, upper section of the slope, largest pores are emptied of water, but the smallest pores are near or at saturation. At the dry, lower slope section, soil is at the initial moisture status.

The slope was estimated to be at least in the field capacity at the width of the irrigation tube and at an average length of three metres in the downslope direction (the moist section in Figure 32). Along the middle line of the experimental field the soil was estimated to be wet until 3.5 m, and at the sides until 2.5 m (Figure 26 b, Figure 32). In the moist, upper section of the slope, a pressure head from -50 cm in the C horizon to -100 cm in the E horizon was estimated to prevail at the lowest, and from -20 cm in the C horizon to -30 in the E horizon was estimated to prevail at the highest. This corresponds to a degree of saturation of 0.5-0.78 in the C, 0.7-0.88 in the BC, 0.67-0.91 in the B and 0.84-0.96 in the E horizon. Around the moistened area, the moisture content was estimated to drop abruptly, within a distance of 1-3 m to the moisture content preceding the irrigation, to a degree of saturation of 0.25-0.45 in the soil profile (Chapter 4.1.2).

The irrigation of the actual tracer experiment on September 6, 2005 is shown in Figure 33. The figure also includes an example of the response data available from a well screen. The small notches in the water level time series in the observation well are the time points when the irrigation was stopped for

about a minute to change the water tank (Figure 33 b). The total duration of the irrigation was 3 hours 30 minutes and the total irrigation amount was 2066 l. Chloride concentrations together with the water levels were observed in the well field for seven hours. When the measuring team returned to the field the next day, no water was found in the wells.

As the irrigation water was spread on an area of about 4.0 m x 0.5 m below the irrigation tube, the average infiltration into the soil within this wet area was 4.9 mm/min. The total amount of irrigation, in terms of rainfall to the wet area was 1033 mm, which is nearly double the amount of rain that would fall on to that area during a whole year. If the irrigation is thought to represent a rain that falls onto the whole moistened area of nearly 50 m^2, the average rainfall intensity would be 0.2 mm/min, and the total rainfall amount 41 mm – a rainfall event that occurs approximately once in five years (e.g. Hyvärinen 1994).

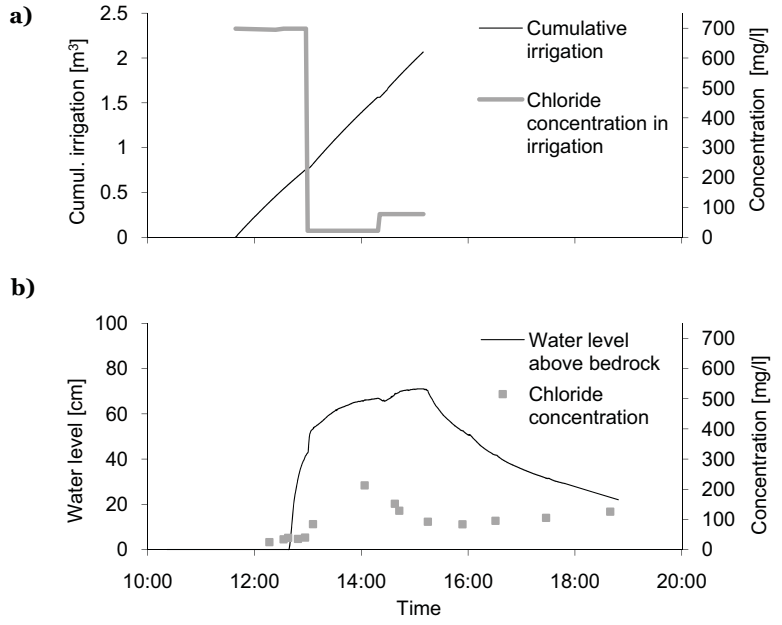

Figure 33. Cumulative irrigation through the perforated pipe (a) and an example of the observed response in a well screen (b).

To demonstrate the lateral flow at different depths in soil, the irrigation water contained chloride from the very beginning. 0.8 m^3 of chloride solution of 700 mg/l, i.e. an approximately 32-fold concentration compared to the natural chloride concentration in the soil water, was irrigated into the soil during one hour and 20 minutes, after which the irrigation was continued with pure water

for two hours and 10 minutes. However, the last 0.5 m^3 of the irrigation water contained slightly increased amounts of chloride since the irrigation tank contained residues of the first chloride solution. As noted in the beginning of Chapter 4.1, the chloride concentration of 700 mg/l is of the same magnitude as the concentrations used in reference studies (e.g. Buttle and McDonald 2002, Tsuboyama et al. 1994).

4.1.4 Inverse modelling of saturated hydraulic conductivity

Water level data available from the chloride tracer experiment can be used in several ways for assessing the magnitude of the saturated hydraulic conductivity in the slope. First, a general estimate of the average saturated hydraulic conductivity of the whole soil profile was calculated directly from Darcy's law, by solving the law for conductivity K [LT^{-1}]:

$$K_S = -\frac{Q\Delta L}{A\Delta H} = -\frac{V\Delta L}{tA\Delta H} \quad . \tag{4}$$

The flow rate Q [L^3T^{-1}] was set equal to the total irrigation volume V [L^3] with duration t [T], the flow distance ΔL [L] to the mean distance that the downslope travelling saturation front reached during this time, area A [L^2] to the product of the mean width and height of the saturation front, and ΔH [L] to the mean head difference of the front within the saturated area. The dimensions related to the saturation front were estimated from the water level data of the well screens.

Second, estimates of the saturated hydraulic conductivity of the different soil horizons were calculated using the recession data on the observation wells at the middle line of the experimental field (Figure 26 b, Figure 27). Since the flow was regarded as one-dimensional between these wells, a simple groundwater model (Equation 5) was fitted to the data of three consecutive wells (Figure 34) and the saturated hydraulic conductivity was inversely solved for each soil horizon. The wells used in the calculation were well screens 1, 4, and 10 (Figure 27). Since the uppermost well, well 1, was located near the irrigation source, it was assumed that only minor amounts of new water flowed into the well during the recession period, after the irrigation was stopped.

The equation used for the inverse model was (e.g. Spitz and Moreno 1996):

$$S\frac{\partial H}{\partial t} = \frac{\partial}{\partial y}\left(T\frac{\partial H}{\partial y}\right) \quad , \tag{5}$$

where S [-] is the storage coefficient, H [L] is the hydraulic head, t [T] is the time, y [L] is the distance in the direction of the slope, and T [L^2T^{-1}] is the transmissivity, i.e. a product of the saturated hydraulic conductivity K [LT^{-1}] and the thickness of the saturated soil profile b [L].

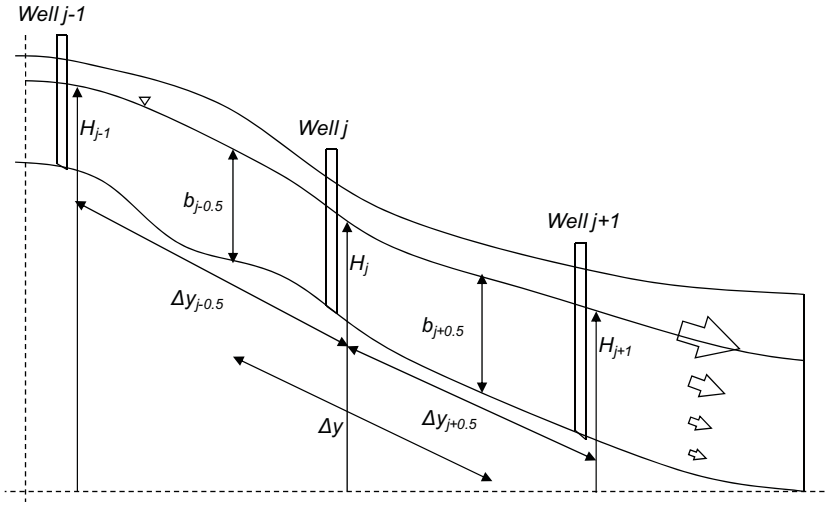

Figure 34. Schematic of a three well system for inverse, 1D-modelling of saturated hydraulic conductivity.

Equation 5 was implicitly solved for the middle well j in the y direction (cf. Figure 34):

$$H_j^{t+1} = \frac{H_j^t + \frac{\Delta t}{\Delta y}\left(\frac{Kb_{j+0.5}}{S}\frac{H_{j+1}^{t+1}}{\Delta y_{j+0.5}} + \frac{Kb_{j-0.5}}{S}\frac{H_{j-1}^{t+1}}{\Delta y_{j-0.5}}\right)}{\left[1 + \frac{\Delta t}{\Delta y}\left(\frac{Kb_{j+0.5}}{S}\frac{1}{\Delta y_{j+0.5}} + \frac{Kb_{j-0.5}}{S}\frac{1}{\Delta y_{j-0.5}}\right)\right]} \quad . \qquad (6)$$

As the hydraulic heads H in wells *(j-1)* and *(j+1)* were considered to be known boundaries, saturated hydraulic conductivity of the middle well *(j)* could be solved using the method of least squares, by setting the calculated hydraulic head for well *(j)* equal to the measured head. To obtain estimates for the saturated hydraulic conductivity of the different soil horizons, the term Kb/S was considered a sum of subterms of all the horizons under saturation. For instance, when the water table was at the level of the interface between the B and BC horizons, the term was calculated by summing $K_{BC}b_{BC}/S_{BC}$ and K_Cb_C/S_C together. Values for the storage coefficients were estimated based on the literature (e.g. Airaksinen 1978), water retention data (Chapter 2.3.2), and porosity data (Chapter 2.3.4).

In an unconfined aquifer, the storage coefficient corresponds directly to the specific yield. The specific yield, for its part, is considered to be as great as, or smaller than the effective porosity (for the definition of effective porosity see Chapter 2.3.4). In Brassington (1998), an indicative value of 16 % is given for the specific yield of sandy and gravelly till, and 6 % for silty till. As for the fraction of the total porosity producing specific yield, an 18 % share is given for till (Brassington 1998). Dunn et al. (2007) received a larger fraction, 40 %, for their conceptual flow and transport model, when testing different hypotheses on the significance of the different hydrological processes and geographic controls in determining the mean residence time in the forested catchment of Maimai in New Zealand. It is to be noted that Dunn et al. (2007) use the term *effective porosity* for the fraction of the total porosity that contributes actively to flow. Thus, the concept of effective porosity used by Dunn et al. (2007) is not related to water retention data similarly, as in this study.

In this study, general estimates presented above as well as estimates derived from the water retention data were used to for the storage coefficient. Water retention data were used to estimate the storage coefficient following the method adopted in the estimation of the macropore volume (Chapter 2.3.4). For instance, the limiting pore diameter of 50 µm was used to make a difference between storage pores, which do not contribute to flow in soil, and transmission pores that correspond to the storage coefficient (cf. Greenland 1977 after Perret et al. 1999). Without a clear relation between the macropores and the storage coefficient, the lowest estimate of the storage coefficient was calculated using the threshold diameter of 100 µm (e.g. Jongerius 1957 after Perret et al. 1999) for a macropore (Chapter 2.3.4).

Based on the different estimates of storage coefficients, the storage coefficient in the 1D-model of this study was given values from a minimum of about 13 % of the total porosity in the C horizon to a maximum of 50% of the total porosity in the E horizon. In all the applications, the storage coefficient decreased with depth, and the stone content was taken into account in the estimates. The range of variation for the storage coefficients are given in Table 4.

Table 4. Minimum, average and maximum of the storage coefficient *S* [%] used in the one-dimensional groundwater model.

Soil horizon	S_{min} *[%]*	S_{ave} *[%]*	S_{max} *[%]*
E	9.1	12.7	16.0
B	7.4	11.2	15.6
BC	4.5	8.5	15.0
C	3.8	6.9	12.7

The stand pipes of the chloride tracer experiment provided the third estimates for the saturated hydraulic conductivity, because the stand pipes can be considered as piezometers. As water was pumped out of the stand pipes to measure the chloride concentration of the water rising to the pipes, the velocity of the water level increase in the pipes was also recorded. The saturated hydraulic conductivity K_S [LT^{-1}] was then calculated with the *Piezometer method* of Luthin and Kirkham (1949), combined with Youngs (1968), as presented in Amoozegar (2002):

$$K_S = \pi r^2 \ln\left(\frac{z_n}{z_{n+1}}\right) \Big/ B\left(t_{n+1} - t_n\right) \quad , \qquad (7)$$

where z_n and z_{n+1} [L] are the water levels in the tube at the time steps n and $n+1$, respectively, r [L] is the radius of the tube, and the deviation $t_{n+1} - t_n$ [T] is the time required for the water table rise. B [L] is a tabulated constant whose value depends on the radius of the pipe and the thickness of the saturated soil profile (e.g. Amoozegar 2002). As no cavity was left below the stand pipes, the conductivity calculated with the Piezometer method corresponds, theoretically, mainly to the vertical component of the saturated hydraulic conductivity of the subsoil.

4.2 Results

4.2.1 Response of the observation wells to the tracer irrigation

During the seven-hour observation period from the beginning of the chloride irrigation on September 6, 2005, water reached two stand pipes, pipe 1 and pipe 15 (Figure 26 b), but the chloride tracer only pipe 1, located at a horizontal distance of 70 cm from the irrigation source. Considering the well screens, saturation reached 12 wells and increased chloride concentrations were observed in 10 wells. Measured water levels and chloride concentrations in the 12 well screens are presented in Figure 35. Each graph presents the data of one well, and the relative locations of the graphs in the double page correspond to the locations of the wells in the field (Figure 26 b).

Considering the water levels in Figure 35, the rapid rise of the levels in the observation wells demonstrates how the irrigation produces an almost vertical, downhill travelling saturation front. The data on the rise period also reveal a nearly exponential increase in the hydraulic conductivity, when the groundwater table reaches the E horizon. Despite the continuous, intensive

irrigation, the water table holds a constant level after reaching the E horizon, without producing any surface runoff (see e.g. WS4 and 7). Another sign of the high conductivities near the soil surface are the small notches in the water level series of wells 3 and 6, situated close to the irrigation source (see e.g. WS3 and 6 in Figure 35): When the irrigation was interrupted for changing the water tank for less than 30 s, water level in the well screens responded immediately to the stop.

In the wells on the sides of the experimental field, the water level rise is not as sharp as in the wells following the middle line downslope (cf. e.g. WS4 and 5). The moisture pulse spreads freely across the slope to the surrounding soil mass on the sides, but in the wells along the middle line, flow is mainly two-dimensional in the vertical direction z and in the downslope direction y. After the irrigation is stopped, the water table starts to withdraw and the moisture conditions in soil start to approach the field capacity. The data on the recession period reflect the hydraulic conductivity of the soil at different depths, and can be used in assessing the saturated hydraulic conductivity of the different soil horizons.

Considering the chloride concentrations, the highest values are recorded in the wells that follow the middle line downslope (WS4, 7, etc. in Figure 27, Figure 35). Concentrations near the magnitude of the irrigation solution are found as far as three metres from the source. The chloride concentrations in the middle line wells rise almost instantaneously to the concentration of irrigation solution due to the high preferential flow rates in soil. If the role of translatory flow – the flow that pushes old, chloride-free water from the soil matrix to the preferential flow routes and to the well screens – was more significant, the rise of the chloride concentration in the well screens would be more moderate. Instead, some of the irrigated water saturates the soil matrix while some of the water bypasses it. The middle line wells also react very rapidly to the change from salted water to fresh water.

The high concentrations and the fast changes in concentrations of the middle line wells (Figure 35) reveal that almost all water entering the wells is new water flowing in the preferential routes. In the wells on the sides of the experimental field, concentrations do not reach as high values, since the salt irrigation was changed into pure water before the water level had reached the highly conductive, upper soil horizons, and the proportion of translatory flow was therefore higher in the side line wells than in the middle wells. However, water observed in the wells around the whole experimental field is predominantly water flowing in the preferential flowroutes or in an active fraction of the soil pore space that contributes to fast runoff generation.

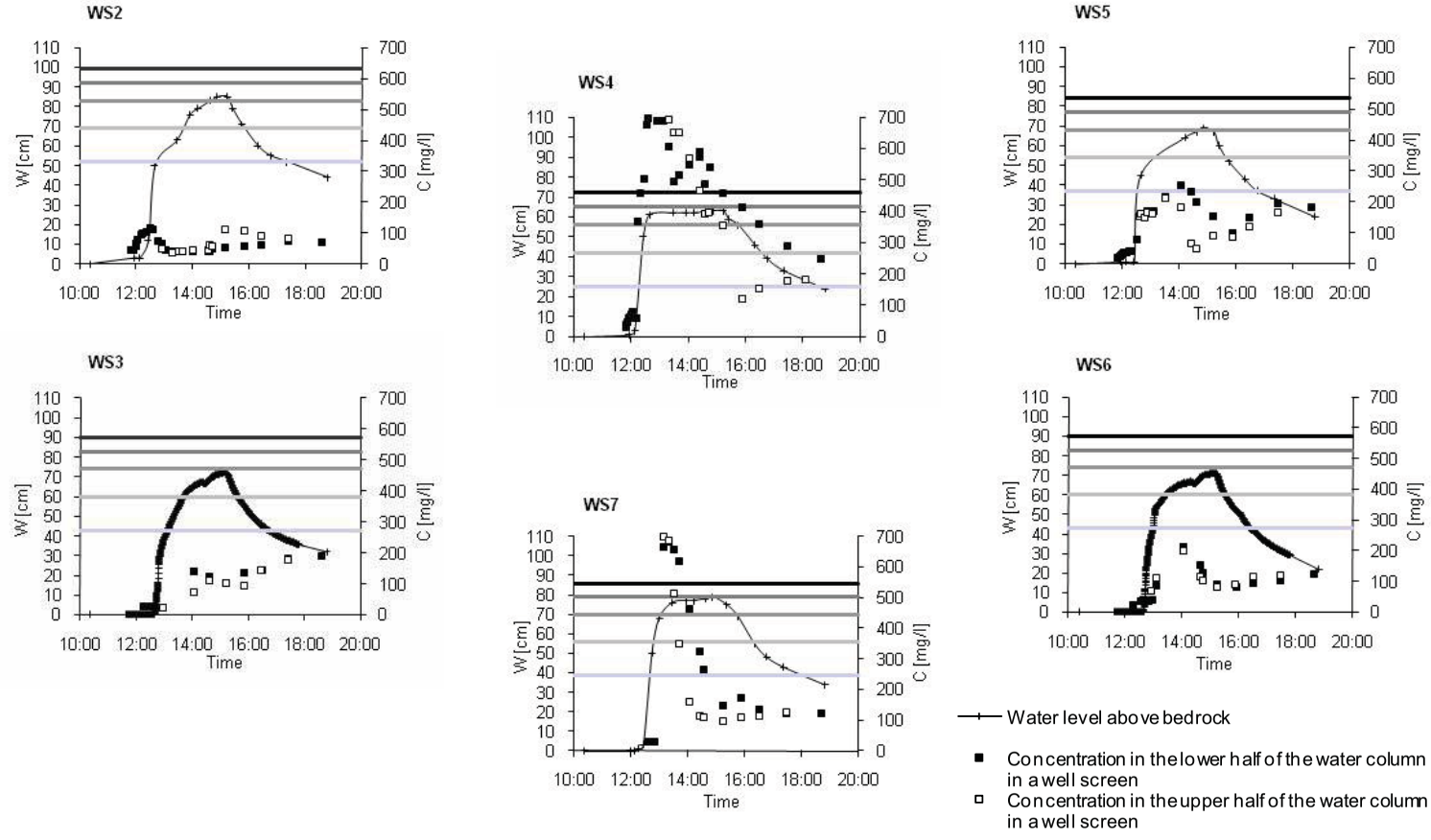
WS2
WS4
WS5
WS3
WS7
WS6
W [cm]
C [mg/l]
Time
10:00
12:00
14:00
16:00
18:00
20:00
Water level above bedrock
Concentration in the lower half of the water column in a well screen
Concentration in the upper half of the water column in a well screen

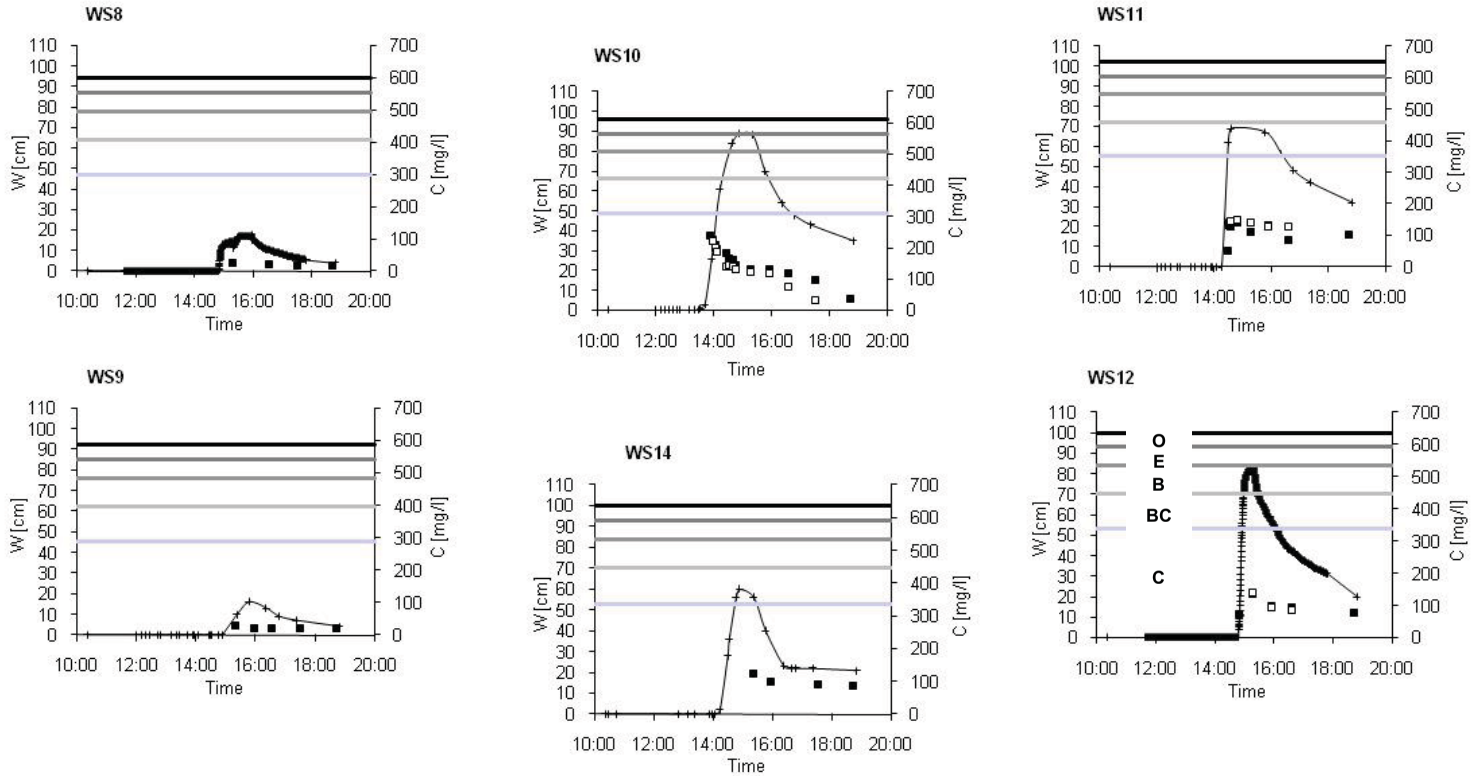

Figure 35. Water level *W* and chloride concentration *C* in the well screens *WS* in the ion tracer experiment of September 6, 2005. Water level zero corresponds to the bedrock, and the five, horizontal, grey-toned lines mark off the different soil horizons. The uppermost black line in each subfigure is the soil surface.

Considering further the response of the concentrations in the wells to the irrigation, the high concentration values as well as the fast changes in the values also demonstrate a fast replacement of water in the wells during the experiment. Thus, the concentration data provide an estimate for the coinciding concentration levels in the soil water, and in particular in the water of the preferential flowpaths around the wells, even if an exact correspondence is not plausible. As for the depth distribution of the concentrations, the data also provides valuable information: The data from two depths in the wells, i.e. from the upper and lower half of the water column, show clear differences in concentrations at different depths during the experiment (Figure 35).

As observed in the field during the experiments (Chapter 4.1.1), the depth distribution of the chloride concentration in a well did not easily mix, and was mainly affected by different flow conditions at different depths in soil, lateral throughflow and replacement of water in the wells, and mechanisms routing water from soil into the wells. Systematic, density driven stratification was not observed. The results (Figure 35) support the field observations, since higher concentrations are recorded both in the lower and upper half of the water column in the well screens. Concentrations recorded at the two depths give an indication of the concentrations in the surrounding soil water – measurements from the lower half of the water column being representative for the C horizon and measurements from the upper half of the water column being representative for the BC, B, and E horizons. However, the representativeness of the data is rather ambiguous after the irrigation is stopped, the water table starts to withdraw, and translatory flow processes start to deliver increasing amounts of old water into the well screens in relation to by-pass flow of new water. Accuracy and representativeness issues are further discussed in Chapter 4.2.2, 4.3.1, 5.1.8 and 5.3.3.

A closer look at the forms of the concentration time series (Figure 35) reveals that the wells generally exhibit three kinds of concentration patterns. Most of the wells (WS3, 4, 5, 6, 7, 11, 12 in Figure 35) exhibit a pattern containing a rising and a falling limb, followed by another rising limb in some of the wells (e.g. WS4 and 5 in Figure 35). The first rising limb is due to translatory flow and initiation of fast preferential flow: the irrigation water pushes away old, chloride-free water to the wells first, but chloride concentrations rise abruptly, as the soil saturates and the fast, preferential flow initiates in the macropore network. When the irrigation is changed into fresh water, concentrations start to dilute, which produces the falling limb. The fast dilution is due to preferential flow, as most of the water entering the wells originates directly from the irrigation. The slight concentration rise in some wells (e.g. WS5 and 6

in Figure 35) after ending the irrigation, results from the decrease of preferential flow rates. Salt has been stored into the soil matrix during the tracer irrigation, and the proportion of the matrix flow starts to rise in relation to preferential flow.

The second plume type is a continuously falling limb without a rise at the beginning of the series (wells 8, 9, 10, 14 in Figure 35). No chloride reached wells 8 and 9, and the slight dilution in the concentration in these wells is due to the low chloride concentration in the fresh water irrigation in relation to the background concentration in the natural soil water. Wells 10 and 14 received high amounts of chloride already in the first drops of water that entered these wells. The absence of a rising limb at the beginning of the series is explained by the initial moisture status. Wells are 10 and 14 are located farther off the irrigation source, and the preliminary irrigation a day before could not saturate the soil around these wells. In the downslope direction, the initial soil moisture at the beginning of the tracer irrigation drops abruptly around well 10 (Figure 32) and the small initial moisture status translates into remarkably smaller amounts of easily mobilizable old water that could contribute to translatory flow into wells 10 and 14.

The third plume type has two chloride peaks (well 2 in Figure 35). The first peak is reached already with a low water level, and the second occurs in the upper half of the water column just before the water level starts to fall after the irrigation is stopped. The double peak behaviour is related to a big stone that impedes the direct water flow from the irrigation source to the well screen. The first peak comes presumably via preferential routes below the stone (cf. Chapter 3.2.2). As the water level rises in the C and BC horizons, the role of translatory flow increases in proportion to bypass, preferential flow. However, as the water level has reached the B horizon with a remarkably higher macropore volume (cf. Chapter 2.3.4 Figure 19), the role of preferential flow starts to rise again, and the second peak concentration is due to preferential routes above the stone.

4.2.2 Lateral flow

The data recorded in the wells following the middle line downslope the experimental field (WS4, 7, 10, etc. in Figure 26 b, 27, 35) illustrate the lateral movement of the salt water front downhill, as the main flow direction follows the direction of the slope between these wells (cf. Chapter 4.2.1). Data from the middle line wells also represent the maximum migration downslope via preferential flowpaths. In Figure 36, estimates of the chloride concentrations

in the preferential flowpaths along the study slope, as interpolated from the data of the middle line wells, are presented for six different time points. In the first time point at 12:00, tracer irrigation has been running for 20 min. During this time, chloride has reached a distance of about 2.0 m from the irrigation source. Concentration levels of the magnitude of the irrigated solution are found at a distance of 1.0 m from the source.

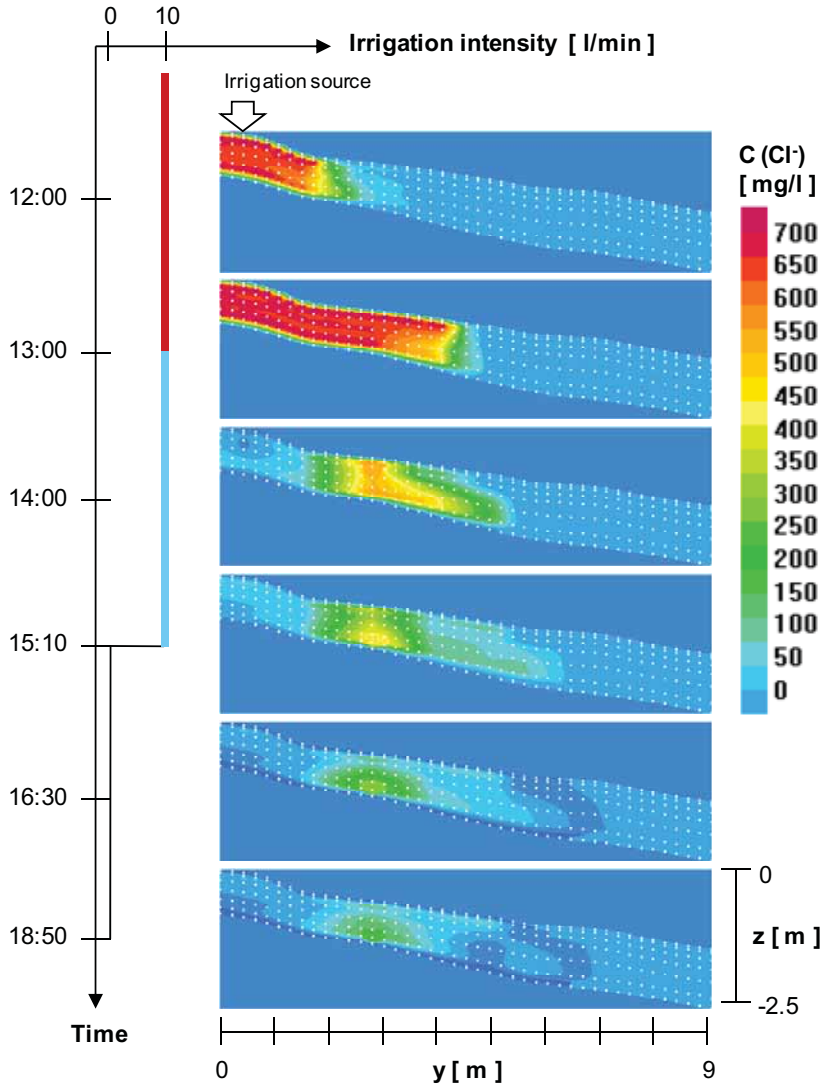

Figure 36. Downslope migrating chloride plume at six time points, presented in the vertical direction *z* and in the downslope direction *y*. The chloride concentrations *C* are interpolated from the data on the middle line well screens (cf. Figure 26 b, 27 and 35) with SurGe (Dressler, the SurGe website).

At the second time point at 13:00, the irrigation has been running for 1 h 20 min and is about to be changed into unsalted water. In this case, the front of the chloride plume has already migrated to a distance of 4.0 m from the irrigation source, and concentrations of the magnitude of the irrigated solution have moved beyond a distance of 3.0 m. During the following two time points at 14:00 and 15:10, irrigation is continued with unsalted water, and the chloride concentration drops fast while the saturation front continues to migrate downhill.

Figure 36 shows a large change in chloride concentrations between the time points 13:00 and 14:00, when the irrigation was changed from salted to unsalted water. The change demonstrates the dominance of new water and preferential flow in the well screens, as well as a fast response of the well screens to changes in the surrounding soil water, in particular to the water in the preferential flowpaths (cf. Chapter 4.2.1). The change is explained by flow from the preferential flow domain, i.e. from the middle line well screens, to the surrounding soil matrix either directly or via preferential flowpaths on the sides of the middle line wells. Even though the intensity of the irrigation remains the same, velocity of the front decreases between 13:00 and 14:00, as the front reaches the drier section of the slope, where the soil was not saturated by the preliminary irrigation a day before (cf. Figure 32, Chapter 4.3.1).

When the irrigation is stopped after a total duration of 3 h 30 min at 15:10, the front is at a distance of about 5.0 m from the irrigation source. After the stop, the migration of the front starts to slow down fast. In 1 h 20 min after the stop at 16:30, the front has proceeded only 1.0 m, and during the last 2 h 20 min the front no longer proceeds. Considering the chloride concentrations, slow dilution is detected during the last two time steps. This is due to a decrease in preferential flow, as well as a decrease in by-pass flow in relation to translatory flow, as noted in Chapter 4.2.1.

Accuracy as well as the representativeness of the data in terms of preferential flow decreases after the irrigation is stopped and saturation starts to withdraw (Chapter 4.2.1). It is also to be noted that the overall accuracy of the data presented in Figure 36 is better for the locations inside the saturated domain, i.e., at the front of the plume the data only provide an estimate based on interpolation between the data recorded in a well screen containing water and a well without water and measured data. For the wells without a water table, the background chloride concentration was used as long as water entered the well. Accuracy and representativeness issues are further discussed in Chapters 4.3.1, 5.1.8 and 5.3.3.

4.2.3 Estimates for the saturated hydraulic conductivity

The Piezometer method gives, using the data available from stand pipe 15 (Figure 37), an average conductivity of 2.4E-3 cm/s for the C horizon.

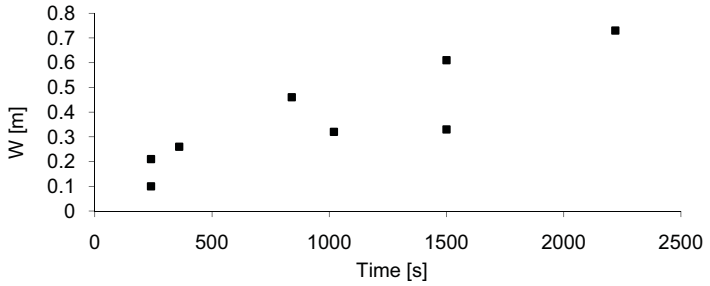

Figure 37. Rise of water level *W* in stand pipe 15, after pumping the pipe empty during the ion tracer experiment of September 6, 2005.

Saturated hydraulic conductivities calculated with the Piezometer method are presented in Figure 38 together with the conductivities obtained with the one-dimensional flow model (Equation 6). The figure also contains the estimated limits for the profile average of the saturated hydraulic conductivity that were calculated directly from Darcy's law (Equation 4), and the profile average related to the results of the 1D-model.

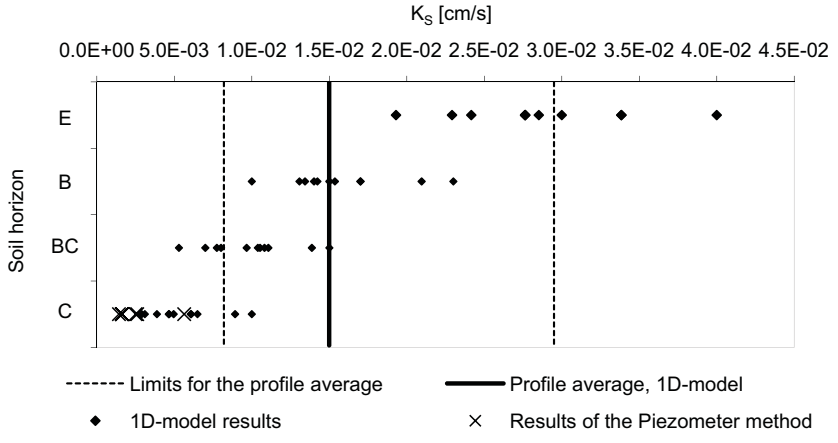

Figure 38. Estimates of the saturated hydraulic conductivity K_S obtained with the inverse, 1D-model application, and the Piezometer method. Estimates of the profile average are calculated from the results of the inverse, 1D-model application, and directly from Darcy's law.

Results obtained with the Piezometer method for the subsoil partially overlap the results obtained with the one-dimensional model. Average conductivity values obtained with the one-dimensional model are 2.9E-2 cm/s for the E horizon, 1.6E-2 cm/s for the B horizon, 1.0E-2 cm/s for the BC horizon, and 6.0E-3 cm/s for the C horizon. The profile average related to the one-dimensional model is 1.5E-2 cm/s, and it fits inside the estimated limits of 8.0E-3 and 3.0E-2 cm/s. The limits were calculated with Equation 4, by assuming an irrigation volume of 1.55-2.07 m^3, an average flow distance of 3.0-4.6 m, a duration of 12600 s, an average cross-sectional area of 3.2-5.0 m^2, and a head difference of 0.8-0.9 m. These assumptions were based on the irrigation data and the data on the wells screens (Figure 35).

4.3 Discussion

4.3.1 Runoff generation and subsurface stormflow

A variety of tracers have widely been used in studying runoff generation in forest soils (e.g. Espeby 1989, McDonnell 1990, Lepistö et al. 1994, Tsuboyama et al. 1994, Buttle and McDonald 2002, Laudon et al. 2004 and 2007). However, detailed studies concentrating on preferential flow and subsurface stormflow in shallow, forested till soils of the Fennoscandian region, as well as for studies on the consistent use of tracer data in developing dual-permeability models for forest soils are called for (cf. Chapter 1.1). The experimental arrangement of this study illustrated preferential flow, subsurface stormflow and conservative solute transport along the Kangaslampi study slope, and produced numerical data for modelling purposes.

Compared to natural rainfall or snow melt events, the chloride tracer experiment was an extreme, hypothetical case both in terms of input intensity and duration. Artificial experiments, however, can provide particularly incisive tests of hydrological theory, since controlled experiments can isolate individual mechanisms and provide a more precisely defined target for the theory to hit (Kirchner 2006). Thus, the intensive experiment of this study is not representative of natural rainfall or snow melt events, but demonstrates the mechanisms behind subsurface stormflow as well as the flow pathways during the runoff generation in soil more clearly than measurements conducted in natural conditions. The data available from the experiment represent, together with the data of the dye tracer experiments (Chapter 3), the saturation and draining of soil, the initiation, steady state and recession

period of subsurface stormflow, and the flowpaths and mechanisms in wet and dry soil.

Combined with the results of the dye tracer experiments (Chapter 3.2, 3.3), the high chloride concentrations recorded at the ion tracer experiment support the finding that individual macropore segments are short in length but have a tendency to self-organize into larger preferential flow systems (cf. Sidle et al. 2001). Intensity and duration of rainfall, initial soil moisture content, and the saturated hydraulic conductivity of the soil matrix determine when macropore flow occurs (Jarvis 2007). Initiation of macropore flow and the water exchange between macropores and the soil matrix have a marked influence on the resulting runoff generation processes (Weiler and Naef 2000). At the beginning of the chloride tracer irrigation, most of the irrigated solution funnelled directly into macropores, as the initial moisture status of soil near the irrigation source was high. Chloride concentration of the magnitude of the irrigation water was observed as far as four metres from the source.

The high chloride concentrations detected far from the irrigation source shortly after the beginning of the irrigation can only be explained with fast, subsurface stormflow along preferential routes. Pressure induced by the irrigation pushed only small amounts of old, chloride-free water from the soil matrix to the preferential flow network and translatory flow was detected only when the soil was wet and saturating, but not yet fully saturated. During lower intensity, natural events, the addition of small amounts of new, event water can mobilize large amounts of old water that can contribute to the runoff generation (Bishop et al. 2004). The data of the tracer experiment of this study rather indicate however that old, chloride-free water in the macropores was pushed into the soil matrix, when new, chlorinated water saturated the soil via macropores and initiated the fast, preferential flow downslope. High amounts of vertical event water fluxes may participate in the slope runoff generation, when a large, saturated layer prevails in soil above the bedrock before and during the event, and the input intensity is high (Buttle and McDonald 2002).

As the saturation front encountered the drier slope section, the velocity of the front decreased as more water was needed to saturate the soil matrix. This supports the finding that in coarse-textured soils the soil matrix saturates via macropores before the preferential flow in the macropores initiates (cf. Aubertin 1971). As saturation started to withdraw after the irrigation was stopped, the proportion of flow in the soil matrix started to grow in relation to the flow in the preferential flow network, illustrating the effect of a change in irrigation intensity on the flow mechanisms in soil. The recorded chloride concentrations imply that during the irrigation, water was mainly funnelled via

macropores into the soil matrix, both in the wet and dry slope section, and after the irrigation, water in the soil matrix and in the preferential routes started to mix, as preferential flow started to drain. A slight rise in the chloride concentration after the irrigation was stopped indicates that water from the soil matrix both entered the preferential routes and drained back to the next matrix pores. Beside the duality of the soil structure and flow formation, the chloride tracer experiment demonstrated the strong increase in hydraulic conductivity as the water table approaches soil surface, as expected based on the findings of e.g. Lind and Lundin (1990).

The observed changes in the origin of water in the preferential flowpaths and in the soil matrix support the finding of Kienzler and Naef (2008), who studied the formation of subsurface stormflow at four hillslopes during controlled tracer experiments and natural rainfall events in Switzerland. Kienzler and Naef (2008) conclude that the intensity of the subsurface stormflow and the fraction of pre-event water in runoff depend on whether subsurface stormflow in preferential flowpaths is fed directly from precipitation or indirectly from saturated parts of the soil. When precipitation feeds directly into preferential flow paths, subsurface stormflow responds quickly and contains low pre-event water fraction. In contrast, subsurface stormflow response is delayed and consists mainly of pre-event water when it is fed indirectly via large saturated zones of the soil.

From the modelling point of view, results of this study and the results of Kienzler and Naef (2008) suggest that the flow between the pores of the soil matrix should be low compared with the flow between the pores of the preferential flow domain, and compared with the exchange of water between the soil matrix and the preferential flow domain, when the soil is saturating or drying. At saturation, the exchange between the domains should be low. In many of the two pore domain modelling approaches (e.g. Gerke and van Genuchten 1993a), flow between the pore domains is governed by the average hydraulic conductivity and the hydraulic gradient between the domains that yields the preferred flow characteristics.

From the modelling point of view, it is also to be noted that the representativeness of the concentration data on the well screens is not fully unambiguous. The turnover of water in the wells was fast, indicating a good correspondence between the data recorded in the well screens and actual concentration levels in the water of preferential flowpaths in soil surrounding the wells (cf. Chapter 4.1.1., 4.2.1, 4.2.2). Most water observed in particular in the middle line wells of the experimental field (cf. Figure 26, 27, 35, 36) was

new water from the irrigation source, and the water presented the fraction of the soil pore space that contributes actively to subsurface stormflow.

However, the measured tracer concentrations at different depths of the wells do not directly correspond to the tracer concentrations in preferential flowpaths at different depths in the soil profile (Chapter 4.1.1., 4.2.1, 4.2.2). In consequence, when the tracer experiment is simulated with a computer model, a strict, direct comparison of the measured and simulated chloride profiles is not justifiable. The observed concentrations only reflect the magnitude of the chloride concentration at different depths. The representativeness issues are discussed further in Chapter 5.1.8 and 5.3.3.

Considering the data available from the stand pipes, the results indicate that the soil-bedrock interface does not provide a broad preferential flow plane for water and solutes in the one metre thick middle part of the experimental slope. Water reached two stand pipes during the experiment (SP1 and 15, Figure 26), and chloride only one (SP1, Figure 26). SP1 was located only at a horizontal distance of 70 cm from the irrigation source. Salt observed on the bedrock so near the irrigation source cannot be considered a sign of a highly conductive layer at soil-bedrock interface.

As for the other stand pipe, SP15, high chloride concentrations were observed in all the nearby well screens, whereas background concentration prevailed in pipe 15 throughout the experiment. This indicates that chloride detected in the surrounding wells originates from the upper soil horizons instead of the soil-bedrock interface or the deepest parts of the subsoil. Salt water detected in the lower half of the well screens did not originate merely from the lateral direction from the preceding subsoil. As the saturation front proceeded downslope, subsoil saturated both from the lateral direction with the water flowing in subsoil, and from the vertical direction with the water flowing in the upper soil horizons. Together with the rapidly rising groundwater tables during the irrigation, concentration results of the tracer-free stand pipe show that the soil saturates before lateral flow initiates, and the conductivity, the amount of macrostructures, and the velocity and amount of flow increase non-linearly with depth.

The study of Saastamoinen et al. (2009) as well as the unpublished data of Saastamoinen and Laine-Kaulio (2007) from dye tracer experiments up- and downslope from the hillslope section presented in this study, support the findings of a poorly conducting subsoil in the midslope section of the Kangaslampi hillslope. Unsaturated soil near the hillslope top and bottom was doused with a dye tracer solution similarly to this study, the soil was sliced and

samples were collected for analyzing phosphorous speciation in preferential flowpaths and in soil matrix at different parts of the slope. The experiments revealed that in the thinner soil columns (cf. Chapter 2.1) up- and downslope from the study area, the dye tracer and hence the preferential flowroutes reached the bedrock.

The findings of Saastamoinen et al. (2009) and Saastamoinen and Laine-Kaulio (2007) correspond to the results of Ilvesniemi et al. (2010), who measured the different components of the water balance in two, small, forested catchments with a shallow till soil cover above impermeable bedrock at the SMEAR-II measurement stations in Hyytiälä, Finland, for a period of about 10 years. The measurements show that in the soil column with an average thickness of 50-70 cm, no surface or surface layer runoff is detected in any conditions, and lateral flow generates in the soil layer above the bedrock when the lower layers saturate (Ilvesniemi et al. 2010). In addition to the low soil profile thickness, stone content that increases with depth explains the runoff generation near bedrock in Hyytiälä.

4.3.2 Saturated hydraulic conductivity

Saturated hydraulic conductivity values produced by the different methods, i.e. the laboratory analyses and the Guelph measurements in the field (Chapter 2.3.3), and the Piezometer method and the one-dimensional model application (Chapter 4.2.3), clearly differ from each other. Depending on the soil horizon, the difference between the lowest and the highest estimate is 44 to 85 fold. Results related to all the different methods presented in this study, together with the results of Möttönen (2000), based on 16 undisturbed soil samples for each soil horizon in the nearby area of Kangasvaara, are presented in Figure 39.

The conductivity values determined with the inverse one-dimensional model clearly exceed the results of the laboratory analysis and the Guelph measurements (Figure 39). The magnitude of the results obtained with the different methods is connected to scale (cf. Jenssen 1990). The smallest conductivity values were obtained from the small, disturbed laboratory samples, and the highest conductivity values were related to the inverse 1D-model application that covered the most extensive soil volume. As noted in Chapter 2.3.3, although the small laboratory samples were disturbed, they indicate the conductivity of the soil matrix, because the matrix properties are strongly controlled by the soil texture (e.g. Jarvis 2007). Small, disturbed soil

samples are thereby clearly unsuitable for determining the overall saturated hydraulic conductivity of forest soil with high amounts of macropores.

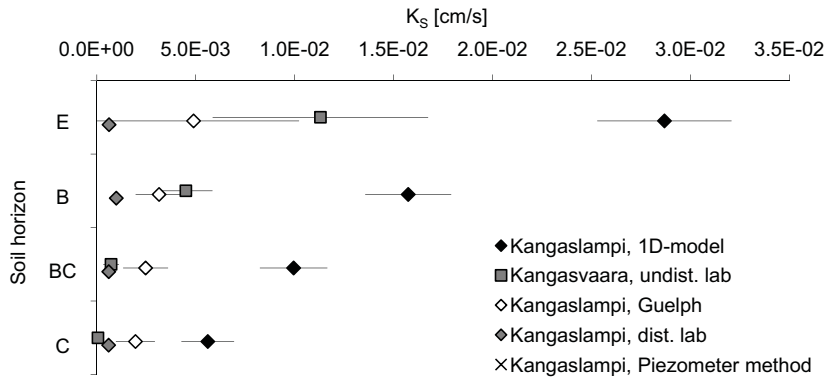

Figure 39. Average saturated hydraulic conductivity with 95 % confidence intervals for Kangaslampi, determined with different methods, and for the nearby area of Kangasvaara (Möttönen 2000), determined from soil samples.

The applicability of the Guelph results remains more questionable. In this study, soil was saturated only around the tip of the Guelph device. To emphasize the difference between the conductivity of widely saturated soil and the small-scale saturation around the Guelph tip, Penttinen (2000) used the term *field saturated hydraulic conductivity* for Guelph measurements conducted in northern Finland. If the Guelph device was used in soil that is saturated over a larger area, the device could give higher estimates for the conductivity. However, according to comparative studies (e.g. Mohanty et al. 1994), the conductivity estimates obtained with the Guelph permeameter are generally considered lower than conductivity values obtained with other field methods, and in some cases also lower than the values measured in the laboratory from undisturbed samples.

The conductivity estimates obtained for the subsoil with the Piezometer method are of the same magnitude as the Guelph results, even though the soil was saturated over a much larger area around the stand pipes used for the Piezometer method. In comparison to the 1D-model application, the Guelph and Piezometer results for the subsoil are smaller. Theoretically, the Piezometer method represents the vertical saturated hydraulic conductivity of subsoil, whereas the results obtained with the 1D-model correspond to the lateral conductivity. In addition, based on one stand pipe at a time, the results of the Piezometer method represent a smaller spatial scale than the 1D-model application.

Lind and Lundin (1990) present a summary of the saturated hydraulic conductivity measured with a variety of field methods in Scandinavian tills. According to the summary, the conductivity varies from about 10^{-6} to 10^{-2} cm/s. Conductivities calibrated with the one-dimensional model in this study exceed this reference range for the E, B and BC horizons. It is noteworthy that none of the field methods cited in Lind and Lundin (1990) correspond to as large a scale as the model applications of this study. Estimates obtained with the one-dimensional groundwater model conform to the total pore space of the studied hillslope section or to the preferential flow domain of the section.

The scale dependency, the dependency on soil structural properties, as well as the with depth changing values of the saturated hydraulic conductivity of tills are a common finding (e.g. Lind and Lundin 1990). Related to these features, no ideal methods for measuring the saturated hydraulic conductivity of tills exist (Jenssen 1990). Methods for separately measuring the conductivity of the soil matrix and the macropores are also not available. Taking into account these facts as well as the analysis presented above and earlier in Chapter 2.3.3, the large-scale conductivity estimates (the inverse 1D model) can be linked to the large pores forming the preferential flowroutes, and the small-scale estimates (the laboratory measurements related to the screened soil samples) to the micropores of the soil matrix, to estimate the saturated hydraulic conductivities of the pore domains of the dual-permeability model in this study (Chapter 5).

5 Modelling of flow and solute transport

5.1 Methods

To simulate the stormflow event produced in the ion tracer experiment in Chapter 4, a flow model based on the three-dimensional form of Richards' equation was coupled with a three-dimensional solute transport model accounting for advection and dispersion. Equations needed were solved numerically and programmed to a simulation model with Java in an object-oriented way, which enabled a simultaneous development of a one and two pore domain model. The model allows for adaptability in parameterising and in fitting the model structurally to the observed event. A similar combination of model features and adaptability is not available in reference models and their applications, which are presented and compared with the model and applications of this study in Chapter 5.3. Considering the model of this study, a summary of the equations, together with the numerical solution methods, development and testing of the computer programme, as well as the principles for determining the initial state, parameterisation and model evaluation are presented in the following subsections. Parameterisation is discussed in detail for each model version and application separately in Chapter 5.2, and analysis of the developed model and its applications is presented in Chapter 5.3.

5.1.1 Equations for flow, advection and dispersion

The Richards' equation (1931) for subsurface flow in unsaturated porous media is:

$$\frac{\partial \theta}{\partial t} = \nabla\left[K(\theta)\nabla H\right] \pm S\,, \tag{8}$$

where θ is the volumetric water content [L^3/L^3], K is the moisture dependent hydraulic conductivity [L/T], H is the hydraulic head [L], and S contains sinks and sources of the system [L^3/L^3T]. The hydraulic head H is defined as a sum of the pressure head h [L] and the elevation head z [L] as:

$$H = h + z \quad . \tag{9}$$

Due to the non-linear relation between the soil moisture θ and the pressure head h, the Richards' equation can be transformed into a more straightforward form for calculations, with the hydraulic head on both sides:

$$C^d(h)\frac{\partial H}{\partial t} = \nabla\left[K(\theta)\nabla H\right] \pm S \quad , \tag{10}$$

where the term C^d [L^{-1}] describes the derivative of the soil moisture characteristic curve, i.e., the curvature of the relation between the soil moisture and the pressure head, and is referred to as the differential moisture capacity.

The relation used to connect the soil moisture with the pressure head in this study is the van Genuchten model (1980):

$$\theta = \theta_R + \frac{\theta_S - \theta_R}{\left[1 + \left(\alpha|h|\right)^{\beta}\right]^{\left(1-\frac{1}{\beta}\right)}} \quad . \tag{11}$$

Analogously to the water retention analysis (Chapter 2.3.1), the lower index *R* denotes *residual* and *S* denotes *saturated* in the water content terms θ [L^3/L^3], and α [L^{-1}] and β [-] are the model parameters. Following van Genuchten (1980), parameters α and β are used to link the hydraulic conductivity *K(h)* [L/T] to the hydraulic head. The hydraulic conductivity is a product of the saturated hydraulic conductivity K_s [L/T] and the relative hydraulic conductivity K_r [L/T]:

$$K(h) = K_r K_s \quad , \tag{12}$$

where the relative conductivity is estimated from:

$$K_r = S_e^{\left(\frac{1}{2}\right)}\left\{1 - \left[1 - S_e^{\left(\frac{1}{\beta}\right)}\right]^{\beta}\right\}^2 \quad , \tag{13}$$

where S_e [-] is the degree of saturation, for which applies:

$$S_e = \left[1 + \left(\alpha|h|\right)^{\beta}\right]^{\left(\frac{1}{\beta}-1\right)} \quad . \tag{14}$$

Since the solute transport model is used in this study to simulate the chloride movement in the tracer experiment, the governing equation for solute transport contained advection and dispersion terms. Derived from Fetter (2001), the transport equation is:

$$\frac{\partial(\theta C)}{\partial t} = \nabla\left[D\nabla(\theta C)\right] - v\nabla(\theta C) \quad , \tag{15}$$

where θ is the soil moisture [-], C is the concentration [M/L³], D is the dispersion coefficient [L²/T], summing up both diffusion and dispersion, and v is the flow velocity in soil pores [L/T]. The flow velocity in direction n is:

$$v_n = \frac{q_n}{\theta} = -\frac{K(\theta)_n \partial H}{\theta \partial x_n} \quad . \tag{16}$$

In the three-dimensional case, n translates into x, y, and z coordinates, denoted in the numerical solutions with indices i, j, and k, respectively. For three-dimensional porous medium, where flow and dispersion are assumed to occur only along the coordinate axes, the dispersion coefficient can be written for each dimension n following Rausch et al. (2005) as:

$$D_n = \alpha^* + \alpha_L \frac{v_n^2}{|v|} + \alpha_{T1} \frac{v_{T1}^2}{|v|} + \alpha_{T2} \frac{v_{T2}^2}{|v|} \quad . \tag{17}$$

The first coefficient α^* is the diffusion term [L²/T] regarded as a constant, α_L denotes the longitudinal dispersivity [L] in the direction of the axis in question, and α_T denotes the transverse dispersivity [L] in the direction of the other two axes. v_{T1} and v_{T2} are the flow velocities [L/T] in transverse directions. The magnitude of the flow velocity $|v|$ is:

$$|v| = \sqrt{v_x^2 + v_y^2 + v_z^2} \quad , \tag{18}$$

where v_x is the flow velocity in the direction x, v_y in the direction y, and v_z in the direction z.

5.1.2 Numerical solution of the partial differential equations

The Richards' equation does not have a closed-form analytical solution for a general case of an arbitrary three-dimensional grid and arbitrarily changing moisture conditions. A suitable numerical method for solving the partial differential equations for both flow and solute transport in a hillslope with moderately varying soil profile is the *finite volume method* (e.g. Rausch et al. 2005), where the soil profile of a slope is divided into an unstructured grid, and the mass balance of water or solute is calculated for each control volume of the grid. Thus, the hydraulic head H or the solute concentration C is located at the centroid of each volume, and the differential form of the governing equation is integrated over all the volumes. The resulting solution satisfies the conservation of mass for any control volume, as well as for the whole computational domain.

The integral form of the flow equation for the finite volume method is:

$$\int_{t}^{t+\Delta t}\int_{z}^{z+\Delta z}\int_{y}^{y+\Delta y}\int_{x}^{x+\Delta x}\left[C^{d}(h)\frac{\partial H}{\partial t}\right]dxdydzdt$$
$$=\int_{t}^{t+\Delta t}\int_{z}^{z+\Delta z}\int_{y}^{y+\Delta y}\int_{x}^{x+\Delta x}\left[\frac{\partial}{\partial x}\left(K_{x}\frac{\partial H}{\partial x}\right)\right. \tag{19}$$
$$\left.+\frac{\partial}{\partial y}\left(K_{y}\frac{\partial H}{\partial y}\right)+\frac{\partial}{\partial z}\left(K_{z}\frac{\partial H}{\partial z}\right)-S\right]dxdydzdt$$

Integration over *x*, *y* and *z*, and implicitly over time *t*, and by denoting the resulting volumes by *V* and areas by *A*, leads for each cell of the grid to:

$$C^{d}(h_{i,j,k}^{t})\frac{V_{i,j,k}}{\Delta t}\left(H_{i,j,k}^{t+1}-H_{i,j,k}^{t}\right)$$
$$=K_{i+0.5,j,k}^{t}A_{i+0.5,j,k}\frac{H_{i+1,j,k}^{t+1}-H_{i,j,k}^{t+1}}{x_{i+1,j,k}-x_{i,j,k}}$$
$$-K_{i-0.5,j,k}^{t}A_{i-0.5,j,k}\frac{H_{i,j,k}^{t+1}-H_{i-1,j,k}^{t+1}}{x_{i,j,k}-x_{i-1,j,k}}$$
$$+K_{i,j+0.5,k}^{t}A_{i,j+0.5,k}\frac{H_{i,j+1,k}^{t+1}-H_{i,j,k}^{t+1}}{y_{i,j+1,k}-y_{i,j,k}}$$
$$-K_{i,j-0.5,k}^{t}A_{i,j-0.5,k}\frac{H_{i,j,k}^{t+1}-H_{i,j-1,k}^{t+1}}{y_{i,j,k}-y_{i,j-1,k}}$$
$$+K_{i,j,k+0.5}^{t}A_{i,j,k+0.5}\frac{H_{i,j,k+1}^{t+1}-H_{i,j,k}^{t+1}}{z_{i,j,k+1}-z_{i,j,k}}$$
$$-K_{i,j,k-0.5}^{t}A_{i,j,k-0.5}\frac{H_{i,j,k}^{t+1}-H_{i,j,k-1}^{t+1}}{z_{i,j,k}-z_{i,j,k-1}}-S_{i,j,k}V_{i,j,k} \tag{20}$$

The implicit solution was chosen to reduce problems of computational instability. The solution of Equation 20 is iterative. To reduce the number of unknown terms in the new time step *t+1* and to avoid problems with convergence of the iteration, the hydraulic conductivity *K* was appointed explicitly to the earlier time steps *t* (van Dam 2000). As the conductivity values are related to the water fluxes between cells, the conductivities were calculated as averages of the cells in question. In the internal cells of the grid, conductivities were calculated as arithmetic means and at the boundaries as geometric means. The geometric mean was used to set the hydraulic conductivity between a water permeable, inner cell and an impermeable boundary cell to zero. Arithmetic mean was used inside the grid to enable higher conductivity values than obtainable with geometric means, when flow is calculated between wet and dry cells. The differential moisture capacity was estimated by the difference quotient (Karvonen 1988, Celia et al. 1990):

$$C_{i,j,k}^{d} = \frac{\theta_{i,j,k}^{t+1} - \theta_{i,j,k}^{t}}{h_{i,j,k}^{t+1} - h_{i,j,k}^{t}} \quad . \tag{21}$$

The finite volume integral of the solute transport equation is:

$$\begin{aligned}
&\int_{t}^{t+\Delta t}\int_{z}^{z+\Delta z}\int_{y}^{y+\Delta y}\int_{x}^{x+\Delta x} \frac{\partial(\theta C)}{\partial t}\, dxdydzdt \\
&= \int_{t}^{t+\Delta t}\int_{z}^{z+\Delta z}\int_{y}^{y+\Delta y}\int_{x}^{x+\Delta x}\left[\frac{\partial}{\partial x}\left(\theta D_x \frac{\partial C}{\partial x}\right)\right. \\
&+ \frac{\partial}{\partial y}\left(\theta D_y \frac{\partial C}{\partial y}\right) + \frac{\partial}{\partial z}\left(\theta D_z \frac{\partial C}{\partial z}\right) \\
&\left. - \frac{\partial}{\partial x}(\theta v_x C) - \frac{\partial}{\partial y}(\theta v_y C) - \frac{\partial}{\partial z}(\theta v_z C)\right] dxdydzdt
\end{aligned} \quad , \tag{22}$$

and the integration leads to the following form:

$$\begin{aligned}
&\frac{V_{i,j,k}}{\Delta t}\left(\theta_{i,j,k}^{t+1} C_{i,j,k}^{t+1} - \theta_{i,j,k}^{t} C_{i,j,k}^{t}\right) \\
&= \frac{C_{i+1,j,k}^{t+1} - C_{i,j,k}^{t+1}}{x_{i+1,j,k} - x_{i,j,k}} \theta_{i+0.5,j,k}^{t+1} D_{i+0.5,j,k}^{t+1} A_{i+0.5,j,k} \\
&- \frac{C_{i,j,k}^{t+1} - C_{i-1,j,k}^{t+1}}{x_{i,j,k} - x_{i-1,j,k}} \theta_{i-0.5,j,k}^{t+1} D_{i-0.5,j,k}^{t+1} A_{i-0.5,j,k} \\
&+ \frac{C_{i,j+1,k}^{t+1} - C_{i,j,k}^{t+1}}{y_{i,j+1,k} - y_{i,j,k}} \theta_{i,j+0.5,k}^{t+1} D_{i,j+0.5,k}^{t+1} A_{i,j+0.5,k} \\
&- \frac{C_{i,j,k}^{t+1} - C_{i,j-1,k}^{t+1}}{y_{i,j,k} - y_{i,j-1,k}} \theta_{i,j-0.5,k}^{t+1} D_{i,j-0.5,k}^{t+1} A_{i,j-0.5,k} \\
&+ \frac{C_{i,j,k+1}^{t+1} - C_{i,j,k}^{t+1}}{z_{i,j,k+1} - z_{i,j,k}} \theta_{i,j,k+0.5}^{t+1} D_{i,j,k+0.5}^{t+1} A_{i,j,k+0.5} \\
&- \frac{C_{i,j,k}^{t+1} - C_{i,j,k-1}^{t+1}}{z_{i,j,k} - z_{i,j,k-1}} \theta_{i,j,k-0.5}^{t+1} D_{i,j,k-0.5}^{t+1} A_{i,j,k-0.5} \\
&+ q_{i-0.5,j,k}^{t+1} A_{i-0.5,j,k}\left[\zeta_{i-0.5,j,k}^{t} C_{i-1,j,k}^{t} + \left(1 - \zeta_{i-0.5,j,k}^{t}\right) C_{i,j,k}^{t}\right] \\
&- q_{i+0.5,j,k}^{t+1} A_{i+0.5,j,k}\left[\zeta_{i+0.5,j,k}^{t} C_{i,j,k}^{t} + \left(1 - \zeta_{i+0.5,j,k}^{t}\right) C_{i+1,j,k}^{t}\right] \\
&+ q_{i,j-0.5,k}^{t+1} A_{i,j-0.5,k}\left[\zeta_{i,j-0.5,k}^{t} C_{i,j-1,k}^{t} + \left(1 - \zeta_{i,j-0.5,k}^{t}\right) C_{i,j,k}^{t}\right] \\
&- q_{i,j+0.5,k}^{t+1} A_{i,j+0.5,k}\left[\zeta_{i,j+0.5,k}^{t} C_{i,j,k}^{t} + \left(1 - \zeta_{i,j+0.5,k}^{t}\right) C_{i,j+1,k}^{t}\right] \\
&+ q_{i,j,k-0.5}^{t+1} A_{i,j,k-0.5}\left[\zeta_{i,j,k-0.5}^{t} C_{i,j,k-1}^{t} + \left(1 - \zeta_{i,j,k-0.5}^{t}\right) C_{i,j,k}^{t}\right] \\
&- q_{i,j,k+0.5}^{t+1} A_{i,j,k+0.5}\left[\zeta_{i,j,k+0.5}^{t} C_{i,j,k}^{t} + \left(1 - \zeta_{i,j,k+0.5}^{t}\right) C_{i,j,k+1}^{t}\right]
\end{aligned} \tag{23}$$

Concentration *C* appears in the numerical solution two times in each advection term, but only one of the two is non-zero at a time. This is due to the switch term ζ, the value of which is either zero or one depending on the flow direction. For instance for the advection term between cells *(i,j,k)* and *(i-1,j,k)* applies:

$$\begin{cases} \xi_{i-0.5,j,k} = 1, & q_{i-0.5,j,k} \geq 0 \\ \xi_{i-0.5,j,k} = 0, & q_{i-0.5,j,k} < 0 \end{cases} . \qquad (24)$$

The switch term is determined analogously for each direction. When water flows into a cell from an adjacent cell, i.e. the source cell, the concentration of the adjacent cell is used in the calculations, i.e., the switch term is 1 for the adjacent cell, but 0 for the destination cell – and vice versa.

The numerical solution of the advection equation causes numerical dispersion (Karvonen 2003):

$$\frac{v_n \Delta x_n}{2} \qquad (25)$$

where v_n is the flow velocity [L/T] in direction n (x, y or z) and Δx_n is the corresponding flow distance [L]. In order to accurately simulate dispersion, numerical dispersion (Eq. 25) was reduced from the dispersion D_n, when the numerical dispersion was smaller than the real dispersion (cf. van Genuchten and Gray 1978). Dispersion was set to zero, if the numerical dispersion exceeded the actual dispersion.

The flow and transport equations formed a set of linear equations that were solved with the help of the tridiagonal *Thomas algorithm* (see e.g. Wang and Anderson 1980) in the computer application. The algorithm is based on solving the governing equations for a whole column of grid cells at the same time. The simultaneous solution is based on matrix calculus and Gaussian elimination. Since the changes in the pressure head and in the chloride concentration were expected to be fastest in the vertical direction, the Thomas algorithm was applied to the cell columns in the z direction. The algorithm was applied to all vertical columns one at a time, and the lateral direction y and horizontal direction x were taken either from the previous iteration step or explicitly from the previous time step at the beginning of iteration.

For the Thomas algorithm, the flow equation was rearranged in the following form:

$$
\begin{aligned}
&-\frac{K^t_{i,j,k-0.5}A_{i,j,k-0.5}}{z_{i,j,k}-z_{i,j,k-1}}H^{t+1}_{i,j,k-1}\\
&+\left[C^d(h^t_{i,j,k})\frac{V_{i,j,k}}{\Delta t}\right.\\
&+\frac{K^t_{i+0.5,j,k}A_{i+0.5,j,k}}{x_{i+1,j,k}-x_{i,j,k}}+\frac{K^t_{i-0.5,j,k}A_{i-0.5,j,k}}{x_{i,j,k}-x_{i-1,j,k}}\\
&+\frac{K^t_{i,j+0.5,k}A_{i,j+0.5,k}}{y_{i,j+1,k}-y_{i,j,k}}+\frac{K^t_{i,j-0.5,k}A_{i,j-0.5,k}}{y_{i,j,k}-y_{i,j-1,k}}\\
&\left.+\frac{K^t_{i,j,k+0.5}A_{i,j,k+0.5}}{z_{i,j,k+1}-z_{i,j,k}}+\frac{K^t_{i,j,k-0.5}A_{i,j,k-0.5}}{z_{i,j,k}-z_{i,j,k-1}}\right]H^{t+1}_{i,j,k}\\
&-\frac{K^t_{i,j,k+0.5}A_{i,j,k+0.5}}{z_{i,j,k+1}-z_{i,j,k}}H^{t+1}_{i,j,k+1}\\
&=C^d(h^t_{i,j,k})\frac{V_{i,j,k}}{\Delta t}H^t_{i,j,k}\\
&+\frac{K^t_{i+0.5,j,k}A_{i+0.5,j,k}}{x_{i+1,j,k}-x_{i,j,k}}H^{t+1}_{i+1,j,k}+\frac{K^t_{i-0.5,j,k}A_{i-0.5,j,k}}{x_{i,j,k}-x_{i-1,j,k}}H^{t+1}_{i-1,j,k}\\
&+\frac{K^t_{i,j+0.5,k}A_{i,j+0.5,k}}{y_{i,j+1,k}-y_{i,j,k}}H^{t+1}_{i,j+1,k}+\frac{K^t_{i,j-0.5,k}A_{i,j-0.5,k}}{y_{i,j,k}-y_{i,j-1,k}}H^{t+1}_{i,j-1,k}
\end{aligned}
\qquad (26)
$$

Denoting the coefficients of the head terms $H^{t+1}_{i,j,k-1}$, $H^{t+1}_{i,j,k}$, $H^{t+1}_{i,j,k+1}$ on the left hand side (Eq. 26) by $A_{i,j,k}$, $B_{i,j,k}$ and $C_{i,j,k}$, respectively, and the remaining expression on the right hand side of the equation by $D_{i,j,k}$, the flow equation can be given in the matrix form for the Gaussian elimination of k vertical cells and for all (i,j) as:

$$
\begin{bmatrix}
B_{i,j,1} & C_{i,j,1} & 0 & 0 & \dots\\
A_{i,j,2} & B_{i,j,2} & C_{i,j,2} & 0 & \dots\\
\dots & \dots & \dots & \dots & \dots\\
\dots & 0 & A_{i,j,k} & B_{i,j,k} & C_{i,j,k}
\end{bmatrix}
\begin{bmatrix}
H^{t+1}_{i,j,1}\\ \dots\\ \dots\\ H^{t+1}_{i,j,k}
\end{bmatrix}
=
\begin{bmatrix}
D_{i,j,1}\\ \dots\\ \dots\\ D_{i,j,k}
\end{bmatrix}
\quad . \qquad (27)
$$

The state of H each time step can be efficiently solved in each iteration step for the whole domain. Application of the Thomas algorithm to the transport equation is equivalent: The equation is rearranged to a form with only terms containing $C^{t+1}_{i,j,k-1}$, $C^{t+1}_{i,j,k}$, and $C^{t+1}_{i,j,k+1}$ on the left hand size. The equation is then written in the matrix form as described above, and the state of C for all (x,y) is solved with the Gaussian elimination.

For the Thomas algorithm, the solute transport equation was rearranged in the following form:

$$
\begin{aligned}
&-\frac{\theta_{i,j,k-0.5}^{t+1} D_{i,j,k-0.5}^{t+1} A_{i,j,k-0.5}}{z_{i,j,k}-z_{i,j,k-1}} C_{i,j,k-1}^{t+1} \\
&+\left(\frac{\theta_{i,j,k}^{t+1} V_{i,j,k}}{\Delta t} \right. \\
&+\frac{\theta_{i+0.5,j,k}^{t+1} D_{i+0.5,j,k}^{t+1} A_{i+0.5,j,k}}{x_{i+1,j,k}-x_{i,j,k}}+\frac{\theta_{i-0.5,j,k}^{t+1} D_{i-0.5,j,k}^{t+1} A_{i-0.5,j,k}}{x_{i,j,k}-x_{i-1,j,k}} \\
&+\frac{\theta_{i,j+0.5,k}^{t+1} D_{i,j+0.5,k}^{t+1} A_{i,j+0.5,k}}{y_{i,j+1,k}-y_{i,j,k}}+\frac{\theta_{i,j-0.5,k}^{t+1} D_{i,j-0.5,k}^{t+1} A_{i,j-0.5,k}}{y_{i,j,k}-y_{i,j-1,k}} \\
&+\left. \frac{\theta_{i,j,k+0.5}^{t+1} D_{i,j,k+0.5}^{t+1} A_{i,j,k+0.5}}{z_{i,j,k+1}-z_{i,j,k}}+\frac{\theta_{i,j,k-0.5}^{t+1} D_{i,j,k-0.5}^{t+1} A_{i,j,k-0.5}}{z_{i,j,k}-z_{i,j,k-1}} \right) C_{i,j,k}^{t+1} \\
&-\frac{\theta_{i,j,k+0.5}^{t+1} D_{i,j,k+0.5}^{t+1} A_{i,j,k+0.5}}{z_{i,j,k+1}-z_{i,j,k}} C_{i,j,k+1}^{t+1} \\
&=\frac{\theta_{i,j,k}^{t} V_{i,j,k}}{\Delta t} C_{i,j,k}^{t} \\
&+\frac{\theta_{i+0.5,j,k}^{t+1} D_{i+0.5,j,k}^{t+1} A_{i+0.5,j,k}}{x_{i+1,j,k}-x_{i,j,k}} C_{i+1,j,k}^{t+1} \\
&+\frac{\theta_{i-0.5,j,k}^{t+1} D_{i-0.5,j,k}^{t+1} A_{i-0.5,j,k}}{x_{i,j,k}-x_{i-1,j,k}} C_{i-1,j,k}^{t+1} \\
&+\frac{\theta_{i,j+0.5,k}^{t+1} D_{i,j+0.5,k}^{t+1} A_{i,j+0.5,k}}{y_{i,j+1,k}-y_{i,j,k}} C_{i,j+1,k}^{t+1} \\
&+\frac{\theta_{i,j-0.5,k}^{t+1} D_{i,j-0.5,k}^{t+1} A_{i,j-0.5,k}}{y_{i,j,k}-y_{i,j-1,k}} C_{i,j-1,k}^{t+1} \\
&+q_{i-0.5,j,k}^{t+1} A_{i-0.5,j,k} \left[\zeta_{i-0.5,j,k}^{t} C_{i-1,j,k}^{t} + \left(1-\zeta_{i-0.5,j,k}^{t}\right) C_{i,j,k}^{t} \right] \\
&-q_{i+0.5,j,k}^{t+1} A_{i+0.5,j,k} \left[\zeta_{i+0.5,j,k}^{t} C_{i,j,k}^{t} + \left(1-\zeta_{i+0.5,j,k}^{t}\right) C_{i+1,j,k}^{t} \right] \\
&+q_{i,j-0.5,k}^{t+1} A_{i,j-0.5,k} \left[\zeta_{i,j-0.5,k}^{t} C_{i,j-1,k}^{t} + \left(1-\zeta_{i,j-0.5,k}^{t}\right) C_{i,j,k}^{t} \right] \\
&-q_{i,j+0.5,k}^{t+1} A_{i,j+0.5,k} \left[\zeta_{i,j+0.5,k}^{t} C_{i,j,k}^{t} + \left(1-\zeta_{i,j+0.5,k}^{t}\right) C_{i,j+1,k}^{t} \right] \\
&+q_{i,j,k-0.5}^{t+1} A_{i,j,k-0.5} \left[\zeta_{i,j,k-0.5}^{t} C_{i,j,k-1}^{t} + \left(1-\zeta_{i,j,k-0.5}^{t}\right) C_{i,j,k}^{t} \right] \\
&-q_{i,j,k+0.5}^{t+1} A_{i,j,k+0.5} \left[\zeta_{i,j,k+0.5}^{t} C_{i,j,k}^{t} + \left(1-\zeta_{i,j,k+0.5}^{t}\right) C_{i,j,k+1}^{t} \right]
\end{aligned}
\tag{28}
$$

The Thomas algorithm is presented in detail for solving the hydraulic head *H*, for instance, in Wang and Anderson (1982) and for the concentration *C* in Rausch et al. (2005).

Calculations with the above equations were performed for each time step in the following order. First, the state of the hydraulic head was iterated with the Thomas algorithm for all columns. When the iteration converged in all cells, i.e. the difference between the head values in consecutive iteration steps in all cells was smaller than a convergence criterion, the value of hydraulic head was set for that particular time step. In the simulations of this study, a value from 10^{-5} to 10^{-3} cm was used as the convergence criterion, depending on the desired accuracy and computation time. Second, values for the other variables, i.e., the pressure head, the soil moisture, the differential moisture capacity, and the hydraulic conductivity were updated. Third, the concentrations were iterated with the Thomas algorithm, with a convergence criterion from 10^{-5} to 10^{-3} µgcm^{-3}. The procedure was repeated in the same manner in all time steps. Boundary conditions are discussed in Chapter 5.1.6.

5.1.3 Equations for the two pore domain case

The dual permeability model can be given in the form (Gerke and van Genuchten 1993a):

$$C^d(h)\frac{\partial H}{\partial t} = \nabla\left[K(\theta)\nabla H\right] \pm S \pm \Gamma_w \qquad (29)$$

where Γ_w describes the exchange of water between the two pore domains. For the matrix domain, the exchange term is positive and for the preferential domain negative. Most of the studies available on dual permeability modelling parameterise the model so that both domains cover the whole pore space in soil alone, which leads to the use of a scaling factor that describes the ratio of the porosity of the preferential flow domain and total porosity in soil (e.g. Gerke and van Genuchten 1993a and 1993b, Šimůnek et al. 2003, Ray et al. 2004, Gerke et al. 2007). In these models, the exchange term of the preferential domain is divided by the scaling factor, and the exchange term of the matrix domain by the difference between one and the scaling factor, i.e., the porosity of the matrix domain in relation to the total porosity.

In this study, the parameterisation is directly scaled, so that no scaling factor is needed in the model. Thus, in this study the exchange term is determined as:

$$\Gamma_w = \alpha_w\left(H_p - H_m\right) \quad , \qquad (30)$$

where H_p [L] denotes the hydraulic head of the preferential domain, H_m [L] the hydraulic head of the matrix domain, and α_w [L^{-1}T^{-1}] is the so-called first-order

water transfer coefficient. The water transfer coefficient is defined following Gerke and van Genuchten (1993a):

$$\alpha_w = \frac{\beta}{a^2} K_a \gamma_w \quad , \tag{31}$$

where β is a factor describing the geometry of the aggregates [-], a represents the distance from a fictitious matrix block to the preferential domain boundary [L], γ_w is an empirical coefficient [-], and K_a is the effective hydraulic conductivity of the preferential-matrix interface [L/T]. Other studies define the water transfer coefficient α_w as a product of the relative hydraulic conductivity between the pore domains [-] and a lumped transfer coefficient [$L^{-1}T^{-1}$] (e.g. Ray et al. 2004). In this study, the definition of Gerke and van Genuchten (1993a) was used, and to reduce the number of unknown parameters, a, β and γ_w were lumped into one parameter α_{wl} [L^{-2}]. Thus, the water transfer coefficient α_w consisted only of one lumped coefficient α_{wl} and average hydraulic conductivity between the pore domains K_a (cf. Ray et al. 1997):

$$\Gamma_w = \alpha_{wl} K_a \left(H_p - H_m \right) \quad . \tag{32}$$

Gerke and van Genuchten (1993b) present five methods to calculate the average hydraulic conductivity K_a between the pore domains: i) dependence upon the pressure head of matrix alone, ii) preferential domain alone, iii) arithmetic mean, iv) geometric mean, and v) an integral form. The highest estimates were obtained by using only the conductivities of the preferential domain. Arithmetic mean yielded the second highest estimates for water exchange and indicated accurate results for matrix block geometries in the form of parallel rectangular slabs. Arithmetic mean was chosen for this study to gain a high exchange rate that is dependent on the moisture status of both the pore domains. The features of the modelled phenomenon helped to choose the way how the hydraulic conductivity between the systems was calculated. Considering the tracer experiment of this study, the conductivity needs to assure a dynamic and fast movement of water and solutes between the two systems.

Integrating the dual version of the Richards' equation with the finite volume method, and arranging the resulting terms in the form suitable for the Thomas algorithm, the equation giving the numerical solution becomes the same for both the matrix and preferential domains:

$$
\begin{aligned}
&-\frac{K^t_{i,j,k-0.5}A_{i,j,k-0.5}}{z_{i,j,k}-z_{i,j,k-1}}H^{t+1}_{i,j,k-1}\\
&+\left[C^d(h^t_{i,j,k})\frac{V_{i,j,k}}{\Delta t}\right.\\
&+\frac{K^t_{i+0.5,j,k}A_{i+0.5,j,k}}{x_{i+1,j,k}-x_{i,j,k}}+\frac{K^t_{i-0.5,j,k}A_{i-0.5,j,k}}{x_{i,j,k}-x_{i-1,j,k}}\\
&+\frac{K^t_{i,j+0.5,k}A_{i,j+0.5,k}}{y_{i,j+1,k}-y_{i,j,k}}+\frac{K^t_{i,j-0.5,k}A_{i,j-0.5,k}}{y_{i,j,k}-y_{i,j-1,k}}\\
&+\frac{K^t_{i,j,k+0.5}A_{i,j,k+0.5}}{z_{i,j,k+1}-z_{i,j,k}}+\frac{K^t_{i,j,k-0.5}A_{i,j,k-0.5}}{z_{i,j,k}-z_{i,j,k-1}}\\
&\left.+\frac{K^t_{i,j,k}+K^t_{DUAL,i,j,k}}{2}\alpha_{wl}V_{i,j,k}\right]H^{t+1}_{i,j,k}\\
&-\frac{K^t_{i,j,k+0.5}A_{i,j,k+0.5}}{z_{i,j,k+1}-z_{i,j,k}}H^{t+1}_{i,j,k+1}\\
&=C^d(h^t_{i,j,k})\frac{V_{i,j,k}}{\Delta t}H^t_{i,j,k}\\
&+\frac{K^t_{i+0.5,j,k}A_{i+0.5,j,k}}{x_{i+1,j,k}-x_{i,j,k}}H^{t+1}_{i+1,j,k}+\frac{K^t_{i-0.5,j,k}A_{i-0.5,j,k}}{x_{i,j,k}-x_{i-1,j,k}}H^{t+1}_{i-1,j,k}\\
&+\frac{K^t_{i,j+0.5,k}A_{i,j+0.5,k}}{y_{i,j+1,k}-y_{i,j,k}}H^{t+1}_{i,j+1,k}+\frac{K^t_{i,j-0.5,k}A_{i,j-0.5,k}}{y_{i,j,k}-y_{i,j-1,k}}H^{t+1}_{i,j-1,k}\\
&+\frac{K^t_{i,j,k}+K^t_{DUAL,i,j,k}}{2}\alpha_{wl}V_{i,j,k}H^{t+1}_{DUAL,i,j,k}
\end{aligned}
\qquad (33)
$$

When using Equation 33 for the matrix domain, the terms denoted with the *DUAL* sub-index refer to the variables of the preferential domain, and when using the equation for the preferential domain, terms denoted with the *DUAL* sub-index refer to variables of the matrix domain.

The dual domain version of the advection-dispersion equation was derived in the similar manner as the flow equation, so that no scaling factor is applied (Gerke and van Genuchten 1993a):

$$\frac{\partial(\theta C)}{\partial t}=\nabla\left[D\nabla(\theta C)\right]-v\nabla(\theta C)\pm\Gamma_s \qquad (34)$$

where Γ_s is the solute exchange term [$ML^{-3}T^{-1}$] that describes the advective and dispersive solute exchange between the pore domains. Analogously to the water exchange term in the flow equation, the positive sign is reserved for the flux to the matrix domain, and the negative sign for the flux to the preferential

domain. For the solute exchange term, varying definitions are available (e.g. Gerke and van Genuchten 1993a, Ray et al. 2004), and the definitions differ for the dispersion part. The dispersive exchange may depend more on the moisture status of the soil matrix, as a function of the pressure head difference and dispersivity of the matrix domain near the matrix-preferential domain interface (Gerke and van Genuchten 1993a), or the dispersive exchange may be dependent upon the relative saturation of the more dynamic preferential flow domain (e.g. Ray et al. 2004, Gerke et al. 2007).

To simplify the solute exchange term and to reduce the amount of unknown parameters, the term of this study was reduced to consist only of advective exchange. The subsurface stormflow event was clearly dominated by advection according to the ion tracer experiment, and therefore the dispersive exchange was neglected. Thus, the following form of the solute exchange term was used in this study:

$$\Gamma_S = (1-d)\alpha_{wl} K_a (H_p - H_m) C_p + d\alpha_{wl} K_a (H_p - H_m) C_m \qquad (35)$$

where α_{wl} [L^{-2}], K_a [LT^{-1}], H_p and H_m [L] define the exchange of water between the systems analogous to the water exchange term Γ_w, C_p and C_m [ML^{-3}] are the solute concentrations of the preferential flow domain p and the soil matrix m, and d [-] is the flow direction switch similar to the advection terms (Equation 28). d is zero, when the flow direction is from the preferential domain to soil matrix, and in the opposite case, d equal the value of one:

$$\begin{cases} d = 0, & (H_{p,i,j,k} - H_{m,i,j,k}) \geq 0 \\ d = 1, & (H_{p,i,j,k} - H_{m,i,j,k}) < 0 \end{cases} \qquad (36)$$

Integrating the dual version of the solute transport equation with the finite volume method, and arranging the resulting terms in the form suitable for the Thomas algorithm, the numerical solution becomes for the soil matrix and for the preferential flow domain as follows. In the equation for the soil matrix (Eq. 37), *DUAL* refers to the preferential domain, and in the equation for the preferential flow domain (Eq. 38), *DUAL* refers to the soil matrix (cf. Eq. 33).

$$
\begin{aligned}
&-\frac{\theta_{i,j,k-0.5}^{t+1} D_{i,j,k-0.5}^{t+1} A_{i,j,k-0.5}}{z_{i,j,k}-z_{i,j,k-1}} C_{i,j,k-1}^{t+1} \\
&+\left[\frac{\theta_{i,j,k}^{t+1} V_{i,j,k}}{\Delta t}\right. \\
&+\frac{\theta_{i+0.5,j,k}^{t+1} D_{i+0.5,j,k}^{t+1} A_{i+0.5,j,k}}{x_{i+1,j,k}-x_{i,j,k}}+\frac{\theta_{i-0.5,j,k}^{t+1} D_{i-0.5,j,k}^{t+1} A_{i-0.5,j,k}}{x_{i,j,k}-x_{i-1,j,k}} \\
&+\frac{\theta_{i,j+0.5,k}^{t+1} D_{i,j+0.5,k}^{t+1} A_{i,j+0.5,k}}{y_{i,j+1,k}-y_{i,j,k}}+\frac{\theta_{i,j-0.5,k}^{t+1} D_{i,j-0.5,k}^{t+1} A_{i,j-0.5,k}}{y_{i,j,k}-y_{i,j-1,k}} \\
&+\frac{\theta_{i,j,k+0.5}^{t+1} D_{i,j,k+0.5}^{t+1} A_{i,j,k+0.5}}{z_{i,j,k+1}-z_{i,j,k}}+\frac{\theta_{i,j,k-0.5}^{t+1} D_{i,j,k-0.5}^{t+1} A_{i,j,k-0.5}}{z_{i,j,k}-z_{i,j,k-1}} \\
&\left.-d\alpha_{wl} K_a\left(H_{DUALi,j,k}^{t+1}-H_{i,j,k}^{t+1}\right) V_{i,j,k}\right] C_{i,j,k}^{t+1} \\
&-\frac{\theta_{i,j,k+0.5}^{t+1} D_{i,j,k+0.5}^{t+1} A_{i,j,k+0.5}}{z_{i,j,k+1}-z_{i,j,k}} C_{i,j,k+1}^{t+1} \\
&=\frac{\theta_{i,j,k}^{t} V_{i,j,k}}{\Delta t} C_{i,j,k}^{t} \\
&+\frac{\theta_{i+0.5,j,k}^{t+1} D_{i+0.5,j,k}^{t+1} A_{i+0.5,j,k}}{x_{i+1,j,k}-x_{i,j,k}} C_{i+1,j,k}^{t+1} \\
&+\frac{\theta_{i-0.5,j,k}^{t+1} D_{i-0.5,j,k}^{t+1} A_{i-0.5,j,k}}{x_{i,j,k}-x_{i-1,j,k}} C_{i-1,j,k}^{t+1} \\
&+\frac{\theta_{i,j+0.5,k}^{t+1} D_{i,j+0.5,k}^{t+1} A_{i,j+0.5,k}}{y_{i,j+1,k}-y_{i,j,k}} C_{i,j+1,k}^{t+1} \\
&+\frac{\theta_{i,j-0.5,k}^{t+1} D_{i,j-0.5,k}^{t+1} A_{i,j-0.5,k}}{y_{i,j,k}-y_{i,j-1,k}} C_{i,j-1,k}^{t+1} \\
&+q_{i-0.5,j,k}^{t+1} A_{i-0.5,j,k}\left[\zeta_{i-0.5,j,k}^{t} C_{i-1,j,k}^{t}+\left(1-\zeta_{i-0.5,j,k}^{t}\right) C_{i,j,k}^{t}\right] \\
&-q_{i+0.5,j,k}^{t+1} A_{i+0.5,j,k}\left[\zeta_{i+0.5,j,k}^{t} C_{i,j,k}^{t}+\left(1-\zeta_{i+0.5,j,k}^{t}\right) C_{i+1,j,k}^{t}\right] \\
&+q_{i,j-0.5,k}^{t+1} A_{i,j-0.5,k}\left[\zeta_{i,j-0.5,k}^{t} C_{i,j-1,k}^{t}+\left(1-\zeta_{i,j-0.5,k}^{t}\right) C_{i,j,k}^{t}\right] \\
&-q_{i,j+0.5,k}^{t+1} A_{i,j+0.5,k}\left[\zeta_{i,j+0.5,k}^{t} C_{i,j,k}^{t}+\left(1-\zeta_{i,j+0.5,k}^{t}\right) C_{i,j+1,k}^{t}\right] \\
&+q_{i,j,k-0.5}^{t+1} A_{i,j,k-0.5}\left[\zeta_{i,j,k-0.5}^{t} C_{i,j,k-1}^{t}+\left(1-\zeta_{i,j,k-0.5}^{t}\right) C_{i,j,k}^{t}\right] \\
&-q_{i,j,k+0.5}^{t+1} A_{i,j,k+0.5}\left[\zeta_{i,j,k+0.5}^{t} C_{i,j,k}^{t}+\left(1-\zeta_{i,j,k+0.5}^{t}\right) C_{i,j,k+1}^{t}\right] \\
&+(1-d)\alpha_{wl} K_a\left(H_{DUALi,j,k}^{t+1}-H_{i,j,k}^{t+1}\right) C_{DUALi,j,k}^{t+1} V_{i,j,k}
\end{aligned}
\tag{37}
$$

$$
\begin{aligned}
&-\frac{\theta_{i,j,k-0.5}^{t+1} D_{i,j,k-0.5}^{t+1} A_{i,j,k-0.5}}{z_{i,j,k}-z_{i,j,k-1}} C_{i,j,k-1}^{t+1} \\
&+\left[\frac{\theta_{i,j,k}^{t+1} V_{i,j,k}}{\Delta t}\right. \\
&+\frac{\theta_{i+0.5,j,k}^{t+1} D_{i+0.5,j,k}^{t+1} A_{i+0.5,j,k}}{x_{i+1,j,k}-x_{i,j,k}}+\frac{\theta_{i-0.5,j,k}^{t+1} D_{i-0.5,j,k}^{t+1} A_{i-0.5,j,k}}{x_{i,j,k}-x_{i-1,j,k}} \\
&+\frac{\theta_{i,j+0.5,k}^{t+1} D_{i,j+0.5,k}^{t+1} A_{i,j+0.5,k}}{y_{i,j+1,k}-y_{i,j,k}}+\frac{\theta_{i,j-0.5,k}^{t+1} D_{i,j-0.5,k}^{t+1} A_{i,j-0.5,k}}{y_{i,j,k}-y_{i,j-1,k}} \\
&+\frac{\theta_{i,j,k+0.5}^{t+1} D_{i,j,k+0.5}^{t+1} A_{i,j,k+0.5}}{z_{i,j,k+1}-z_{i,j,k}}+\frac{\theta_{i,j,k-0.5}^{t+1} D_{i,j,k-0.5}^{t+1} A_{i,j,k-0.5}}{z_{i,j,k}-z_{i,j,k-1}} \\
&\left.+(1-d)\alpha_{wl} K_a\left(H_{i,j,k}^{t+1}-H_{DUALi,j,k}^{t+1}\right) V_{i,j,k}\right] C_{i,j,k}^{t+1} \\
&-\frac{\theta_{i,j,k+0.5}^{t+1} D_{i,j,k+0.5}^{t+1} A_{i,j,k+0.5}}{z_{i,j,k+1}-z_{i,j,k}} C_{i,j,k+1}^{t+1} \\
&=\frac{\theta_{i,j,k}^{t} V_{i,j,k}}{\Delta t} C_{i,j,k}^{t} \\
&+\frac{\theta_{i+0.5,j,k}^{t+1} D_{i+0.5,j,k}^{t+1} A_{i+0.5,j,k}}{x_{i+1,j,k}-x_{i,j,k}} C_{i+1,j,k}^{t+1} \\
&+\frac{\theta_{i-0.5,j,k}^{t+1} D_{i-0.5,j,k}^{t+1} A_{i-0.5,j,k}}{x_{i,j,k}-x_{i-1,j,k}} C_{i-1,j,k}^{t+1} \\
&+\frac{\theta_{i,j+0.5,k}^{t+1} D_{i,j+0.5,k}^{t+1} A_{i,j+0.5,k}}{y_{i,j+1,k}-y_{i,j,k}} C_{i,j+1,k}^{t+1} \\
&+\frac{\theta_{i,j-0.5,k}^{t+1} D_{i,j-0.5,k}^{t+1} A_{i,j-0.5,k}}{y_{i,j,k}-y_{i,j-1,k}} C_{i,j-1,k}^{t+1} \\
&+q_{i-0.5,j,k}^{t+1} A_{i-0.5,j,k}\left[\zeta_{i-0.5,j,k}^{t} C_{i-1,j,k}^{t}+\left(1-\zeta_{i-0.5,j,k}^{t}\right) C_{i,j,k}^{t}\right] \\
&-q_{i+0.5,j,k}^{t+1} A_{i+0.5,j,k}\left[\zeta_{i+0.5,j,k}^{t} C_{i,j,k}^{t}+\left(1-\zeta_{i+0.5,j,k}^{t}\right) C_{i+1,j,k}^{t}\right] \\
&+q_{i,j-0.5,k}^{t+1} A_{i,j-0.5,k}\left[\zeta_{i,j-0.5,k}^{t} C_{i,j-1,k}^{t}+\left(1-\zeta_{i,j-0.5,k}^{t}\right) C_{i,j,k}^{t}\right] \\
&-q_{i,j+0.5,k}^{t+1} A_{i,j+0.5,k}\left[\zeta_{i,j+0.5,k}^{t} C_{i,j,k}^{t}+\left(1-\zeta_{i,j+0.5,k}^{t}\right) C_{i,j+1,k}^{t}\right] \\
&+q_{i,j,k-0.5}^{t+1} A_{i,j,k-0.5}\left[\zeta_{i,j,k-0.5}^{t} C_{i,j,k-1}^{t}+\left(1-\zeta_{i,j,k-0.5}^{t}\right) C_{i,j,k}^{t}\right] \\
&-q_{i,j,k+0.5}^{t+1} A_{i,j,k+0.5}\left[\zeta_{i,j,k+0.5}^{t} C_{i,j,k}^{t}+\left(1-\zeta_{i,j,k+0.5}^{t}\right) C_{i,j,k+1}^{t}\right] \\
&-d\alpha_{wl} K_a\left(H_{i,j,k}^{t+1}-H_{DUALi,j,k}^{t+1}\right) V_{i,j,k} C_{DUALi,j,k}^{t+1}
\end{aligned}
\tag{38}
$$

5.1.4 Programme development

The model was programmed with Java in an object-oriented way. The distributed and iterative calculation of hydraulic head and solute concentration requires computing power and memory. To avoid long calculation times and capacity overflow, the programme was structured in five classes as described in the simplified UML (for more information on the *Unified Modelling Language* UML, see e.g. Fowler 2004) class diagram (Figure 40). The diagram presents the main components of the programme. In addition, the classes contain methods for reading data from and writing data into files, keeping track of water and solute balance, performance factors, etc.

The five classes work together so that a model can run one or multiple calculations, a calculation may contain one or two (or several) pore domains, a calculation is linked to a grid, which can also provide data directly to the pore domains, and a grid may include several soil horizons i.e. parameterisations of soil properties, related to each pore domain. The pore domains interact with each other both directly and via the calculation class, i.e., the domains may refer to each other directly or via the calculation class, to transmit the necessary data from one pore domain to another during each time step for water and solute exchange.

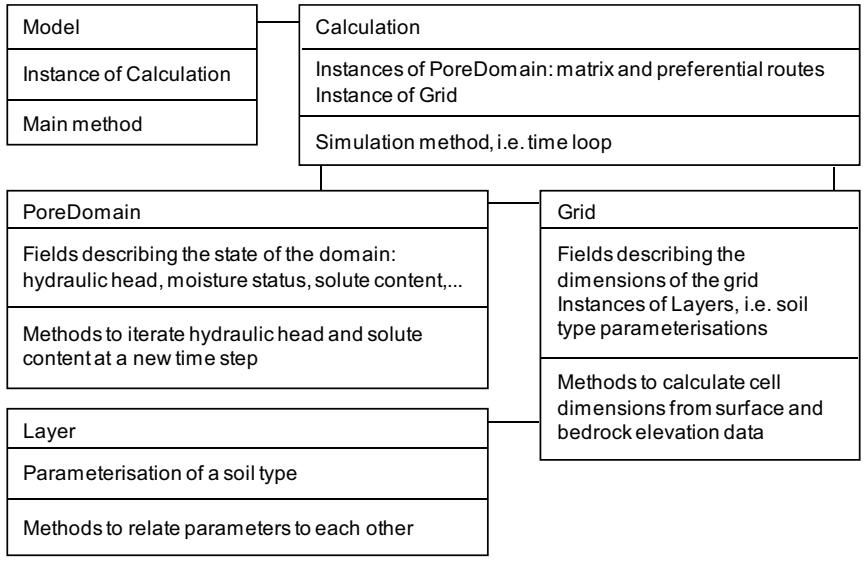

Figure 40. Simplified UML class diagram of the main components of the model programme.

In the programme, time dependent variables are stored in four-dimensional (*t, x, y, z*) matrices during a calculation. The time dimension is limited to only

three computational time steps to minimize the amount of buffer storage needed. Thus, the matrices always contain values from the time step in question and from two previous time steps. Other steps of interest are written into files.

5.1.5 Programme verification

The validity of the programme was tested during the programming process by running the code on fictitious hillslopes, with differing slope angles, grid spacing, initial moisture status, boundary conditions, parameterisation, and irrigation, and by observing water and solute mass balances of the model runs. After completing the programme code, the model was tested against analytical solutions. The Richards' equation-based flow model was tested against the one-dimensional example presented in Tracy (1995), and the solute transport model against the analytical solution of a one-dimensional step change concentration example derived by Ogata and Banks (1961, in Fetter 2001). Since the numerical model was programmed so that a pore domain was built up as its own class, tests against the analytical solution could be made for a one pore domain model: the tests verify the correctness of the calculation routines related to a pore domain class.

The analytical solution presented in Tracy (1995) applies to one-dimensional movement of water pressure. The analytical solution was compared to the numerical model of this study so that the hydraulic head was set as a constant at the initial state in two directions. This way flow occurred in one dimension even though the calculation was run in the three-dimensional mode (Figure 41).

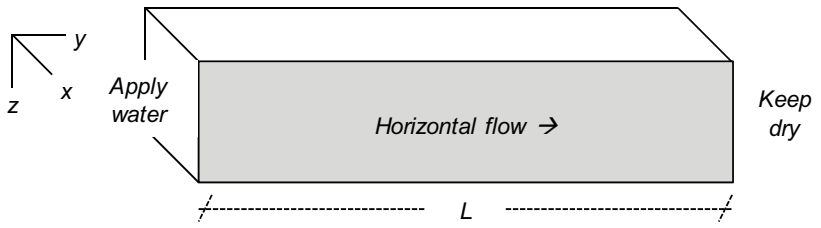

Figure 41. Set up for the analytical solution of Tracy (1995) for one-dimensional flow in a three-dimensional block.

In the solution of Tracy (1995), the initial values for the pressure head h_I [L] are determined with:

$$h_I = h_r\left[1-\frac{1}{6}\left(\frac{y-L}{L}\right)^2\right] \tag{39}$$

where h_r is the lowest possible pressure head [L], y is the distance [L], and L is the total length of the grid block in the flow direction. The pressure head in the first cell column on the left hand side, where water is applied, h_o [L], was changed, related to time according to:

$$h_0 = h_r\left(1-\frac{1}{6-5\frac{t}{T}}\right) \tag{40}$$

where t is the time [T] and T is the total calculation time [T], which is determined by:

$$T = -5L^2\frac{\theta_S-\theta_R}{6h_rK_S} \tag{41}$$

where θ_S is the water content at saturation [L^3/L^3], θ_R is the residual water content [L^3/L^3], and K_S is the hydraulic conductivity at saturation [L/T]. In the analytical solution, the time and space dependent pressure head h [L] is determined by:

$$h = h_r\left[\frac{1-\left(\frac{y-L}{L}\right)^2}{6-\frac{5t}{T}}\right] \quad . \tag{42}$$

The numerical model needed one change in order to be comparable with the analytical solution, since the water content and the hydraulic conductivity are assumed to follow linear relations in the analytical model instead of the van Genuchten model (Eq. 1, Chapter 2.3.2). Thus, in the numerical model, the water content θ [L^3/L^3] was calculated as:

$$\theta = \theta_R + \frac{\theta_S-\theta_R}{h_s-h_r}\left(h-h_r\right) \quad , \tag{43}$$

and the relative hydraulic conductivity K_R [-] as:

$$K_R = \frac{h-h_r}{h_s-h_r} \quad . \tag{44}$$

Several parameterisations were tested with the analytical and numerical models. Results related to one parameterisation (Table 5) are presented in

Figure 42. Dimensions of the given grid and the parameter values are of the same magnitude as the average values used in simulating the chloride tracer experiment in this study.

Table 5. Parameterisation of the Tracy (1995) model.

Parameter	*Value*	*Unit*
θ_R	0.05	-
θ_S	0.50	-
Δt	60	s
T	3000	s
dx, dy, dz	20	cm
h_r	-9680	cm
h_s	0	cm
K_S	0.01	cm s^{-1}
L	880	cm

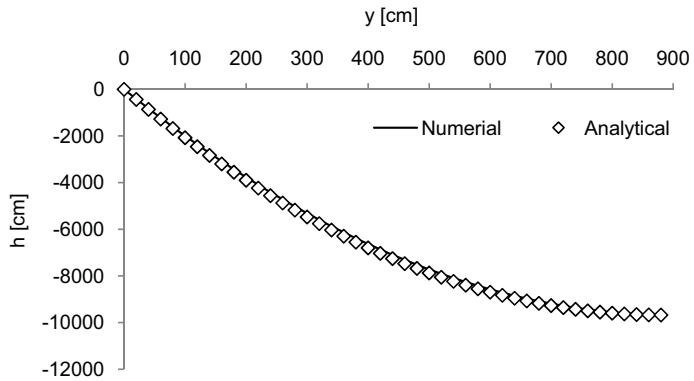

Figure 42. Analytical solution and numerical solution of the Tracy (1995) model for the pressure head *h* along the grid in the *y* direction, related to the parameterisation given in Table 5.

The coefficient of determination between the numerical solution and the analytical solution of Tracy (1995) exceeds 0.9999 (Figure 42). Thus, the programme code is verified in terms of the comparison with the Tracy (1995) model.

In testing the solute transport model, the same grid as in testing the flow model was used. In the example case of Ogata and Banks (1961, in Fetter 2001), flow velocity through the system is constant and only the concentration is changed in one time step, at one end of the system (Figure 43).

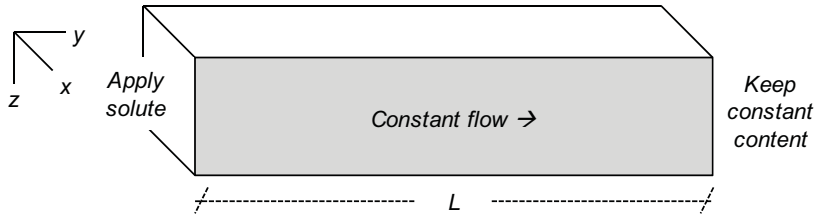

Figure 43. Set up for the analytical solution of Ogata and Banks (1961) for one-dimensional solute transport controlled by advection and dispersion in a three-dimensional block.

Initial solute concentration in the system is set to zero, and the step change in concentration at one end spreads through the system based on advection and dispersion. To create one-dimensional transport to the system, transverse dispersivity is set to zero. Concentration C [M/L^3] at different locations x [L] of the grid and at different observation time steps t [T] is determined as:

$$C = \frac{C_0}{2}\left[erfc\left(\frac{y - v_y t}{2\sqrt{\alpha_L v_y t}} \right) + \exp\left(\frac{v_y y}{\alpha_L v_y} \right) erfc\left(\frac{y + v_y t}{2\sqrt{\alpha_L v_y t}} \right) \right] \qquad (45)$$

where C_o is the new concentration [M/L^3] at location y=0, v_y is the flow velocity [L/T], and α_L is the longitudinal dispersivity [L^2/T]. The error function *erf* is a special case of the gamma function and can be written as:

$$erf(y) = 1 - \left(a_1 b + a_2 b^2 + a_3 b^3 + a_4 b^4 + a_5 b^5 \right) \exp(-y^2) \qquad (46)$$

where the term b is determined as

$$b = \left(1 + a_6 y \right)^{-1} \qquad (47)$$

Values of the coefficients a_1 to a_6 are listed in Table 6 below, together with one of the parameterisations used in testing the model. The complementary function of the error function *erfc* is calculated with:

$$erfc(y) = 1 - erf(y) \qquad (48)$$

and

$$erfc(-y) = 1 + erf(y) \qquad (49)$$

Table 6. Parameterisation of the numerical solute transport model, related to the example case of an analytical solution (Ogata and Banks 1961).

Parameter	*Value*	*Unit*
v_y	0.02	cm s^{-1}
α_L	50	cm
Δt	60	s
dx, dy, dz	20	cm
C_0	1000	µg cm^{-3} = mg l^{-1}
θ_s	0.5	cm
K_S	0.01	cm s^{-1}
a_1	0.254829592	-
a_2	-0.284496736	-
a_3	1.421413741	-
a_4	-1.453152027	-
a_5	1.061405429	-
a_6	0.3275911	-

Results of the analytical and numerical model are compared in Figure 44.

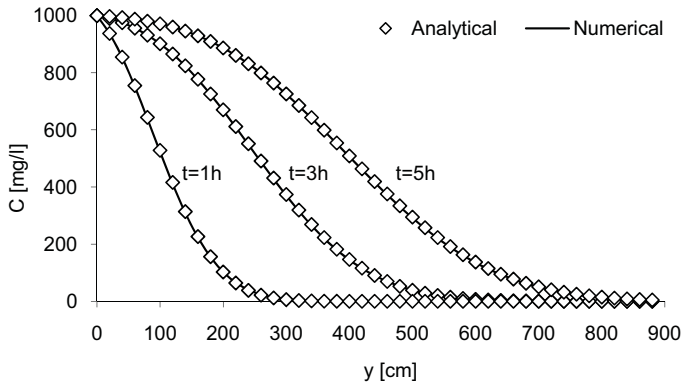

Figure 44. Analytical solution and numerical solution of the Ogata and Banks (1961) model for concentration *C* for three time points, along the test grid in the *y* direction, related to the parameterisation given in Table 6.

At each of the three time points of 1, 3 and 5 h, the coefficient of determination exceeds 0.9999. The close correspondence between the numerical and the analytical solution is guaranteed by the elimination of the numerical dispersion in the numerical model. Numerical dispersion did not exceed the actual dispersion in this example case and was fully eliminated with the correction presented in Chapter 5.1.2 (Equation 25). Water and solute mass balance errors of the numerical model are further discussed below in Chapter

5.1.7, together with the assessment of the discretisation and performance criteria for a test run.

5.1.6 Boundary conditions and model domain

The modelled area was bounded at a distance of 1.0 m above the irrigation source and 2.0 m below the maximum distance that the chloride pulse reached during the experiment (cf. e.g. Figure 26 and 35). On both the sides, the area was extended 0.7 m wider than the irrigation tube and 1.5 m wider than the well screen field. Thus, the model covered an area of 5.0 m in the *x* direction, times 9.0 m in the *y* direction, i.e. 45 m^2, in total (cf. Figure 26 b). The volume of the domain was approximately 40 m^3 as the average soil thickness was about 0.9 m. At each of the six boundaries of the model domain, the grid was surrounded with an additional layer of imaginary cells. The calculations were performed in the inner cells of the domain – the values of the state variables or fluxes from or into the imaginary cells were assumed to be known for all time steps.

For the upper and lower imaginary layer in the *z* direction (i.e. soil surface and bedrock), the hydraulic conductivity was set to zero to prevent fluxes in and out. Thus, the values of the state variables in the imaginary cells did not affect the inner cells. The chloride irrigation of the tracer experiment was inserted into the system by the source term *S* (Equation 29), into the surface cells of the columns residing below the irrigation source. All the side boundaries in the *x* and *y* directions were set partly open (cf. Neumann type boundary conditions, e.g. in Wang and Anderson 1982): fluxes out from the domain were allowed to simulate the outflow of water and chloride from the domain during the irrigation, but fluxes into the domain were not allowed. The hydraulic head in an imaginary cell at a side boundary was determined at the end of each time step, based on the head gradient between the boundary cell and the adjacent cell inside the domain:

$$H_{imaginary} = H_{boundary} - \left(H_{inside} - H_{boundary}\right) \quad , \qquad (50)$$

where $H_{imaginary}$ is the hydraulic head in the imaginary cell, $H_{boundary}$ is the hydraulic head in the boundary cell, and H_{inside} is the hydraulic head in the cell adjacent to the boundary cell inside the grid. When the difference $(H_{inside} - H_{boundary})$ was negative, the conductivity in the imaginary cell was set to zero, which resulted in no inflow. Otherwise, the conductivity in the imaginary cell was calculated based on the known head values. To simplify the calculations,

dispersion was prevented at the boundaries. Advection at the boundaries was based on the fluxes described above.

5.1.7 Performance factors, discretisation and numerical error

In addition to the comparisons between the numerical and analytical solutions (Chapter 5.1.5), three performance factors were taken into account when choosing a time step and grid spacing for the simulations. First, laminarity of flow within the domain, i.e. the applicability of Richards' equation to describe flow in the domain, was evaluated in terms of the *Reynolds number* (e.g. Airaksinen 1978):

$$Re = \frac{v_n \Delta x_n}{\nu} \quad , \tag{51}$$

where v_n is the flow velocity [L/T] in direction n (i, j or k), Δx_n is the characteristic length [L] in direction n, and ν is the kinematic viscosity of water [L^2/T]. For the kinematic viscosity, a constant value of 1.31E-2 cm^2/s was used since the average temperature of the soil water during the chloride tracer experiment was 10 °C. To ensure laminar flow, the Reynolds number should be less than 10. The characteristic length influences the value of the Reynolds number.

The *Courant number* (e.g. Rausch et al. 2005)

$$Co = \frac{v_n \Delta t}{\Delta x_n} \quad , \tag{52}$$

was used for assessing the time step length Δt [T] in relation to the grid spacing Δx_n. In the equation, v_n is the flow velocity [L/T] in direction n. To minimize numerical dispersion and to avoid problems with stability of the solution, the Courant number should be near 1. If the Courant number is remarkably higher, the solution of the flow model may turn unstable. If the Courant number is remarkably smaller, numerical dispersion may grow higher than the physical dispersion. Magnitude of the numerical dispersion was also observed though the *Peclet number* (e.g. Rausch et al. 2005):

$$Pe = \frac{\Delta x_n}{\alpha_L} \quad , \tag{53}$$

where Δx_n is flow distance [L] and α_L is the longitudinal dispersivity [L]. If the Peclet number is smaller than 2, real dispersion is larger than the numerical

dispersion, and the numerical dispersion can be corrected by subtracting the numerical dispersion from the physical dispersion.

The highest and lowest values of the performance criteria in the grid were recorded at each time step. In order to keep the Peclet number, as well as the Reynolds number low, the grid spacing should be dense. A denser grid translates, however, into longer calculation times as the amount of grid cells increase. A long time step helps to limit the calculation time, but it may result in instability issues noted above. Also, when simulating the intensive chloride tracer experiment of this study and using a long time step, the amount of the irrigation to be fed into a surface grid cell, may exceed the pore volume of that cell, which easily restrains the convergence of the calculation. Taking into account the performance factors on one hand, and the calculation time on the other, most of the simulations were performed with a time step of 60 s and a grid spacing from about 10 to 20 cm on average in the vertical direction z, and with a spacing of 20 cm on average in the slope transversal direction x and longitudinal direction y.

The model grid was created by interpolating the bedrock and soil surface from the vertical survey and soil depth data related to the observation wells. In the x direction, the grid consisted of 25 cells and in the y direction of 45 cells with the grid spacing of 20 cm. In the vertical direction z, the soil profile was divided into five layers. Thickness of the E, B and BC layers corresponded directly to the mean thickness of each of the horizons, and the remarkably thicker subsoil horizon C was divided into two layers. The variation in the soil profile thickness was taken into account by adjusting the thickness of the subsoil layers in the grid. To simulate the chloride tracer experiment of seven hours with the 60 s time step and in the altogether 5625 grid cells, both the flow and transport equations needed to be solved nearly 1.2 million times per a run. Depending on the parameterisation and iteration criteria used, the amount of iterations needed in finding the solution for one time step could exceed 300 in the flow model and 20 in the solute transport model at the end of the irrigation period.

To verify the suitability of the grid spacing and time step, performance factors are analysed below for a test run that contains extreme parameter values that change with depth (Table 7) and a clear head gradient in the slope at the initial state (cf. Figure 32). At the initial state, a constant value was set for the hydraulic head within the dry, lower section of the slope so that the minimum pressure head value was -345 cm. Within the upper slope section, the pressure head was set to a value of -65, -59, -50, and -35 cm in the E, B, BC, and C horizons, respectively, to emulate the average pressure head gradient

prevailing in the slope prior to the chloride irrigation (cf. Chapter 4.1.2, 4.1.3). Between the wetter and drier slope sections, the pressure head was set to change linearly. The test run covered the same time span of about seven hours as the observations in the field. In assessing the test run, values of the performance criteria were not taken into account for the cells where the irrigation was fed into.

Table 7. Parameterisation of a test run using extreme values. Near soil surface, water retention capacity is low and saturated hydraulic conductivity high, near bedrock vice versa. The magnitude of the parameter values are based on the measurements and computational estimates available (Chapter 2.3, Chapter 4.3.2).

Soil horizon	α [cm^{-1}]	β [-]	θ_R [-]	θ_S [-]	K_S [cms^{-1}]	α^* [cm^2s^{-1}]	α_L [cm]	α_T [cm]
E	0.08	1.4	0.0	0.32	4E-2	1E-6	50	5
B	0.04	1.5	0.0	0.32	2E-2	1E-6	50	5
BC	0.02	1.6	0.0	0.32	4E-3	1E-6	50	5
C	0.01	1.7	0.0	0.32	2E-3	1E-6	50	5

For the test run, the Reynolds number exceeded the limit for laminar flow, 10, in the downslope direction y. The limit was exceeded in the cells adjacent to the cells where the irrigation was fed into and it rose up to a maximum value of 23. The Courant number stayed clearly below the limit of 1 and the Peclet number clearly below the limit of 2 during the whole run inside the whole grid. Numerical dispersion was for all time steps and all cells lower than the real dispersion, and numerical dispersion could be eliminated as described in Chapter 5.1.2, Eq. 25. The total water volume and mass of the solute within the model domain, as well as the amount of water and solute flowing out from the domain were recorded for each time step. During the test run, both the water and solute mass balance errors were of magnitude 10^{-3} % (0.0019 % of water and 0.0010 % of solute was lost), when the convergence criterion of the iterations was set to 0.0001 cm in solving the flow model (hydraulic head) and 0.0001 μgcm^{-3} in solving the solute transport model (concentration). Considering only the time after irrigation was stopped, the water balance error was of magnitude 10^{-4} % and the solute mass balance error 10^{-7} %. The magnitude of the water and solute mass balance error grew in relation to the irrigation intensity and amount of iterations needed to solve the flow and solute transport equations during each calculation step.

Increasing the grid density by a factor of two in each direction multiplied the time required for running the model by a factor of eight, when the convergence criteria were kept at 0.0001 cm and 0.0001 μgcm^{-3}. Reducing the time step

additionally to one third of the original, i.e. to 20 s, not changing the iteration criteria, multiplied the time required for running the model by a factor of 16. The denser grid lowered the maximum values of the Reynolds number, when the characteristic length was based on the cell dimensions. At the cost of a longer calculation time, the maximum value of the Reynolds number dropped to 13.5 in the y direction. The shorter time step did not improve the values of the performance criteria. To conclude, most of the simulations were performed with the time step of 60 s and with the average grid spacing of 20 cm, accepting an excessively high Reynolds number nearby the irrigation source cells, and accepting a maximum water and solute balance error of about 0.001 %. To demonstrate the effect of a denser grid and a shorter time step on the flow and solute transport results, one of the model versions was run with a grid composing of two separate layers in the E, B and BC horizons, and three layers in the C horizon, and a time step of 20 s (Chapter 5.2.5).

5.1.8 Initial state, principles for parameterisation and evaluation of the model results

Most of the simulations were restricted to cover the seven hour observation period of the chloride tracer experiment. The initial irrigation with tracer-free water a day before the experiment was not included in the first simulations in order to keep the calculation time as short as possible, and to be able to concentrate on investigating the parameterisation required for the initiation, steady-state, and recession stages of the observed, subsurface stormflow event. The effect of the initial irrigation period on the model results was investigated at the end with one of the final model versions (Chapter 5.2.6). Estimates of the initial state were based on measured soil moisture values (cf. Chapter 4.1.2). Use of a warm-up period at the beginning of the simulations was not possible because of a long calculation time and processes required in longer simulations. The model did not contain, for instance, the simulation of root water uptake and evapotranspiration.

Estimates of the initial state are given in Table 8 (cf. Chapter 4.1.2). The moist upper slope section was estimated to be at least at the field capacity at the beginning of the tracer irrigation. Between the moistened and dry slope sections, the degree of saturation was estimated to drop linearly. Depending on the definition used for a macropore (cf. Chapter 2.3.4), and assuming the moisture conditions described in Chapter 4.1.3 for the beginning of the tracer irrigation, 30-65 % of the irrigation volume is needed to saturate the soil matrix and 35-70 % the preferential flowpaths.

Table 8. Range of variation and average values (in brackets) of the estimates of the degree of saturation and the corresponding pressure head values in the initial state of the simulations, based on the average water retention data (cf. Chapter 2.3.2). Moist estimates are used for the upper slope section and dry estimates for the lower slope section, when the calculation is started from the beginning of the chloride tracer experiment. Dry estimates are used for the whole slope, when the initial irrigation period is included in the simulation.

Soil horizon	$S_{r\,Moist}$ *[-]*	$S_{r\,Dry}$ *[-]*	h_{Moist} *[cm]*	h_{Dry} *[cm]*
E	0.50 – 0.78 (0.64)	0.25 – 0.33 (0.29)	-100 – -30 (-65)	-428 – -244 (-336)
B	0.70 – 0.88 (0.79)	0.38 – 0.45 (0.42)	-90 – -28 (-59)	-615 – -374 (-495)
BC	0.67 – 0.91 (0.79)	0.27 – 0.33 (0.30)	-75 – -25 (-50)	-348 – -258 (-303)
C	0.84 – 0.96 (0.90)	0.33 – 0.39 (0.36)	-50 – -20 (-35)	-278 – -221 (-250)
Mean	0.68 – 0.88 (0.78)	0.31 – 0.38 (0.35)	-79 – -26 (-52)	-417 – -274 (-346)

The model was parameterised based on the results of the soil analysis (Chapter 2.3.2 - 2.3.4) and the inverse one-dimensional model application (Chapter 4.2.3). Corresponding to the podzol profile, both the one and the two domain models were parameterised soil horizon-wise. In the two domain case, each soil horizon was separately parameterised for the soil matrix and the preferential flow domain. The model parameters include the water retention parameters of the van Genuchten model (α, β, θ_R, and θ_S, Equation 1), the saturated hydraulic conductivity (K_S, Equation 12), and the diffusion, longitudinal and transverse dispersivity coefficients (α^*, α_L, and α_T, respectively, Equation 17). The exchange coefficient (α_{wl}, Equation 32) was introduced in the dual-permeability model for simulating water and solute exchange between the two pore domains.

In the one pore domain model, the average van Genuchten parameter values were used so that stones were taken into account by lowering the values of the porosity parameters in relation to the stone content of soil at different depths (Chapter 2.2.1, Table 1 and Figure 11 in Chapter 2.3.2). The saturated hydraulic conductivity values were selected from the results of the one-dimensional groundwater model (Figure 38 in Chapter 4.2.3). The diffusivity, and longitudinal and transverse dispersivity were assessed based on the literature. Diffusivity was given a constant value of 10^{-6} cm^2. The longitudinal dispersivity was assessed using the rule presented in Spitz and Moreno (1996), according to which the longitudinal dispersivity is about 10 % of the total travel distance.

Hence, the longitudinal dispersivity was estimated to be 10 % of the travel distance of chloride solution in the tracer experiment of this study. The transverse dispersivity is reported to vary from 1 to 30 % of the longitudinal dispersion (e.g. Klotz and Seiler 1980, Pickens and Grisak 1980, in Rausch et al. 2005), and it was given a value of 10 % of the longitudinal dispersivity. Since the chloride transport was dominated by advection in the tracer experiment, same dispersivity coefficients were used in all soil horizons for simplicity.

In the two pore domain model, parameters of the gently sloping water retention curves were assigned to the preferential flowroutes, and parameters of the sharp curves to the soil matrix (Table 2 and 3, Figure 13 and 14 in Chapter 2.3.2). Laboratory results of the saturated hydraulic conductivity were set to the soil matrix, and results of the one-dimensional groundwater model to the preferential routes (Figure 15 b in Chapter 2.3.3, Figure 38 in Chapter 4.2.3). Saturated hydraulic conductivity of the preferential flow domain was also given higher values than available from any measurements, depending on the pore space allocated to the preferential flow routes, the value of the exchange coefficient, and the initial state. The diffusivity was given a constant value of 10^{-6} cm^2 for both pore domains. In the preferential flow domain, the longitudinal dispersivity was estimated to be 10 % of the travel distance of chloride solution in the tracer experiment, and the transverse dispersivity was given an estimate of 10 % of the longitudinal dispersivity, similarly to the one pore domain model. For the soil matrix, the longitudinal and transverse dispersivity were set to 10 % of the values used in the preferential flow domain. The same values were used for the dispersivity coefficients in all soil horizons.

Both in the one and two pore domain models, the van Genuchten parameters, the total porosity, and the diffusivity and dispersivity coefficients were *a priori* fixed. In the two pore domain model, also the saturated hydraulic conductivity of the soil matrix was fixed. Although the small, partly disturbed water retention samples presumably give an erroneous conception of the water retention properties on the hillslope scale, these parameters were fixed, since the study focuses on saturated or near saturated conditions, and the phenomenon is not as sensitive to the water retention values as to the other parameters. In addition, no data were available to produce any other estimates for the water retention parameters, and the intensive tracer data on subsurface stormflow does not support any detailed assessments of the water retention parameters used.

The parameters that were based on measurements but allowed adjustments or calibration were the saturated hydraulic conductivity of the preferential flow

domain and the porosity of the preferential flow domain in relation to the porosity of the soil matrix. The total porosity was assumed to be known based on the water retention and stone content data. The only unknown parameter without any direct estimates based on measurements was the exchange coefficient between the pore domains (α_{wl}, Equation 32). Limits for the value of the exchange coefficient were evaluated in relation to different values of the saturated hydraulic conductivity of the preferential flowroutes and to fractioning of the pore space between the soil matrix and the preferential flow domain. In addition to the changes in these parameters, irrigation fed into each pore domain was changed in different model runs. If the exchange coefficient was small, the exchange of water and solutes between the systems was also small, and the amount of irrigation fed into each of the domains affected the model outcome. With high values of the exchange coefficient, water and solute were rapidly mixed already in the cells where the irrigation was fed into, and the value did not affect the results.

The main criteria for assessing the goodness of fit of the model results and the suitability of the model versions to describe the phenomenon were the *Nash-Sutcliffe model efficiency coefficient,* R_{eff}, and the *coefficient of determination*, R^2, between the observed and simulated chloride concentration values along the middle line of the study slope at two time points (Figure 26 b, 27, 35, 36). In addition to evaluating the two criteria of goodness of fit, the shape and the location of the saturation front and chloride plume were visually examined. The two measures describe the goodness of fit from different viewpoints. The coefficient of determination describes the proportion of the variance of the measured data that the modelled values explain, whereas the Nash-Sutcliffe efficiency coefficient is a dimensionless transformation of the sum of squared errors, accounts for the systematic bias in the modelled series, and is widely used in hydrological model applications (e.g. Seibert 1999).

The use of the concentration data as the evaluation criterion aimed at demonstrating the usability and importance of the tracer data for the model development and identifiability (cf. Chapter 1.2). The goodness of fit measures were calculated by comparing the observed and simulated chloride concentrations at each point of the two-dimensional grid (lateral cross-section of the soil column along the middle line of the study slope). In the case of the one pore domain model, chloride concentrations simulated in the only one pore domain of the model were used in the comparison. In the case of the two pore domain model, chloride concentrations simulated for the preferential flow domain were used in the comparison, since the concentration data were

considered to mainly represent the water flowing in the larger soil pores (cf. Chapter 4.1.1, 4.2.1, 4.2.2).

In addition to presenting the model development process based on the measured and simulated chloride concentrations in the preferential flow domain along the middle line of the study slope (Chapters 5.3.1-5.3.3), chloride concentration in the soil matrix as well as groundwater levels of both the pore domains along the middle line are presented in Chapter 5.2.4, as predicted with the best dual-permeability model found in this study. The solute mass balance of the entire 3D calculation grid is also presented in Chapter 5.2.4, as predicted with the best dual-permeability model, to further describe the characteristics of the two pore domain system.

The two-dimensional, interpolated concentration data from the middle line observation wells were considered most suitable for the model development for several reasons. First, the data represent the maximal transport along the slope during the observed stormflow event. Second, the representativeness of the data is more transparent than that of the side line wells. As noted above and in Chapter 4.1.1, 4.2.1 and 4.2.2, the data of the middle line wells clearly represent water in the preferential flowroutes in particular during the irrigation, whereas the data from the side line wells represent more an unknown mixture of matrix water and macropore water. Third, the data from the middle line wells are more comprehensive, because on the sides the water table did not rise as high as in the middle line wells and the saturated period did not last as long, which lead into a small amount of recorded concentration values that mainly represent the subsoil. Thus, the data available from the study slope do not support a direct and unambiguous three-dimensional comparison with the model results, even though a three-dimensional model is needed in describing the spreading of the irrigated tracer plume in the slope.

Two time points were selected for closer evaluation, 13:00 and 15:10 (cf. Figure 36). At the first time point at 13:00, the irrigation has been running for 1 h 20 min and the time point represents the maximal tracer concentration in the preferential flow domain in the slope, as the irrigation is about to be changed into pure water. In addition, the migration velocity of the plume is at its highest during the 1 h 20 min, since the plume is flowing downhill in the upper section of the slope, where the initial moisture content was high due to the initial irrigation one day prior to the experiment. At the second time point at 15:10, irrigation has been running for 3 h 30 min and the front has reached the drier slope section. The second time point represents the maximal transport and dilution in the preferential flow domain, as well as the loss of water and solute into the soil matrix, as the irrigation is about to be stopped.

The set of structurally different model versions with different parameterisations were considered hypotheses of how the subsurface system works under the recorded stormflow event (cf. Beven 2008). The resulting model outcomes were compared with each other to investigate the model structure against the experimental data, and vice versa. The results are partly discussed already in Chapter 5.2 to justify the choice of the next model version presented. The model was rather developed for investigative than for predictive or operational use. The model development process thereby followed the loop presented in Refsgaard and Henriksen (2004), reproduced from Schlesinger et al. (1979), where analysis of the observed reality leads to a conceptual model, leading to a model code, leading to a model set-up and simulations, which close the loop with the comparison with the observation of reality. Thus, the study did not only concentrate on searching for a parameter set that produces the highest goodness of fit, did not follow the traditional procedures for calibrating and validating a model for predictive use (cf. e.g. Klemes 1986, Refsgaard 2000), and did not apply pre-defined uncertainty analyses such as the GLUE procedure (Beven and Binley 1992).

5.2 Results

5.2.1 Simulation of the total pore space with a one pore domain model

The first model developed was a traditional one pore domain model, where the whole soil pore space is simulated as a single storage. Based on the soil analysis (Chapter 2.2 and 2.3), the results of the inverse one-dimensional model application (Chapter 4.2.3 and 4.3.2), and reference studies available (e.g. Lind and Lundin 1990, Buttle and House 1997, James et al. 2010) it is evident that the estimates available for the saturated hydraulic conductivity from the soil analysis cannot produce the flow velocities that were observed in the field during the chloride tracer experiment.

As described in Chapter 5.1.8, simulation of the tracer experiment was started by parameterising the one pore domain model with the average values of the saturated hydraulic conductivity that were calibrated with the one-dimensional groundwater model (Figure 38 in Chapter 4.2.3). The water retention parameters were set to the average values presented in Table 1 (Chapter 2.3.2), so that the volumetric fraction of stones was reduced from the residual and saturated water contents. For diffusivity, longitudinal and

transverse dispersivity, constant values were used as described in Chapter 5.1.8. The resulting parameterisation is presented in Table 9.

Table 9. Parameterisation of the one pore domain model with average water retention parameters, and average or maximum saturated hydraulic conductivity of each soil horizon, related to the one-dimensional, inverse model application.

Soil hor.	α [cm^{-1}]	β [-]	θ_R [-]	θ_S [-]	$K_{S\,mean}$ [cm s^{-1}]	$K_{S\,max}$ [cm s^{-1}]	α^* [cm^2 s^{-1}]	α_L [cm]	α_T [cm]
E	0.036	1.504	0.000	0.324	2.9E-2	4.0E-2	1E-6	50	5
B	0.025	1.353	0.001	0.331	1.6E-2	2.3E-2	1E-6	50	5
BC	0.018	1.708	0.000	0.328	9.9E-3	1.5E-2	1E-6	50	5
C	0.013	1.813	0.000	0.305	5.6E-3	1.0E-2	1E-6	50	5

Using the time step of 60 s and the average grid spacing of 20 cm (cf. Chapter 5.1.7) and the parameter set presented in Table 9, the simulation produces the plume presented in Figure 45, with two estimates of the initial state.

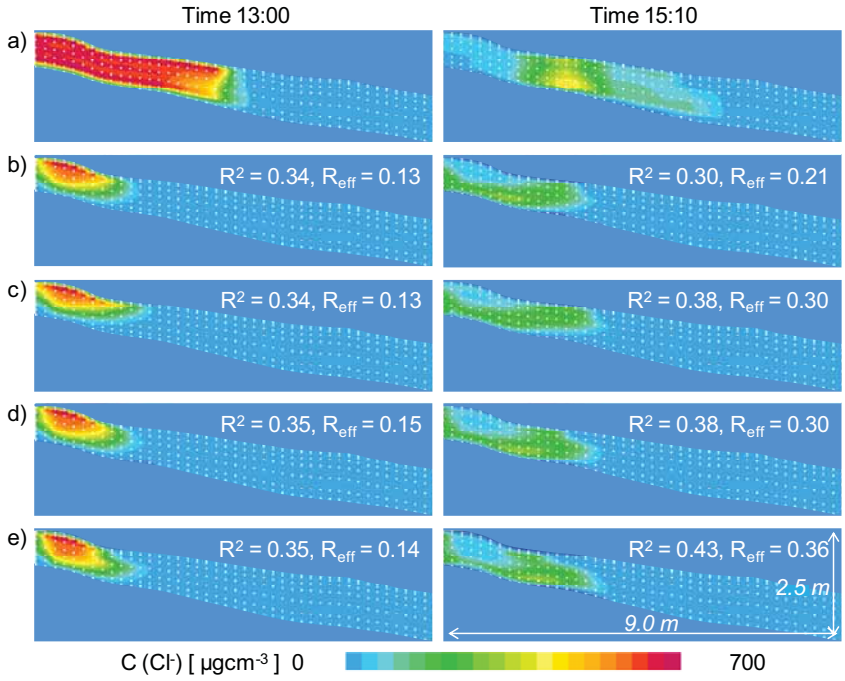

Figure 45. Observed chloride plume at two time points (a), modelled plume related to the parameterisation of Table 9, with the average estimate of the saturated hydraulic conductivity ($K_{S\,mean}$) and for the initial state (b), with the average estimate of the saturated hydraulic conductivity and with the highest estimate of the initial state (c), with the highest estimate of the saturated hydraulic conductivity ($K_{S\,max}$) and the initial state (d), and with the highest estimate of the saturated hydraulic conductivity multiplied by 1.5 and with the highest estimate of the initial state (e).

The first initial state used represents the estimated, average moisture content in the slope, and the second one the highest estimate of the upper slope section and lowest estimate of the lower section that results in a high moisture gradient along the slope (Table 8 in Chapter 5.1.8).

In Figure 45, the modelled plume is presented below the observed plume for two time points (cf. Chapter 4.2.2, Figure 36, and Chapter 5.1.8). The observed plume (Figure 45 a) describes water and chloride in the well screens along the middle line of the experimental field, i.e., in the preferential flowpaths along the middle line (cf. Chapter 4.1.1, 4.2.1, 4.2.2, 5.1.8), whereas the modelled plume is calculated with the one pore domain model that accounts for the total pore space of soil. This leads into the mismatch between the observed and modelled plumes. At the first time point at 13:00, the modelled salt water front is about 200 cm behind the observed front, and at the second time point at 15:10, about 250 cm behind the observed front. The correspondence between the modelled and observed concentration is poor regardless of the initial state or saturated hydraulic conductivity used (cf. Figure 45 a to e). The R^2 value is only 0.34-0.35 at the first and 0.30-0.43 at the second time point, and the R_{eff} value is only 0.13-0.15 at the first and 0.21-0.36 at the second time point. Higher saturated hydraulic conductivities and higher initial soil moisture conditions improve the model result mainly for the second time point.

The slow, simulated flow velocity and the low, simulated concentration are a consequence of simulating the whole pore domain of soil. As the dye and chloride tracer experiments indicate (Chapter 3.3 and 4.3), only a portion of the total pore volume is able to transport water and solute fast, and the remaining part of the pore volume functions more as storage for water and solutes. Averaging a similar flow to all the pores leads into a too slow transport for the chloride plume as seen in Figure 45. In general, the flow and transport velocity can be increased with higher values of the saturated hydraulic conductivity, by raising the initial soil moisture content and moisture gradient downslope, and by restricting the flow to only a portion of the total pore space. According to several test runs (not shown), and as the results in Figure 45 imply, the effect of higher conductivity values on the transport velocity is in this case minor: As the conductivity values grow, the irrigation intensity is not enough to saturate the E and B horizons, and the potential, maximum velocity is not reached. Also, higher conductivity values do not increase the chloride concentrations.

Thus, the only way to obtain a higher migration velocity for the salt water front in the one pore domain model is to limit the simulations to a fraction of the total pore space that contributes actively to the runoff generation and to the

formation of preferential flow. The term active pore space is used in this study to describe this fraction of the pore space instead of the concept of effective porosity, since effective porosity was defined earlier in this study as the difference between saturated porosity and porosity corresponding to a pressure head of -100 cm (Chapter 2.3.4). In addition to limiting the simulations to an active pore domain, the downhill migrating plume can be modified further by fine-tuning the model parameters and the initial moisture status in the soil profile.

5.2.2 Simulation of the active pore space with a one pore domain model

The search for the porosity of the active pore domain was started by using linearly decreasing porosity values that were of the same magnitude as the average storage coefficients used in the one-dimensional, inverse calibration of saturated hydraulic conductivity (Table 4 in Chapter 4.1.4). Similarly to simulating the total pore domain (Chapter 5.2.1), average and maximum values available from the inverse model application were used for the saturated hydraulic conductivity, and the average estimate and the estimate with a high pressure head gradient were used for the initial state (cf. Table 8 in Chapter 5.1.8). For the water retention parameters, the gently sloping curves, appointed for the preferential flowroutes were used (cf. Table 2 and 3, Figure 13 and 14 in Chapter 2.3.2) as described in Chapter 5.1.8. The resulting parameterisation is presented in Table 10. As noted in Chapter 5.1.8, at least 30 % of the irrigation is needed to saturate the soil matrix. Therefore, 70 % of the irrigation was fed into the active pore domain (Chapter 5.1.8).

Table 10. Parameterisation of the one pore domain model, when simulating an active pore space fraction, using gently sloping water retention curves, linearly decreasing porosity values, and two estimates of the saturated hydraulic conductivity, available from the inverse model application.

Soil hor.	α [cm^{-1}]	β [-]	θ_R [-]	θ_S [-]	$K_{S\,mean}$ [$cm\ s^{-1}$]	$K_{S\,max}$ [$cm\ s^{-1}$]	α^* [$cm^2\ s^{-1}$]	α_L [cm]	α_T [cm]
E	0.080	1.380	0.000	0.130	2.9E-2	4.0E-2	1E-6	50	5
B	0.039	1.375	0.000	0.110	1.6E-2	2.3E-2	1E-6	50	5
BC	0.032	1.440	0.000	0.090	9.9E-3	1.5E-2	1E-6	50	5
C	0.025	1.544	0.000	0.070	5.6E-3	1.0E-2	1E-6	50	5

The results show (Figure 46) that both the velocity and concentration of the tracer plume improved clearly compared to modelling the total pore domain (Figure 45 in Chapter 5.2.1): The R^2 value rose from 0.34-0.35 to 0.62-0.74 for

the first, and from 0.30-0.43 to 0.37-0.59 for the second time point, and the R_{eff} value rose from 0.13-0.15 to 0.53-0.68 for the first, and from 0.21-0.36 to 0.32-0.56 for the second time point. However, to reach the observed flow velocity, all of the irrigation needed to be fed into the modelled, active pore domain (Figure 46 e). This means that no water is left to flow into the soil matrix, and the soil matrix does not moisten at all.

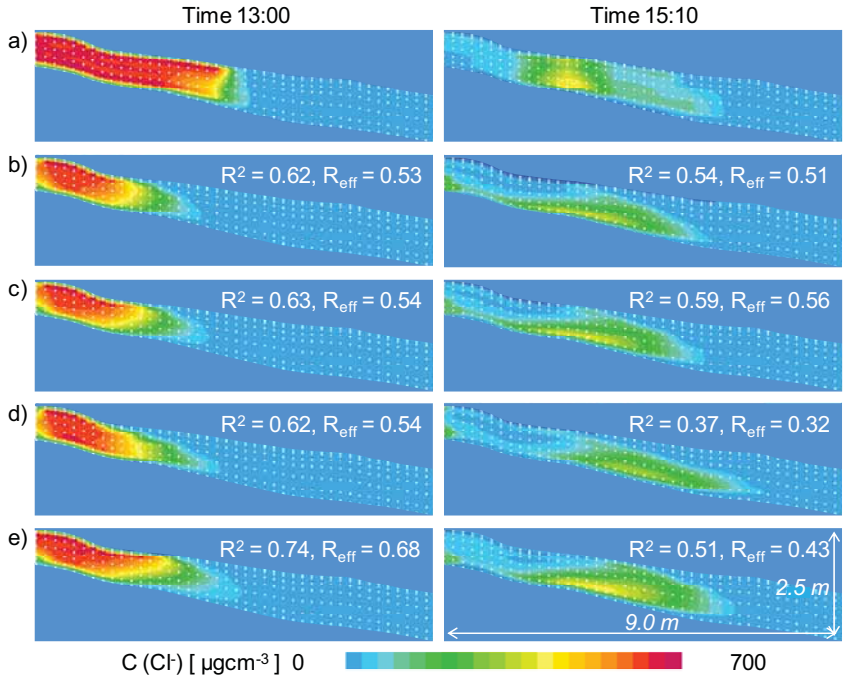

Figure 46. Observed chloride plume at two time points (a), modelled plume when 70 % of the irrigation is fed into the modelled domain, and the parameterisation of Table 10 is used, with the average estimate of the saturated hydraulic conductivity ($K_{S\ mean}$) and of the initial state (b), with the average estimate of the saturated hydraulic conductivity and with the highest estimate of the initial state (c), with the highest estimate of the saturated hydraulic conductivity ($K_{S\ max}$) and initial state (d), and with the average estimate of the saturated hydraulic conductivity and the highest estimate of the initial state, and by feeding 100 % of the irrigation into the modelled domain (e).

Even though the simulated tracer front reached the migration velocity of the observed front, the concentration of the simulated front does not correspond to the observed concentrations (Figure 46 e). The concentration at the first time point is too low, because the flow velocity is too low to push the old, salt-free water further downslope fast enough. Also, all of the salt-free water that was in the modelled pore domain at the beginning of the tracer irrigation remains in the domain, when no transfer of the water into the soil matrix is possible in the one pore domain model. Unlike in the first time point, the

concentration at the second time point is too high, because the tracer fed into the modelled domain remains in the domain. Thus, the results imply that a pore domain model cannot produce the observed tracer plume because it cannot capture the mechanism that exchanges water and solute between the large and small soil pores in changing moisture conditions. Also, the porosity estimates of the active pore domain given in Table 10 are probably too high, since all the irrigation is needed in saturating the modelled active pore domain.

To improve the results related to a one pore domain model, applied to an active fraction of the total pore space, lower estimates are needed for the modelled porosity in order to lower the irrigation amount fed into the modelled domain. In addition, to improve the shape of the plume and the location of the maximum chloride concentration of the second time point, the previous results (Figure 46) imply that the porosity should decrease in a non-linear manner with depth. Table 11 shows the parameterisation used for the next model version.

Reflected against the average water retention data (Table 1 in Chapter 2.3.2), the porosity values used (Table 11) correspond to an estimate of 67-88 µm for a macropore, and reflected against the most gently sloping water retention data (Table 2 and 3 in Chapter 2.3.2) the porosity values correspond to an estimate of 111-133 µm for a macropore, based on Equation 2 (Chapter 2.3.4). The inverse model application presented in Chapter 4.1.4 was used in searching for suitable, adjusted estimates of the saturated hydraulic conductivity, with the porosity estimates given (Table 11). For the initial state, only the average estimate was used (Chapter 5.1.8), because the high moisture estimates were not considered possible with increasing hydraulic conductivity values and gently sloping water retention curves. A 50 and a 60 % share of the irrigation was used for the active pore domain.

Table 11. Parameterisation of the one pore domain model, when simulating an active pore space fraction, using gently sloping water retention curves, non-linearly decreasing porosity values and two estimates of the saturated hydraulic conductivity, available from the inverse model application.

Soil hor.	α [cm^{-1}]	β [-]	θ_R [-]	θ_S [-]	K_{S1} [$cm\ s^{-1}$]	K_{S2} [$cm\ s^{-1}$]	α^* [$cm^2\ s^{-1}$]	α_L [cm]	α_T [cm]
E	0.080	1.380	0.000	0.090	2.5E-2	4.5E-2	1E-6	50	5
B	0.039	1.375	0.000	0.060	1.2E-2	1.0E-2	1E-6	50	5
BC	0.032	1.440	0.000	0.045	5.0E-3	3.5E-3	1E-6	50	5
C	0.025	1.544	0.000	0.035	2.8E-3	3.0E-3	1E-6	50	5

In terms of the R^2, Figure 47 shows a clear improvement in the results as compared with the two earlier model versions (Figure 45 in Chapter 5.2.1, Figure 46). Compared with the results in Figure 46, R^2 rises from 0.62-0.74 to 0.75-0.85 for the first, and from 0.37-0.59 to 0.48-0.59 for the second time point. In terms of the R_{eff}, the model presented in Figure 47 is better for the first but worse for the second time point, the value of R_{eff} rising from 0.53-0.68 to 0.69-0.81 for the first, and dropping from 0.32-0.56 to 0.21-0.44 for the second time point. The R_{eff} value captures more of the mismatch between the measured and modelled chloride concentration at second time point.

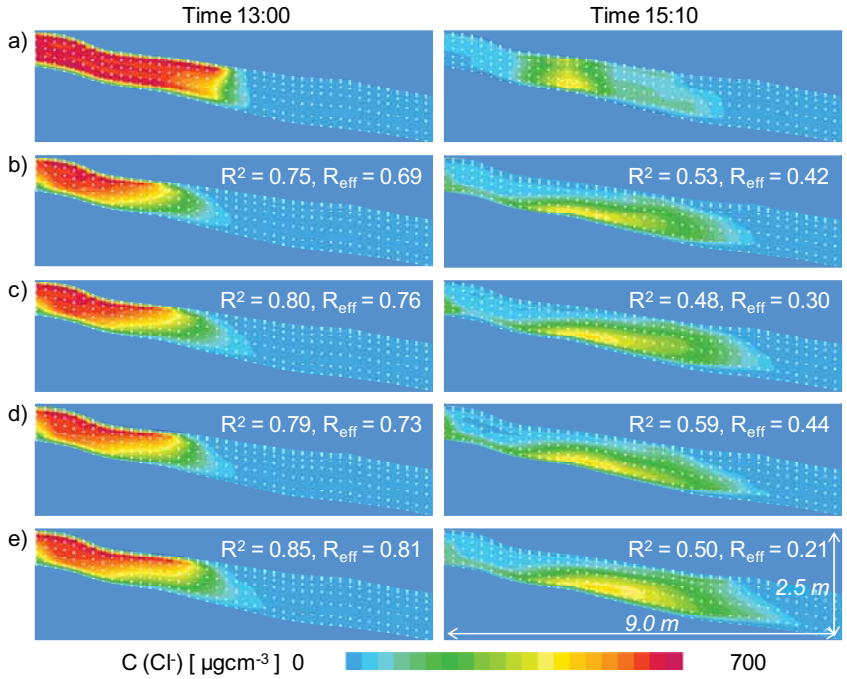

Figure 47. Observed chloride plume at two time points (a), modelled plume related to the parameterisation of Table 11, using the saturated hydraulic conductivity K_{S1} and feeding 50 % of the irrigation into the modelled domain (b), using the saturated hydraulic conductivity K_{S1} and feeding 60 % of the irrigation into the modelled domain (c), using the saturated hydraulic conductivity K_{S2} and feeding 50 % of the irrigation into the modelled domain (d), and using the saturated hydraulic conductivity K_{S2} and feeding 60 % of the irrigation into the modelled domain.

Considering both the goodness of fit measures, the velocity of the front as well as the concentration in general improved for both the time points as compared with the earlier model versions (Figure 45 in Chapter 5.2.1, Figure 46). As expected, the changes in the parameterisation were not able to remove the problems of too much fresh water remaining in the system at the first time point, and too much salt remaining in the system at the second time point.

Thus, the new parameterisation was only able to produce a better shape for the plume and move the location of the maximum, modelled chloride concentration closer to the observed location at the second time point.

The results in Figure 47 also indicate that the changes made in the irrigation amount and saturated hydraulic conductivity cannot improve the results for both the time points at the same time. The more non-linearly dropping estimates of the saturated hydraulic conductivities produce better results for both the time points. However, a better correspondence between the observed and modelled chloride concentration is obtained for the first time point with the higher irrigation amount (Figure 47 c and e), for the second time point with the lower irrigation amount (Figure 47 b and d). This demonstrates the importance of taking into account the exchange of water and solute between the large and small soil pores in changing moisture conditions.

The results presented so far show, together with hundreds of other, similar test runs (not shown) that the model results cannot be further improved for both the time points at the same time through changes in parameterisation and initial state. To further improve the outcome of the one pore domain model, the model would need a structural change, e.g. a sink term that describes the loss of water and salt into the soil matrix, as the saltwater front reaches the dry reaches of the slope. The loss cannot be taken into account by reducing the irrigation amount fed into the active pore domain, because the dilution of the solution is too slow already with the irrigation amount used so far.

Even though a sink term in the cells of the lower part of the slope would improve the model outcome, the observed chloride concentration would be very difficult to reach. The loss of water to the soil matrix is not constant, but depends on the moisture conditions (e.g. Jarvis 2007). Therefore, modelling was continued with the two pore domain version that enables a parallel and coupled simulation of the slow and fast flow regimes. The two pore domain model developed was a dual-permeability model to enable a slow flow between the soil pores of the soil matrix. On the other hand, as a simplification of the dual-permeability approach, a dual-porosity option is directly built in the dual-permeability model.

Before moving into the dual-permeability modelling it is to be noted that inclusion of the initial irrigation period into the simulations with the one pore domain model was not considered reasonable in this study. The results obtained so far already show that the one pore domain model is incapable in capturing the mechanisms related to exchange of the water and solute between the larger and smaller soil pores. It is therefore evident that including the

initial irrigation period in the simulation would reduce the goodness of fit of the model results. The moisture status that is presumed to prevail in the soil at the beginning of the tracer irrigation cannot be produced with the one pore domain model. On the other hand, the estimates used for the moisture status at the beginning of the tracer irrigation cannot be assessed with the results of the one pore domain model. The initial state and its effects on the results can be assessed only when the main mechanisms behind the observed event are adequately captured with the model.

5.2.3 Parallel simulation of slow and fast flow domains with a dual-permeability model

The dual-permeability model was first parameterised using the same parameters for the active or preferential flow domain as in the last version of the one pore domain model (Table 11 in Chapter 5.2.2). The soil matrix was parameterised with the values collected from the water retention data and hydraulic conductivity data as presented in Chapter 5.1.8, i.e., parameters of the sharp water retention curves (Table 2 and 3, Figure 13 and 14 in Chapter 2.3.2) and laboratory results of the saturated hydraulic conductivity (Figure 15 b in Chapter 2.3.3) were used. The water exchange coefficient was set to 0.01 and 0.0001 cm^{-2} that yield a high and a low exchange between the two pore domains, representing the extreme values of the exchange. The resulting parameterisation is given in Table 12.

With the higher value of the exchange coefficient, 0.01 cm^{-2}, and with a constant difference in the hydraulic head, the maximum ratio of the water flux between the two pore domains and between two matrix cells varies from 5.33 in the C horizon up to 199.29 in the E horizon, and the maximum ratio of the water flux between the two pore domains and between two preferential flow cells varies from 3.20 in the C horizon to 1.54 in the E horizon. With the lower value of the exchange coefficient, 0.0001 cm^{-2}, and with a constant difference in the hydraulic head, the maximum ratio of the water flux between the two pore domains and between two matrix cells varies from 0.05 in the C horizon up to 1.99 in the E horizon, and the maximum ratio of the water flux between the two pore domains and between two preferential flow cells varies from 0.03 in the C horizon to 0.02 in the E horizon. Similarly to the previous model versions (Chapter 5.2.1, 5.2.2), the average estimate of the initial moisture conditions was used for both the pore domains (cf. Table 8 in Chapter 5.1.8).

Table 12. Parameterisation of the dual-permeability model, using gently sloping water retention curves for the preferential flow domain and sharp curves for the matrix domain. Results available from the laboratory analysis are used for the saturated hydraulic conductivity of the soil matrix, and values based on the one-dimensional groundwater model K_{S1} as well as adjusted values K_{S2} are used for the preferential flow domain. Constant values are used for the dispersivity and diffusion coefficients in all soil horizons. Two values are tested for the exchange coefficient that yield a high and a low exchange between the pore domains. Porosity of the preferential flow domain is the same as used in the last version of the one pore domain model (Table 11 in Chapter 5.2.2). Porosity of the soil matrix is calculated as a difference of the total porosity and the porosity of the preferential flow domain.

Soil hor.	α [cm^{-1}]	β [-]	θ_R [-]	θ_S [-]	K_{S1} [$cm\ s^{-1}$]	K_{S2} [$cm\ s^{-1}$]	α^* [$cm^2\ s^{-1}$]	α_L [cm]	α_T [cm]
E_p	0.080	1.380	0.000	0.090	4.5E-2	1.0E-1	1E-6	50	5
B_p	0.039	1.375	0.000	0.060	1.0E-2	5.0E-2	1E-6	50	5
BC_p	0.032	1.440	0.000	0.045	3.5E-3	7.0E-3	1E-6	50	5
C_p	0.025	1.544	0.000	0.035	3.0E-3	2.0E-3	1E-6	50	5
E_m	0.013	1.861	0.000	0.234	6.2E-4	6.2E-4	1E-6	5	0.5
B_m	0.008	1.600	0.019	0.271	9.8E-4	9.8E-4	1E-6	5	0.5
BC_m	0.012	1.990	0.007	0.283	6.0E-4	6.0E-4	1E-6	5	0.5
C_m	0.012	1.898	0.000	0.270	6.0E-4	6.0E-4	1E-6	5	0.5
α_{wl1} [cm^{-2}]	0.01								
α_{wl2} [cm^{-2}]	0.0001								

The results (Figure 48) again show an improvement as compared with the previous model versions (Figure 45 in Chapter 5.2.1, Figure 46-47 in Chapter 5.2.2). For the first time point and compared with the model presented in Figure 47, the R^2 value rises from 0.75-0.85 to 0.83-0.94, and the R_{eff} value from 0.69-0.81 to 0.81-0.92. For the second time point, the the R^2 value stays at the same level, being 0.48-0.59 for the previous (Figure 47) and 0.46-60 for the current (Figure 48) model version. The R_{eff} value rises from 0.21-0.44 (Figure 47) to 0.39-0.55 (Figure 48), corresponding to the R_{eff} values of the model in Figure 46.

Even though the goodness of fit measures are about the same for the second time point and for the models in Figure 48, and in Figures 46 and 47, the plume looks different. In the one pore domain model, the location of the maximum chloride concentration is 40 cm (i.e. two grid cells) downslope from the observed maximum (Figure 47 a-e), and in the two pore domain model the location of the maximum chloride concentration is 40 cm downslope from the observed maximum in the model versions b and c (Figure 48), and 40 cm upslope from the observed maximum in the model versions d and e (Figure 48). A look at the concentrations behind the results in Figure 47 and 48 also

reveals that the shortcomings of the one pore domain model are related to a too high chloride concentration, whereas the shortcomings of the two pore domain model are related to a too low chloride concentration in the preferential flow domain.

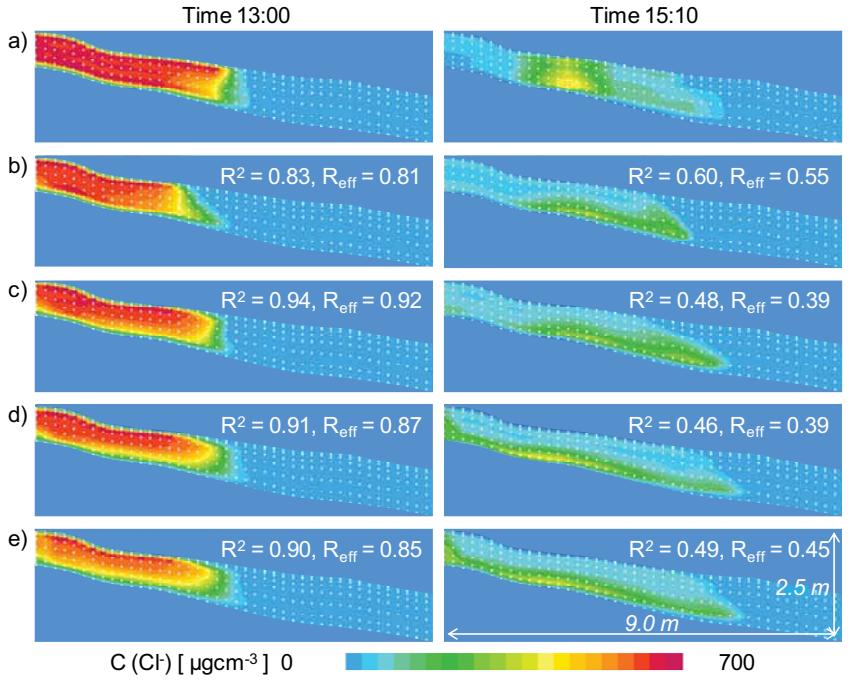

Figure 48. Observed chloride plume at two time points (a), modelled plume when feeding 90 % of the irrigation to the preferential flow domain and 10 % to the soil matrix, and using the parameterisation of Table 12, with the saturated hydraulic conductivity K_{S1} and with the exchange coefficient α_{wl1} (b), with the saturated hydraulic conductivity K_{S2} and with the exchange coefficient α_{wl1} (c), with the saturated hydraulic conductivity K_{S2} and with the exchange coefficient α_{wl2} (d), and feeding 70 % of the irrigation to the preferential flow domain and 30 % to the soil matrix, and using the parameterisation of Table 12, with the saturated hydraulic conductivity K_{S2} and with the exchange coefficient α_{wl2} (e).

The first estimate used for the saturated hydraulic conductivity, K_{S1}, which was the same as in modelling the active pore domain with a one pore domain model (cf. K_{S2} in Table 11 in Chapter 5.2.2), was too low for reaching the observed migration velocity of the front at the first time point (Figure 48 b). Adjusting the conductivity to gain a higher goodness of fit for the first time point, lowered the fit for the second time point, similarly as in modelling the active pore domain with a one pore domain model (cf. Figure 48 b with c, d, and e). Thus, to reach a higher goodness of fit for both the time steps, changes are needed not only in the values of the saturated hydraulic conductivity, but also in the porosity values.

The results also show that the saturated hydraulic conductivity affects the results the most: When using the saturated hydraulic conductivity K_{S2}, the different exchange coefficient and the different fractioning of the irrigation into the two domains have a minor effect on the results, even when the effect of the fractioning of the irrigation is investigated using a small exchange coefficient (Figure 48 c-e). As noted in Chapter 5.1.8, with high values of the exchange coefficient, water and solute rapidly mix already in the cells where the irrigation is fed into, and a different fractioning of the irrigation does not affect the model outcome. A minor fraction of the irrigation can be fed into a matrix cell for the reason that the conductivity of the soil matrix is low and the amount of iterations rises if too much water is forced into the matrix domain, especially if the exchange coefficient is small.

The highest goodness of fit for the first observation step (i.e. R^2 0.94, R_{eff} 0.92), was reached with the higher exchange coefficient (Figure 48 c), and the highest goodness of fit for the second observation step (i.e. R^2 0.60, R_{eff} 0.55), with the smaller exchange coefficient (Figure 48 b). Considering the first time point, the lower correspondence related to the results of Figure 48 d and e, as compared to the results of Figure 48 c, are a consequence of the use of the lower exchange coefficient that yields a lower chloride concentration. Thus, a too high share of old, chloride-free water remains in the preferential flow domain at the first time point.

Considering the results for the second time point, the best correspondence with the modelled and observed plume applies to a model that produces a correct location for the maximum chloride concentration and a similar shape for the chloride plume in general (Figure 48 b). This correspondence is due to a proper combination of the values of the saturated hydraulic conductivity and the exchange coefficient used. Considering the assumption that the soil matrix moistens via preferential flow routes in coarse-textured soils (cf. Chapter 3 and Aubertin 1971), the use of a relatively high exchange coefficient is preferable in the coming model versions.

To parameterise the next, further improved model version, even more non-linearly dropping porosity values were chosen for the preferential flow domain (Table 13). Reflected against the average water retention data (Table 1 in Chapter 2.3.2), the porosity values used for the preferential flow domain correspond to an estimate of 103-150 µm for a macropore, and reflected against the most gently sloping water retention data (Table 2 and 3 in Chapter 2.3.2) the values correspond to an estimate of 188-250 µm for a macropore, based on Equation 2 (Chapter 2.3.4). The porosity values of the preferential flow domain represent about the same magnitude than the air capacity

presented in Chapter 2.3.4. The air capacity is closely related to the concept of effective macroporosity (Germann and Beven 1981). As the shape of the modelled plume in the previous model version (Figure 48 c-d) corresponded to the shape of the observed plume, new values for the saturated conductivity K_{S1} were first determined by keeping the ratio K_S/θ_S in each soil horizon the same as in the previous model version (Table 12, Figure 48).

Table 13. Parameterisation of the dual-permeability model, using gently sloping water retention curves for the preferential flow domain and sharp curves for the matrix domain. Results available from the laboratory analysis are used for the saturated hydraulic conductivity of the soil matrix, adjusted values K_{S1} and K_{S2} are used for the preferential flow domain. Constant values are used for the dispersivity and diffusion coefficients in all soil horizons. Two values are tested for the exchange coefficient that yield a high and a medium exchange. Porosity values of the two pore domains are adjusted, but the total porosity is kept the same as in the previous model versions.

Soil hor.	α [cm^{-1}]	β [-]	θ_R [-]	θ_S [-]	K_{S1} [$cm\ s^{-1}$]	K_{S2} [$cm\ s^{-1}$]	α^* [$cm^2\ s^{-1}$]	α_L [cm]	α_T [cm]
E_p	0.080	1.380	0.000	0.070	8.0E-2	6.5E-2	1E-6	50	5
B_p	0.039	1.375	0.000	0.035	3.0E-2	3.0E-2	1E-6	50	5
BC_p	0.032	1.440	0.000	0.020	3.0E-3	8.0E-3	1E-6	50	5
C_p	0.025	1.544	0.000	0.015	1.0E-3	2.0E-3	1E-6	50	5
E_m	0.013	1.861	0.000	0.254	6.2E-4	6.2E-4	1E-6	5	0.5
B_m	0.008	1.600	0.020	0.296	9.8E-4	9.8E-4	1E-6	5	0.5
BC_m	0.012	1.990	0.008	0.308	6.0E-4	6.0E-4	1E-6	5	0.5
C_m	0.012	1.898	0.000	0.290	6.0E-4	6.0E-4	1E-6	5	0.5
$\alpha_{wl\,1}$ [cm^{-2}]	0.01								
$\alpha_{wl\,2}$ [cm^{-2}]	0.001								

Two values for the exchange coefficient were again taken into account. To ensure a high enough concentration for the first time point, the high value of 0.01 cm^{-2} was used as previously. As the low value used for the exchange coefficient so far, i.e. 0.0001 cm^{-2}, was more suitable than the high value only for the second time point, and as the model outcome for the second time point was poor compared with the first time point even with the more suitable parameter values, this low value of the exchange coefficient was no longer used. Instead, based on several test runs (not shown), a value of 0.001 cm^{-2} seemed to produce the best results for the second time point, and was therefore chosen for closer evaluation. For the initial moisture status, the average estimate was used for both the pore domains as previously (cf. Table 8 in Chapter 5.1.8). For the fractioning of the irrigation volume into the pore domains, a constant share of 90 % was used for the preferential, and 10 % for the matrix domain. As noted in Chapter 5.1.8 and as the results of the previous

model version (Figure 48) imply, the fractioning does not affect the results when a relatively high value is used for the exchange coefficient.

The results (Figure 49) show a very high R^2 and R_{eff} value for the first time point, 0.98, when using the saturated hydraulic conductivity K_{S1}, and with both the exchange coefficients used (Figure 49 b and d). For the second time point, the highest possible goodness of fit, 0.61-0.62 for the R^2, was reached by adjusting the saturated hydraulic conductivity to values K_{S2}, and with both the exchange coefficients used (Figure 49 c and e). The highest value of R_{eff} was 0.52 (Figure 49 d). At the first time point, differences in the R^2 and R_{eff} values related to the use of K_{S1} and K_{S2} are in particular due to the shape of the front of the plume. As noted in Chapter 4.2.2, the data describing the front are only an interpolation of the data available from the nearest observation wells and wells containing no water for measurements, and cannot be considered accurate. Therefore, the lower goodness of fit resulting from a slightly different shape of the front plume cannot be considered a factor for rejecting that model for the first time point.

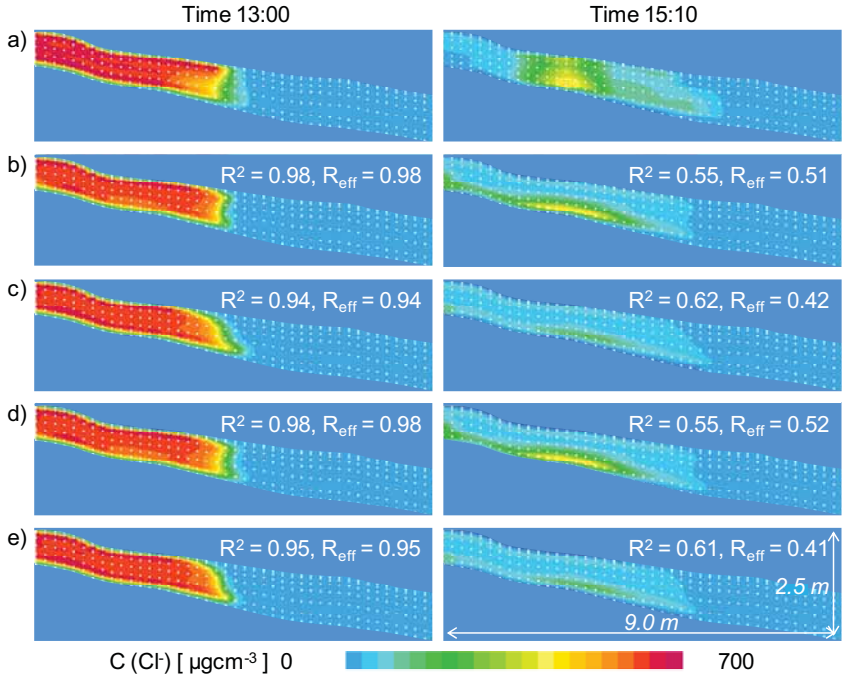

Figure 49. Observed tracer plume at two time points (a), modelled plume at two time points, related to the parameterisation of Table 13, with the saturated hydraulic conductivity K_{S1} and with the exchange coefficient α_{wl1} (b), with the saturated hydraulic conductivity K_{S2} and with the exchange coefficient α_{wl2} (c), with the saturated hydraulic conductivity K_{S1} and with the exchange coefficient α_{wl2} (d), and with the saturated hydraulic conductivity K_{S2} and with the exchange coefficient α_{wl1} (e).

At the second time point, the highest R^2 is related to a parameterisation with which almost all of the tracer disappears from the preferential flow domain into the soil matrix. It is therefore questionable whether the model with the higher R^2, but almost no tracer in the domain (Figure 49 c and e), is better than a model with a lower goodness of fit, but a little too broad area of tracer left in the subsoil, containing the same maximum chloride concentration as observed in the field (Figure 49 b and d). Based on the highest R_{eff} value, the most representative model version for the second time point is the same as for the first time point (Figure 49 d). The two goodness of fit measures used weight different features of the underlying data as described in Chapter 5.1.8, which explains the contradictory results.

It is also to be noted that similarly to the first time step, the accuracy of the interpolated data can be considered unreliable for the second time point. A look at the original data (Figure 35 in Chapter 4.2.1) behind the interpolated, lateral plume (Figure 49 a) at the second time point reveals that the tracer remains of the E and B horizons in the interpolated data are caused by only one high concentration value of about 350 mg/l measured in the well screen 4. In the other nearby well screens, i.e. wells 7 and 10, concentrations recorded for the second time point are only about 100 mg/l and correspond closer to the modelled values in the E and B horizon. In the interpolated data, values exceeding 100 mg/l are found in several grid cells due to the one, high measured concentration value.

Locally anomalous soil material as well as the interpolation routine used affect the recorded retardation of the tracer in the E and B horizons at the second time point, and result in the mismatch between the interpolated and modelled concentration. If the interpolated values of the E and B horizons at the location of the tracer remains are not taken into account, the R^2 value rises from 0.55 to 0.60 for the models in Figure 49 b and d, and the R_{eff} value from 0.51 to 0.57 for the model in Figure 49 b and from 0.52 to 0.58 for the model in Figure 49 d. This implies that both the depth distributions used for the saturated hydraulic conductivity produce the tracer remains of the BC and C horizons in a similar manner, and the lower conductivity values of the E and B horizons are only needed to produce at least some of the observed tracer remains in the E and B horizons.

Considering both the goodness of fit measures, the representativeness of the interpolated data (Chapter 4.2.1, 4.2.2, 5.1.8) and the assessment of the results in Figure 49, the smaller exchange coefficient α_{wl2} and the more non-linearly dropping saturated hydraulic conductivity K_{S1} are regarded as optimal for describing the observed stormflow event in this study. Even though traditional

testing procedures were not applied, the model presented in Table 13 and Figure 49 can be compared with the split-sample test (Klemeš 1986), where data are split in two parts, the first of which is used for calibration and the second part for validation of a model. Having adjusted the parameterisation to gain as high a goodness of fit as possible for the first part and using the second part for validation, the parameterisation is then adjusted to produce the highest possible goodness of fit for the second part, and the first part is used for validation. In this study, the model was first calibrated against the data of the first time point by using the saturated hydraulic conductivity K_{S1}, and the second time point was considered a validation period (Figure 49 b and d). By using the saturated hydraulic conductivity K_{S2}, the model was calibrated against the data of the second time point, and the first time point was considered a validation period (Figure 49 c and e).

5.2.4 Further results of the dual-permeability model

The dual-permeability model produces versatile results on the variables of the two pore domain system that were not presented or directly used in the model evaluation during the model development process (Chapters 5.2.1-5.2.3). The model development was mainly based on the tracer data available from Chapter 4.2.2, as described in Chapter 1.2 and 5.1.8. Further results, i.e. the concentration levels in the soil matrix and the groundwater levels in both the pore domains along the middle line of the study slope, as well as the solute mass balance in the entire 3D calculation grid, are presented in the following, to describe the functioning of the most representative model version and parameterisation (cf. Table 13, Figure 49 in Chapter 5.2.3).

Simulation results for the concentration prevailing in the soil matrix along the middle line of the experimental field are presented in Figure 50. The results are presented for the model that produced the concentrations presented in Figure 49 for the preferential flow domain. Since no concentration data are available for assessing the reliability of the results of the soil matrix (cf. Chapter 4.2.1, 4.2.2), the results can only be considered predictions, related to the model that is developed specifically for capturing the dynamics of the preferential flow domain. Figure 50 b-e shows that concentrations in the soil matrix remain low compared to concentrations in the preferential flow domain (Figure 50 a).

Due to the high pore volume space, concentration levels do not reach high values in the soil matrix in the middle line of the experimental slope (Figure 50 b-e), even though salted water is considered to flow from the preferential

flowpaths into the soil matrix when the irrigation is changed from salted to unsalted water. As noted in Chapter 4.2.2, the rapid change in concentration in the preferential flow domain after changing the irrigation from salted to unsalted water (Figure 50 a) is explained by flow from the preferential flow domain into the surrounding soil matrix either directly or via preferential flowpaths on the sides of the middle line wells.

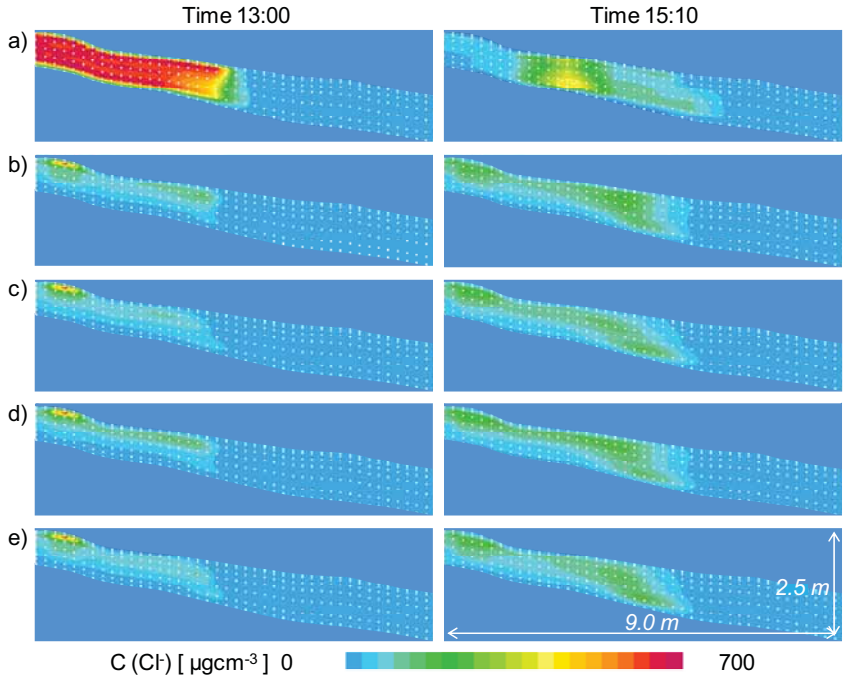

Figure 50. Observed tracer plume at two time points (a), and simulated chloride concentrations for the soil matrix for the model parameterised with the values presented in Table 13. The predictions for the soil matrix (b, c, d, e) correspond directly to the results of the preferential flow domain presented in Figure 49 (b, c, d, e).

The mass balance results from the whole 3D grid further describe the concentration levels in the soil matrix and in the preferential flow domain. Based on the results of the most representative model application (cf. Table 13, Figure 49 d and 50 d), at the time point 13:00 41 % of the irrigated chloride mass is in the preferential flow domain, 45 % in the soil matrix, and 14 % has flown outside the total model domain. At 15:00, 11 % of the irrigated chloride mass resides in the preferential flow domain, 63 % in the soil matrix, and 26 % has flown outside the total model domain. As presented in Chapter 5.1.7, water and solute mass balance errors of the model solution are minor, only about 10^{-3} %, whereby all the water and solute fed into the system is either stored in the

preferential flow domain or the soil matrix, or has flown out of the model domain.

Groundwater levels for the model presented in Table 13, Figure 49 d and 50 d are shown in Figure 51. The groundwater level, i.e. the level between the saturated and unsaturated grid cells in the model, is presented separately for the two, modelled pore domains for the middle line along the study slope.

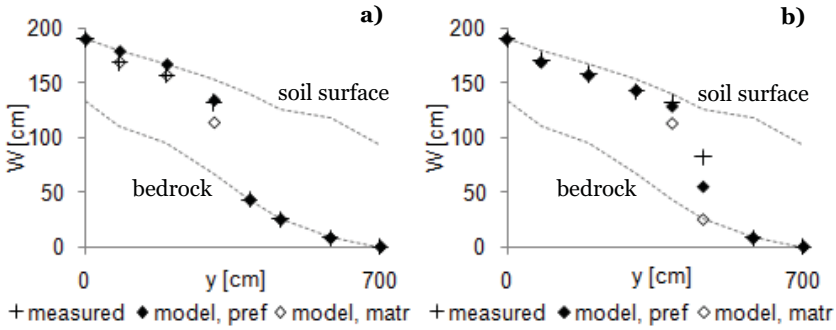

Figure 51. Measured and modelled groundwater level *W* along the study slope in the *y* direction at 13:00 (a), and at 15:10 (b), related to the model presented in Table 13 and Figure 49 d and 50 d.

The R^2 and R_{eff} values are both 1.0 for the time point of 13:00, and 0.98 for 15:10, when comparing the measured groundwater levels with the simulated levels in the preferential flow domain. To include the effect of the soil matrix water content on the simulated levels in the comparison, a combined groundwater level was estimated as the average of the levels of the two pore domains. The average was weighted by the proportions of the pore domains in the total porosity. Using the combined groundwater levels, R^2 and R_{eff} values are 0.99 and 0.99, respectively, for 13:00, and 0.94 and 0.91, respectively, for 15:10. In the advection driven system of this study, a good correspondence between the measured and modelled tracer concentration (Figure 49), and between the measured and modelled migration velocity of the tracer front led into a good correspondence between the measured and modelled groundwater levels.

5.2.5 Effect of time step and grid spacing on the results

To test the effect of a shorter time step and a denser grid spacing on the results, the model presented in Table 13 was run with a shorter time step of 20 s and a denser grid spacing, where the E, B and BC horizons consisted of two layers each, and the C horizon consisted of three layers. In the x and y

direction the density of the grid resolution was doubled to 10 cm. In the parameterisation (Table 13), the saturated hydraulic conductivity K_{S1} and the exchange coefficient α_{wl2} were used. The average estimate was used for the initial moisture conditions as previously (cf. Chapter 5.1.8), and a 90 % share of the irrigation was used for the preferential flow domain and a 10 % share for the matrix domain. The results are presented in Figure 52.

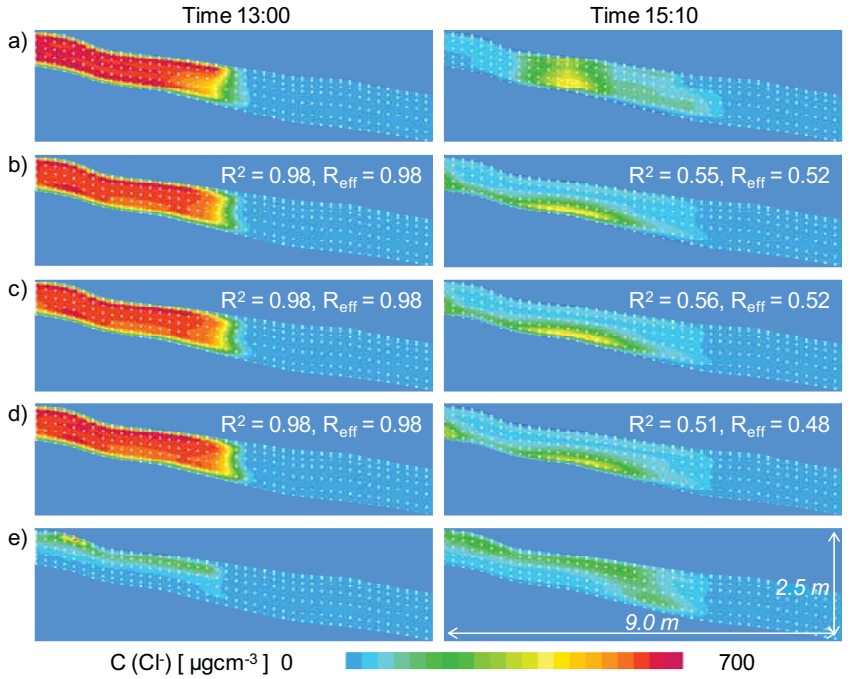

Figure 52. Observed tracer plume at two time points (a), modelled plume related to the parameterisation of Table 13, using the saturated hydraulic conductivity K_{S1} and the exchange coefficient α_{wl2}, the average estimate of the initial state, and the original time step length of 60 s (b), using a short time step length of 20 s (c), using a short time step length of 20 s and a doubled grid resolution (d), and results for the soil matrix in the case of a short time step length of 20 s and a doubled grid resolution (e).

The results (Figure 52) show that the original time step was short enough and the original grid spacing dense enough for numerically accurate results. Comparing Figure 52 b with c shows that the use of a shorter time step does not affect the results, whereas comparing Figure 52 b with d shows that the denser grid spacing has a minor effect on the results for the second time point. The small differences in the plume shape at the second time point in Figure 52 b and d are, however, not a proof of more accurate results in numerical sense. The outcome of the model looks a little different when each of the parameterisations is used for two layers in the model instead of one.

Compared with the earlier model versions, the predicted chloride concentration in the soil matrix also does not change with a shorter time step and a denser grid spacing (cf. Figure 50 d and 52 e).

5.2.6 Effect of the initial irrigation period on the results

The initial state used for the moisture conditions of the slope affects the results as shown already for the one pore domain applications (e.g. Figure 46 in Chapter 5.2.2). The effect of the initial state on the results can be investigated, when a model structure and parameterisation are found that adequately describe the observed phenomenon. In this study, the initial state at the beginning of the tracer irrigation was estimated as described in Chapter 5.1.8. The simulations were restricted to the period of the tracer experiment in order to limit the computing time, and to concentrate on finding a model that captures the observed stormflow event, produced by the tracer irrigation.

To investigate the reliability of the estimates used for the initial state, and the effect of the changes in the initial state on the results, the initial irrigation period with chloride-free water a day before the tracer experiment was included in the simulation, using the model presented in Table 13 (Chapter 5.2.3). The saturated hydraulic conductivity K_{S1} and the exchange coefficient α_{wl2} were again used. For the initial state, prior to the initial irrigation period, values used for the dry slope section in the earlier model versions were used for the whole slope (cf. h_{Dry} in Table 8 in Chapter 5.1.8). The results are presented in Figure 53.

When starting the simulation from the beginning of the initial irrigation period, using the average estimate of the initial state (average of h_{Dry} in Table 8 in Chapter 5.1.8), the model produces a lower moisture status for the slope to the beginning of the tracer irrigation as estimated earlier. Therefore, the R^2 and R_{eff} values (Figure 53 b) are lower for both time points than when only simulating the tracer experiment period (Figure 49 d in Chapter 5.2.3). The initial irrigation is not enough to moisten the soil with the given parameterisation as much as was estimated. Several test runs implied (not shown) that increases in the saturated hydraulic conductivity could not improve the results, and therefore, the higher estimate of the initial state at the beginning of the initial irrigation period (maximum of h_{Dry} in Table 8 in Chapter 5.1.8) was tested next. The improvement in the results is minor (cf. Figure 53 b to c).

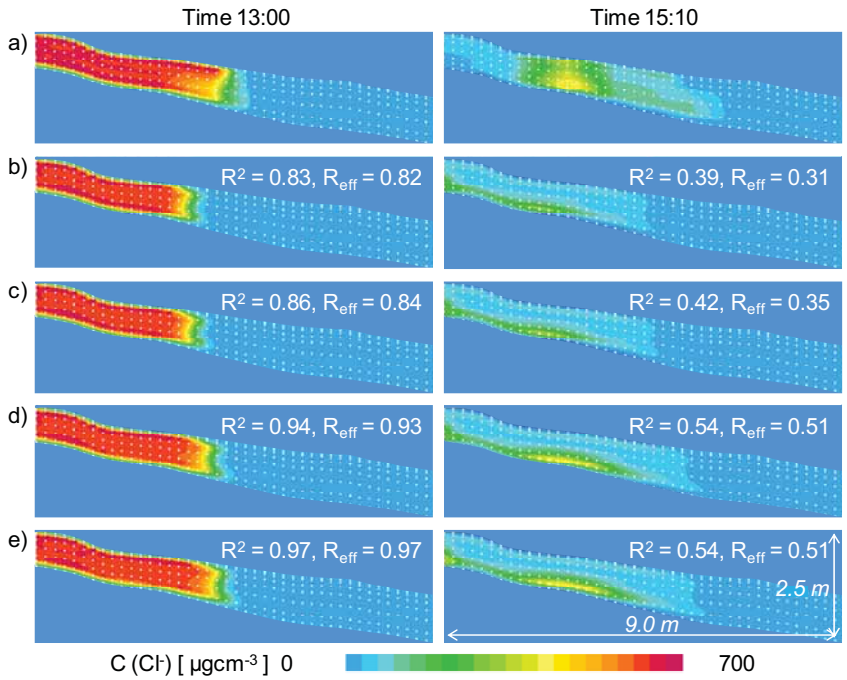

Figure 53. Observed tracer plume at two time points (a), modelled plume at two time points, related to the parameterisation of Table 13, using the saturated hydraulic conductivity K_{S1} and the exchange coefficient α_{wl2}, and using the average of h_{Dry} in Table 8 (Chapter 5.1.8) for the initial state, prior to the initial irrigation period and for the whole slope (b), using the maximum of h_{Dry} in Table 8 for the initial state, prior to the initial irrigation period and for the whole slope (c), using an initial state, prior to the initial irrigation period, of 50 % higher pressure head than the estimated average of h_{Dry} in Table 8 (d), and using the maximum of h_{Dry} in Table 8 for the initial state, prior to the initial irrigation period and for the whole slope, but with a 30 % smaller porosity in each soil horizon of the soil matrix than in Table 13; the porosity of the preferential flow domain was kept the same (e).

To investigate whether a drastic rise in the soil moisture in the initial state prior to the initial irrigation period is able to create high enough soil moisture conditions for the beginning of the tracer experiment, the average estimates of the initial state were raised by 50 % and the model was run with the resulting values. The model result improves clearly (cf. Figure 53 c to d). However, the soil moisture values used are unrealistically high compared to the measured values prior to the experiments in the field. If the model parameterisation as a whole or the model structure is considered inadequate for simulating the moistening of the soil during the initial irrigation, or if the measured values for the initial moisture conditions can be found erroneous, the use of the 50 % higher pressure head compared to the measured maximum is justified, in order to produce a higher goodness of fit for the tracer experiment. However, because the use of e.g. higher values for the saturated hydraulic conductivity

does not help in creating higher moisture conditions for the beginning of the tracer irrigation, the effect of a smaller total porosity soil on the moisture conditions was tested next, using the average estimate of the initial state prior to the initial irrigation period. The porosity estimates were reduced by 30 % for the soil matrix as compared to the values presented in Table 13 (Chapter 5.2.3). The porosity values of the preferential flow domain were kept the same as in Table 13. The results are presented in Figure 53 e.

Reducing the porosity of the soil matrix by 30 % improved the results more than the high rise in the initial moisture conditions at the beginning of the initial irrigation period (cf. Figure 53 d to e). The R^2 and R_{eff} values, i.e. 0.97 for the first, and 0.54 and 0.51, respectively, for the second time point (Figure 53 e), approach the highest values gained in the previous model versions that did not include the initial irrigation period, i.e. 0.98 for the first, and 0.55 and 0.52, respectively, for the second time point (Figure 49 d). If the estimates of the total porosity can be found erroneous, or if it can be proven that the soil does not fully saturate during the tracer experiment (cf. Chapter 2.3.4), the use of the smaller porosity values is justified. The fact that i) the lower porosity values improved the results clearly, ii) the high rise in the initial moisture status prior to the initial irrigation period improved the model outcome less, and iii) the previous model version not containing the initial irrigation period (Figure 49 in Chapter 5.2.3) was able to catch the moistening event when the plume reached the drier slope section during the tracer experiment, indicate that unrepresentative porosity values are an equally probable source of error as an error in the estimates of initial moisture conditions prior to the initial irrigation.

It is also noteworthy that the estimates of the initial state that were used in the simulations without the initial irrigation period, are also inaccurate. The results of the different model versions indicate that inaccuracies in the data on the initial moisture conditions, combined with inaccuracies in all the measurements, including the porosity and stone content of soil, are the most probable causes for the weaker goodness of fit of the model presented in Figure 53 than in Figure 49. The results do not directly imply that the dual-permeability model used is structurally inadequate in describing the observed stormflow event, since the model captures the plume with justifiable parameter values.

The inclusion of the initial irrigation period into the simulation can be compared with a differential split-sample test (Klemeš 1986). In a differential split-sample test, a model is used for an area to simulate new conditions of which no data were available in the model development, i.e. in calibrating and

validating the model for the area. In this study, the initial irrigation period was not included in the model development and represented thereby new conditions for simulations before tuning the parameterisation (Figure 49 d in Chapter 5.2.3, Figure 53 b).

5.3 Discussion

5.3.1 Model structures

Several studies (e.g. Espeby 1989, Jansson 2005, James et al. 2010) report the inadequacy of the traditional, one pore domain, physics-based models to describe runoff generation in forested hillslopes. By taking into account the effect of preferential flow on runoff generation, two pore domain models are expected to describe better in particular the fast subsurface flow processes of hillslopes. However, applications of two pore domain models are still few, and the vast majority of the applications are developed for agricultural soils (e.g. Gärdenäs et al. 2006, Köhne et al. 2006, Vogel et al. 2007, Warsta 2007, Dusek et al. 2010). Considering the two pore domain approaches presented in e.g. Gerke and van Genuchten (1993a, 1993b), Šimůnek et al. (1999, 2003), Vogel et al. (2000), Jansson and Karlberg (2001), Larsbo and Jarvis (2003), Ray et al. (2004), Gerke et al. (2007), and Šimůnek and van Genuchten (2008), the use of i) various governing equations for flow in the preferential flow domain, ii) various routines for determining the exchange of water and solutes between the pore domains, as well as iii) varying dimensionality (1D, 2D or 3D flow) in the models complicate a direct comparison of the applications of the different models.

The model developed in the present study is a full three-dimensional, Richards' equation-based, object-oriented, one to two pore domain description of flow and solute transport, allowing for adaptability in parameterising and in fitting the model structurally to the observed event. A similar combination of preferred features is not available in other models. The one-dimensional, two pore domain model COUP (Jansson and Karlberg 2001) simulates flow in the soil matrix using the Richards' equation, and contains a simple bypass routine for flow in the preferential flow domain. In the bypass routine, water entering the soil at a rate higher than the sorption capacity of the soil matrix, is routed directly to the next underlying soil layer. In the one-dimensional, two pore domain model MACRO (Larsbo and Jarvis 2003), preferential flow is described by the gravity-driven, kinematic wave equation and the exchange of

water between the pore domains by a sink-source term, dependent upon the degree of saturation of the soil matrix. Flow in the micropore region is governed by the Richards' equation.

The one-dimensional, two pore domain version of the HYDRUS model (Šimůnek et al. 1999 and 2003, Šimůnek and van Genuchten 2008) can be used both as a dual-porosity and dual-permeability type models. Richards' equation is used for the preferential flow domain in the dual-porosity model, while water in the soil matrix is being stagnant, and for both the pore domains in the dual-permeability model. In the dual-permeability model, the kinematic wave equation can also be used for the preferential flow domain. The exchange of water and solutes between the domains is pressure driven (cf. Gerke and van Genuchten 1993a, Ray et al. 2004) or driven by fluid saturation (Šimůnek et al. 2003). The dual-porosity type HYDRUS is also available as a two- to three-dimensional version (Šimůnek et al. 2006).

In addition to HYDRUS, the one-dimensional, two pore domain S1D Dual model (Vogel et al. 2000, Ray et al. 2004) and the two-dimensional, two pore domain 2D-DPERM model (Gerke et al. 2007, based on Vogel et al. 2000 and Ray et al. 2004) use the Richards' equation for flow in both pore domains and are similar to HYDRUS. Considering the models cited above, the model developed in this study corresponds closest to the HYDRUS, S1D Dual and 2D-DPERM models. The main differences are the dimensionality of the models, combined with the dual domain approach used (dual-porosity or dual-permeability type of model). In addition, the definition used for the pressure driven exchange term (Gerke and van Genuchten 1993a, Ray et al. 2004) as well as the adjustment of the models to the site and phenomenon in question vary in the different applications of the models mentioned. Structural compatibility of the different model versions of the present study is discussed in the following chapters, reflected against the applications available from different land-use and soil types, representing the variably comparable modelling approaches presented above. Applications of the HYDRUS, S1D Dual and 2D-DPERM models are mainly used as references for the applications of the dual-permeability model.

5.3.2 Analysis of the one pore domain approach

In the present study, simulations with the traditional, Richards' equation-based, three-dimensional, one pore domain flow and solute transport model showed that the observed stormflow event cannot be reproduced with the model with any parameterisation, when flow and solute transport are

simulated in the total pore space of soil. The parameterisation was adjusted for the saturated hydraulic conductivity in the different soil horizons, and the effect of initial moisture conditions on the results was tested. Both the modelled migration velocity of the front of the tracer plume down the study slope, as well as the tracer concentration along the slope did not correspond to the observations for the tested parameterisations and initial states. The simulations therefore showed a structural incompatibility between the one pore domain approach and the modelled phenomenon. The result complements the findings made in Sweden at a small, forested catchment with a shallow till soil cover, where a two pore domain model was concluded more suitable for simulating the instant infiltration and runoff peak immediately after rainfall, compared to a traditional one pore domain model (Jansson et al. 2005).

A further comparison to the results from the Swedish site is challenging due to the differences in the model structures and in the data used for parameterisation and running the models. Jansson et al. (2005) used the one-dimensional COUP model (Jansson and Karlberg 2001), where water entering the soil at a rate higher than the sorption capacity of the soil matrix, is routed directly as bypass flow to the next underlying soil layer. Despite the differences in the model structure and data used, it is noteworthy that Jansson et al. (2005) found a traditional, one pore domain model more suitable for describing the general behaviour of the study slope throughout the melting season. The data on the tracer experiment in Kangaslampi are not applicable to detailed assessments of the suitability of the dual-permeability model to describe slower, natural processes. The study of Jansson et al. (2005) indicates that a one pore domain model is better fitted for slow, natural events than for fast stormflow generation in the Kangaslampi slope as well. However, the study of Jansson et al. (2005) does not directly indicate that a one pore domain model would be better for slow processes in Kangaslampi than the dual-permeability model, because of the above presented differences.

Reference studies (presented in the following) rather imply that a dual or even multi domain approach is preferable for forest soils in various conditions. A detailed analysis of the three-dimensional, one pore domain, physics-based TOUGH2 model (Pruess 2004) revealed that the results of a rainfall-runoff event in the forested Panola hillslope, USA, deviate from observations for both internal storage dynamics and downslope delivery mechanisms (James et al. 2010). The Panola study (James et al. 2010) called for a better description of the soil-bedrock permeability, with parameter values declining with depth for

the saturated hydraulic conductivity, and a dual domain approach, to further develop the model representation of the slope.

Considering other land-use types than forested areas, Vogel et al. (2007) note that the one-dimensional, Richards' equation-based, dual domain model S1D Dual (Vogel et al. 2000, Ray et al. 2004) corresponds better to the observed movement of cadmium in agricultural, sandy-loam soil in Slovakia during a ponded infiltration experiment, than the original one pore domain approach. In comparison to one pore domain models, Gärdenäs et al. (2006) also consider the two-dimensional, dual-porosity and dual-permeability versions of the HYDRUS model (Šimůnek et al. 1999) better for capturing the observed dynamics of pesticide concentrations in a tile-drained, till soil field in southern Sweden during a period of 6 weeks following a spray application of the pesticide. For a tile-drained, clayey till field in northern Germany, Gerke et al. (2007) report a two-dimensional, dual-permeability approach to simulate better bromide concentrations in tile-drain effluent than a single-porosity model.

In the present study, restricting the one pore domain model to simulate flow and solute transport in an active pore fraction of the soil pore space clearly improved the model outcome (Chapter 5.2.2). Yet, the dual-permeability model conformed even better to simulating the subsurface stormflow event (Chapter 5.2.3). Restricting the simulation with the one pore domain model to a fraction of the total soil pore space was the first step towards the development of the dual-permeability model. Dunn et al. (2007) also used a fraction of the total pore space when performing virtual experiments with a one pore domain, semi-distributed, conceptual flow and solute transport model for the forested catchment of Maimai in New Zealand. A 40 % share of the total porosity was considered suitable for the Dunn et al. (2007) model, which is of the same magnitude as the share considered suitable for the uppermost soil horizon in the physics-based, one pore domain model of this study.

In simulating the active fraction of the pore space with the one pore domain approach in the present study, means to improve the outcome of the model included i) the amount of irrigation fed into the modelled domain, ii) the initial moisture status, iii) the saturated hydraulic conductivity, and iv) the porosity of the active pore domain of the different soil horizons. Having adjusted the parameter values, the results showed that a higher amount of irrigation was needed to improve the model outcome at the first observed time point, and a smaller amount to improve the outcome at the second observed time point (Figure 47 in Chapter 5.2.2). The results thereby demonstrated the

importance of taking into account the exchange of water and solute between the preferential flow domain and the soil matrix. As the compatibility between the modelled and observed plume could not be further improved for both time points at the same time, only by tuning the parameterisation, the one pore domain model was not developed further. As described in Chapter 5.2.2, a structural improvement such as a sink term would improve the model outcome, but the observed plume would still be very difficult to capture with the model, as the loss of water to the soil matrix is not constant in changing moisture conditions (e.g. Jarvis 2007).

5.3.3 Analysis of the two pore domain approach

Compared with the improved one pore domain model of an active fraction of the soil pore space, the two pore domain approach further improved the model outcome by allowing for a parallel and coupled simulation of flow and solute transport in the soil matrix and in the preferential flow domain. The outcome of the dual-permeability model was influenced by i) the fractioning of the total porosity into the soil matrix and the preferential flow domain, ii) the saturated hydraulic conductivity of the preferential flow domain, and iii) the exchange coefficient between the domains. The same value of the exchange coefficient produced the highest goodness of fit for both the observed time points, but a different depth distribution was needed for the saturated hydraulic conductivity at the first and at the second time point observed (Chapter 5.2.3).

Similarly as in developing the one pore domain model, adjusting of the parameters of the dual-permeability model reached a point where the model outcome could not be further improved for both the observed time points at the same time. In the one pore domain model, however, the contradiction between the observed time points was mainly related to the irrigation amount fed into the modelled pore domain. Whereas in the dual-permeability model, the contradiction was mainly due to the parameter values needed for the preferential flow domain in order to capture the observed dynamics of the tracer plume at each time point. Considering the most representative model outcomes (Figure 49 in Chapter 5.2.3), the dual-permeability model could explain almost all of the observed variation in the chloride concentration at the first time point, and more than half of the variation at the second time point.

Four main factors explain why the model was able to capture better the concentrations at the first than at the second time point, i.e., why the model could not reproduce the observed tracer remains in particular in the E and B horizons when the tracer plume reached the drier slope section,

simultaneously to the dilution of the concentration along the slope. First, the representativeness of the two-dimensional, interpolated concentration data is unclear at some locations of the slope, as described in Chapter 4.2.1, 4.2.2, 5.1.8. Thus, concentration values that may not correspond to the actual concentrations along the slope are possible in the interpolated data against which the model outcome was compared.

Second, locally anomalous soil material can cause the observed retardation of the tracer in the E and B horizons at the second time point, and result into the mismatch between the interpolated and modelled tracer concentration, as described in Chapter 5.2.3. The model was parameterised horizon-wise, and the model does not take into account the small scale variability in the soil properties in the downslope direction. Taking into account the high variability in the soil physical and hydraulic properties (Chapter 2), it is likely that the average values used for the different soil horizons cannot produce accurate estimates of the concentrations at each specific location of the slope. Together with the representativeness issues of the interpolated data, locally anomalous soil material differing from the average parameterisation are considered most influential for the lower goodness of fit at the second observed time point.

Third, the lower goodness of fit for the second time point is also influenced by the simplified form of the exchange term used. Considering the simulation of solute transport, the exchange term only accounted for advective exchange between the pore domains, and the same value of the exchange coefficient was used for all soil horizons. The simplified form of the exchange term was chosen in order to reduce the number of unknown parameters, and problems with the model identifiability and parameter equifinality. In addition, the subsurface stormflow event was expected to mostly consist of advective transport processes. Introducing a dispersive exchange coefficient in the exchange term in the solute transport model (e.g. Gerke and van Genuchten 1993a, Ray et al. 2004, Gerke et al. 2007), and using different values for the advective and dispersive exchange coefficients for different soil horizons, increase the possibilities to adjust the simulated concentrations to correspond closer to the observed concentrations. The model versions developed and analysed so far create the basis for examining the effect of a more complex exchange term on the results in future studies.

In addition to the simplified form of the exchange term, the chosen dependence of the exchange on pressure head affects the results. The exchange was considered to depend on the moisture status of both the soil matrix and the preferential flow domain, and the hydraulic conductivity between the domains was determined as arithmetic mean of the conductivities of the two

domains, similarly to the study of e.g. Gärdenäs et al. (2006). The use of the conductivity of the soil matrix alone, the geometric mean of the conductivities of the two pore domains or an integral form would lead to a slower exchange between the domains, whereas the use of the conductivity of the preferential flow domain alone would lead to a higher exchange (Gerke and van Genuchten 1993b). A fast exchange between the domains is also obtained, if the exchange is controlled by the relative saturation of the dynamic preferential flow domain alone (cf. Ray et al. 2004, Gerke et al. 2007).

Based on the findings made in the tracer experiments and during the model development process about the dynamic nature of the exchange, a further analysis of the dual-permeability model calls for testing the effect of a dispersive coefficient alongside the advective coefficient, and the effect of coefficients that only depend on the moisture status of the more dynamic, preferential flow domain. Other studies that have so far applied a Richards' equation-based, dual-permeability approach contain both an advective and dispersive exchange coefficient at sites representing other land-use types than forest areas (e.g. Gärdenäs et al. 2006, Dusek 2010). The model outcome is also expected to benefit from the use of at least two different values for the water exchange coefficient, one for the soil horizons that contain remarkable amounts of preferential flowpaths, i.e. the E and B horizons, and one for the BC and C horizons. The suitable value of the exchange coefficient is discussed in the Parameterisation Chapter 5.3.4.

Fourth, the lower goodness of fit of the second time point may be linked to the pore structure of soil: The two pore domain approach may be insufficient for describing flow and solute transport in the Kangaslampi soil with varying soil properties and in changing moisture conditions. In particular the investigation of the effect of the initial irrigation period on the results raised the question whether a two pore domain model provides an adequate representation of the Kangaslampi soil, or even a three domain approach is needed. Inclusion of the initial irrigation period to the simulation yielded a lower estimate of the soil moisture along the slope at the beginning of the tracer irrigation than estimated in Chapter 5.1.8. The lower initial moisture status resulted into a too slow flow and solute transport during the tracer experiment. Increasing of the moisture status prior to the initial irrigation and increasing of the saturated hydraulic conductivity values did not raise the tracer transport velocity to the observed level. Instead, lowering of the total porosity of the soil matrix by 30 % was able to raise the velocity to the observed level and the R_{eff} value to the same level than in simulations without the initial irrigation period.

The 30 % correction of the porosity values of the soil matrix can be explained by a missing third pore domain that describes, for instance, a stagnant matrix storage. The possible stagnant matrix storage may either contain water that does not contribute to runoff generation, or the storage may contain air that is trapped in the pores. If the stagnant storage is filled with water, the water retention capacity is high and permeability low, and flow inside the domain as well as the exchange of water between the stagnant storage and the larger pores is low. Thus, flow in soil only consists of meso- and macropore flow, and the solute exchange between the matrix storage and larger pores is based on diffusion.

If air is always trapped in the smallest pores of a possible, stagnant storage, the soil never fully saturates in natural conditions. The study of Vakkilainen (1982) showed that the real porosity of sandy loam soil (measured in the laboratory by saturating soil samples) was a third higher than the porosity estimated for the soil in the field by determining the saturated moisture content of field lysimeters. The study of Vakkilainen (1982) thereby supports the possibility of a third pore domain that does not saturate in natural conditions, as the porosity values of this study also were determined by saturating soil samples in the laboratory. This air-filled pore space can then be corrected in a simulation model by the 30 % correction factor for the porosity estimates. It is to be noted, however, that the 30 % correction factor of this study produces porosity estimates that fit inside the high variation in the measured porosity values (Chapter 2.3.4). Thus, variation and inaccuracy in the porosity measurements can alone lead into the incompatibility between the used irrigation amounts and observed saturation velocities and degrees.

Studies supporting a three pore domain description of soil with micro-, meso- and macropores include the analysis of ion concentrations in the pore water of soil cores collected from forested till soil (Kareinen and Ilvesniemi 2002), and the statistical analysis of breakthrough curves of conservative tracers in an upland, sandy loam soil block in Scotland (Deeks et al. 2008). However, no studies of hillslope-scale, physics-based, three pore domain flow and solute transport models are available. If the Kangaslampi soil is considered to consist of three pore domains, a dual-permeability model can be used as a simplification of the three domain system similarly than the one pore domain model was used as a simplification of a two domain system in this study.

This study does not directly support or call for the development of a three pore domain approach. Instead, a re-examination of the porosity (i.e. the saturated moisture content), the stone content and the soil moisture estimates is considered most important for the future development and analysis of the

dual-permeability model. This is due to the inability of the model to capture the plume when the initial irrigation period is included in the simulations, since the model could not reach the observed migration velocity of the tracer plume only by raising the saturated hydraulic conductivity and initial moisture content. Thus, shortcomings of the model are considered to result from the variation and inaccuracies of measurements, including the porosity, stone content and moisture status estimates, not the dual-permeability structure of the model. In addition, changing surface boundary fluxes, such as changing rainfall intensities, may cause changes in the size of the dominant macropore conducting water (Jarvis 2007). Therefore, the shortcomings of the model may partly result from the constant fractioning used for the soil matrix and preferential flow domain.

Considering the features of the most representative results obtained with the dual-permeability model, the use of at least two different values for the water exchange coefficient and the use of a dispersive exchange coefficient alongside the advective coefficient support the future analysis and development of the model, in particular for different conditions. The results were influenced by the horizon-wise parameterisation routine, as well as by the form and the constant value used for the exchange coefficient. Despite the shortcomings referred to above, the dual-permeability model was able to capture the main mechanisms behind the observed stormflow and solute transport event, and thereby provides a profound basis for further model development.

5.3.4 Parameterisation

Advances in measurement methods and in the usability of measurements in reducing model and parameter uncertainty are most important for model development (McDonnell and Tanaka 2001). In assessing parameterisations as well as structures of models, chemical data related to manipulation experiments provide powerful means to test whether a model version is giving the right answers for the right reasons, by isolating individual mechanisms (Kirchner 2006). In this study, soil physical and hydraulic properties were determined with a variety of traditional methods, and the representativeness of the results was analysed by comparing the results against each other and against literature references. In addition, estimates of the saturated hydraulic conductivity were supplemented by means of inverse modelling. Together with the ion tracer data, data describing the soil physical and hydraulic properties formed a unique combination that could be used in parameterising the dual-permeability model, and in assessing the structural compatibility of the model

(Chapter 5.3.1, 5.3.2, 5.3.3). The model development process provided assessments of the reliability and usability of the measured parameter values, when the model versions were run against the ion tracer data, specifically designed to demonstrate the different phases of a subsurface stormflow event. Parameterisation is closely linked to the model structure.

Overparameterisation and tuning of the parameter values usually makes the model behaviour less dependent on the structure and overparameterised models can be forced to fit the data in many cases even though they are structurally wrong (Kirchner 2006). Also, models based on current theories rely on calibration to account for the lack of knowledge of the spatial heterogeneities in landscape properties and to compensate for the lack of understanding of actual processes and process interactions (McDonnell et al. 2007). In this study, fixing the majority of the parameter values in the different model versions, and adjusting the remaining parameter values to enable a successful simulation of the observed stormflow event made the assessment of different model structures possible and led to the rejection of some model structures and parameter values. The different model versions with different parameterisations, run against tracer data, were considered to be hypotheses of how to capture the observed event with the model. The data available provided means to test the different hypotheses (cf. Beven 2008).

The parameterisation principle used in this study differs from other studies applying the Richards' and van Genuchten equations (e.g. Gärdenäs et al. 2006, Köhne et al. 2006, Vogel et al. 2007, Gerke et al. 2007, Dusek et al. 2010, James et al. 2010). In this study, parameters were split into three groups of fixed, adjusted and calibrated parameters, and the hillslope was parameterised soil horizon-wise. The fixed parameter values (i.e. water retention properties, saturated hydraulic conductivity of the soil matrix, total porosity) and adjusted parameter values (saturated hydraulic conductivity of the total, active and preferential pore domains, active fraction of the total pore space and fractioning of the total pore space into the soil matrix and the preferential flow domain) originated from soil core analyses and inverse modelling of groundwater tables. The parameterisation focused on linking the measured parameter values to the model parameters that they most likely describe in terms of scale and pore domain (cf. Chapter 2.3.2, 2.3.3, 2.3.4, 4.3.2). The unknown parameter value without estimates based on measurements (water exchange coefficient between the pore domains) was calibrated.

In the reference studies, fixed parameter values originating from soil core analyses have more commonly been used. For instance, James et al. (2010)

used fixed and constant soil core estimates for the saturated hydraulic conductivity and for the van Genuchten parameters in the whole soil profile when simulating flow in the Panola hillslope, USA, with the one pore domain version of the three-dimensional TOUGH2 model. Different values for the conductivity at the soil bedrock interface and drainable porosity of soil were tested. The model failed to capture the observed internal storage dynamics and trench flow due to the structural inadequacy of the model, and the parameterisation used.

Gärdenäs et al. (2006) fixed all parameters with values obtained from pedotransfer functions when simulating flow and pesticide transport in a tile-drained field with the single and dual pore domain versions of the two-dimensional HYDRUS model. Different parameter values were used for different parts and depths of the field. The dual-permeability model most accurately simulated the measured dynamics of pesticide leaching from the field, even though it overestimated the total drainage. Gärdenäs et al. (2006) note that a better agreement between measured and simulated drainage rates could probably be obtained by adjusting the parameterisation.

Vogel et al. (2007) fixed most of the parameter values based on soil core analyses and literature values when simulating the penetration of cadmium into an agricultural sandy-loam field with the one-dimensional S1 Dual model. The van Genuchten model parameters α and β (cf. Equation 1) related to the soil matrix, and the saturated hydraulic conductivity and the exchange coefficient related to the preferential flow domain were optimized by means of inverse modelling. The model was considered most sensitive for these parameters in terms of the infiltration rate. The inverse modelling was based on the observed and simulated cumulative infiltration. The amount of optimised parameters was kept low to avoid problems with non-uniqueness of the solution. Despite the use of optimised parameter values in the dual-permeability model, a single continuum model was concluded to provide a good alternative explanation for the deep cadmium penetration.

Dusek et al. (2010) also modelled the penetration of cadmium into clayey and loamy soils in an agricultural area with the S1Dual model. Similarly to Vogel et al. (2007), Dusek et al. (2010) used measured water retention parameters for the soil matrix and parameters of coarse sand presented in the literature for the preferential flow domain. The use of literature-derived values was justified by the fact that the water retention properties of the preferential pathways are of less importance than their conductivities. The saturated hydraulic conductivities were estimated from in situ tension infiltrometer measurements. Water and solute transfer coefficients were set near the values

calibrated by Vogel et al. (2007). However, a sensitivity analysis for the exchange coefficients was presented, and the results indicated only a slight effect of the transfer coefficients on the simulated cadmium leaching. Since the study aimed to predict the leaching of cadmium at three sites, no comparison to observations was presented and a further analysis of the parameterisation was not possible.

Using the flow data on laboratory soil columns of loam and sand, and bromide transport data from a tile-drained field, Köhne et al. (2006) analysed the identification of soil hydraulic parameters of dual-permeability models by inverse modelling. Most of the parameters of the one-dimensional HYDRUS model were optimised. The successful simulation of field-scale preferential solute transport, concurrently with estimating the hydraulic and solute transport parameters suggests that effluent solute concentrations contain indirect information about preferential water flow, and the information can be used to identify hydraulic dual-permeability model parameters. Gerke et al. (2007) based the parameterisation on earlier calibrations when simulating the bromide transport with the two-dimensional 2D-DPERM model. Even though the simulations could not reproduce the observed movement of the bromide, the study of Gerke et al. (2007) also demonstrated the importance of tracer data for the model development. The study concludes that drainage curves may be simulated comparably with different model approaches, whereas the tracer data contains information on the flow and transport processes.

Compared with the parameterisations discussed above, this study showed the effectiveness of tracer data in adjusting and calibrating parameters that cannot be directly measured, when the majority of the model parameters are fixed with measured values that they most probably represent. The adjusted and calibrated parameters of the dual-permeability model functioned as a group in a way that supported the model identifiability and capturing of the observed stormflow event with the model. The search for the horizon-wise changing parameter values was enabled by the versatility of the tracer data that exhibited the initiation, steady-state and recession period of a stormflow event, as well as flow and exchange of water and solute between the pore domains in varying moisture conditions. Correspondence of the measured and simulated groundwater levels also demonstrated the power of the tracer data in the model development process, when the model was fitted to the concentration data and migration velocity along the slope (Chapter 5.2.4).

As noted in Chapter 5.3.3, small porosity and high conductivity values were needed in the preferential flow domain of the dual-permeability model to reach the observed, high migration velocity of the saturation front at the first

time point. The depth distribution of these parameter values was controlled by the observed shape of the tracer plume in the slope. Small porosity values and a high exchange coefficient were, for their part, important in reaching the observed, high concentrations in the slope for the first time point and the fast dilution at the second time point. In general, the same value of the exchange coefficient produced the highest goodness of fit for both the observed time points, but a different depth distribution of the saturated hydraulic conductivity was optimal for the first and at the second time point observed (Chapter 5.2.3).

Summarising the interplay of adjusted and calibrated parameters, small porosity and high conductivity values of the preferential flow domain, combined with a high exchange coefficient between the pore domains ensured a high enough flux and a low enough discharge for the preferential flow domain, combined with a fast exchange of water and solute between the domains. This combination raised both the saturation velocity and the degree of saturation, as well the concentrations along the slope to the observed level. In general, the model outcome was mainly controlled by the fractioning of the total porosity into the soil matrix and the preferential flow domain, the saturated hydraulic conductivity of the preferential flow domain, and the exchange coefficient between the domains. The model was less sensitive to the saturated hydraulic conductivity of the soil matrix and to the water retention properties that were fixed.

The data available in this study do not support a detailed analysis of the representativeness of the fixed parameter values. For instance, the lack of soil moisture data during the irrigations restricts a detailed analysis of the water retention parameters. The soil analysis (Chapter 2.3.2) implies that the reliability of the water retention parameters is uncertain, due to the small amount of undisturbed soil cores, combined with the high variability in the results. The inaccurate parameter values may produce an unrealistic infiltration pattern in particular in simulating the initial irrigation period and moistening of dry soil. However, the results indicated that the shortcomings of the model, such as the difficulties in capturing the observed stormflow event when the initial irrigation period is included in the simulation, cannot be fixed with different water retention parameters or saturated hydraulic conductivities of the soil matrix. The shortcomings did therefore not result from the values of the fixed parameters. The bottleneck of the parameterisation was rather related to the saturated moisture content of soil that was presumed equal to the total porosity, measured by saturating soil cores (cf. Chapter 5.3.3).

The saturated moisture content turned out to be the most critical factor in assessing the adequacy of the dual-permeability model. This is in line with the findings of e.g. Kettunen (1993), who studied the identifiability of a one-dimensional, Richards' equation-based model for soil moisture in 12 field lysimeters in southern Finland. The lysimeters represented different soil types and were originally used for evapotranspiration studies by Vakkilainen (1982). According to Kettunen (1993), saturated moisture content and the empirical parameter β of the van Genuchten model (cf. Eq. 1, Chapter 2.3.2) are the most influential parameters in terms of the structural sensitivity of the soil moisture model.

In the present study, the saturated moisture content of soil was *a priori* fixed, since porosity was considered a good estimate of the moisture content, and the measurement of porosity was considered reliable. However, the variation of the porosity values was high (Chapter 2.3.4), as was the variation in the stone content estimates that were used to correct the data to represent the soil pore space on the hillslope scale. In addition, porosity values, determined by saturating soil cores, are necessarily not good estimates for the saturated moisture content in the field, as noted in Chapter 5.3.3. To capture the observed stormflow event with the dual-permeability model in this study, when the initial irrigation period was included in the simulation, a 30 % correction of the average values was needed for the porosity of the soil matrix. The correction fits inside the variation of the measured porosity values (Chapter 2.3.4), but can also be justified by the fact that soil does not fully saturate in natural conditions. Verification of the porosity and stone content data is therefore important for future studies.

Considering the porosity values further, the simulations suggest that *a priori* determination of the fractioning of the pore space into soil matrix and preferential flowroutes is not crucial for the model development. The model outcome, especially the simulated tracer concentration, is strongly influenced by the fractioning used, but a suitable value for the fractioning can be found when fitting the model to correspond to the observed tracer event. Thus, the model development process rather gave an estimate of the macroporosity of soil than the assessments presented in the soil analysis using e.g. the water retention data (Chapter 2.3.4). Values used at the end for the porosity of the preferential flow domain correspond to the definition of about 100-250 μm for a macropore, depending on the water retention data used in the determination with Equation 2.

Experimental evidence suggests that pores larger than 300 μm in equivalent cylindrical diameter allow rapid non-equilibrium flow (Jarvis 2007). The

estimates used in this study, i.e. 100-250 μm, correspond to the estimate of 300 μm, if stone content is not taken into account and the soil material is considered on the soil core scale. In addition, the estimates used correspond roughly to the estimates available from saturated, undisturbed water retention samples after draining for 24 hours (Chapter 2.3.4). Thus, in future studies, an indicative value for the macroporosity can be estimated by determining the air-capacity of soil samples that is closely related to *effective macroporosity* (Germann and Beven 1981). Pore size -based techniques may yield estimates not corresponding to channelling macroporosity (Beven and Germann 1982).

The only parameter without any initial estimate was the water exchange coefficient between the pore domains in the dual-permeability model. The lack of a direct measurement method and the use of variously determined exchange terms in different models (Chapter 5.3.1) restrain a direct comparison and assessment of the values of the exchange coefficient. In this study, the optimal value range for the lumped exchange coefficient, i.e. 0.001-0.01 cm^{-2}, was found simultaneously to adjusting the porosity and conductivity parameters. In the HYDRUS model (Šimůnek et al. 1999, 2003), the definition of Gerke and van Genuchten (1993a) can be used for the water exchange similarly to this study. Köhne et al. (2006) obtained a value of 0.0035 cm^{-2} for the coefficient as a result of inverse modelling, when simulating one-dimensional flow in loam and sand soil columns, and one-dimensional bromide transport in a tile-drained, loamy field in Germany. Gärdenäs et al. (2006) set the value of the coefficient to 0.004 cm^{-2}, following the definitions presented in Gerke and van Genuchten (1993a, 1993b), when simulating two-dimensional pesticide transport from a tile-drained, loamy till soil field in Sweden.

The values used by Köhne et al. (2006) and Gärdenäs et al. (2006) for the lumped exchange coefficient are of same magnitude than was considered suitable in this study. The studies of Köhne et al. (2006) and Gärdenäs et al. (2006) apply to tile-drained fields with fine-fractured soils whereas this study applies to forest soil with the parent material sandy till. The suitability of about the same value for the different sites implies that the same value may be usable for various sites in general. However, more studies on the exchange term and suitable values for different sites are needed in order to create a more reliable conception on the variation of suitable values in different conditions. This study emphasizes the importance of tracer data in searching for a value for the exchange coefficient and in analysing the exchange mechanisms in general.

6 Conclusions

This study presented a unique combination of experimental data to quantify the physical and hydraulic properties, to visualize the flowpaths and patterns, and to capture a subsurface stormflow event dominated by preferential flow in a Finnish, forested hillslope with a shallow, sandy till cover above impermeable bedrock. The dataset enabled the development, parameterisation and analysis of a full three-dimensional, Richards' equation-based dual-permeability model for flow and conservative solute transport. The dual-permeability model was clearly more suitable for simulating subsurface flow and transport processes in the study slope than a traditional, one pore domain model. The dual-permeability model contained the main mechanisms required for reproducing the recorded, subsurface stormflow event. Concentration data of the tracer experiment was crucial both for interpreting the subsurface flow and transport processes in the slope and for developing the dual-permeability model.

The soil analysis showed that heterogeneity of the soil physical properties causes variation in the soil hydraulic properties, together with inaccuracies and scale issues related to the different measurement methods. However, the depth distribution of the soil properties followed a consistent pattern in the soil profile: granularity, stone content, porosity, and hydraulic conductivity, as well as the variances of these properties all decreased non-linearly with depth. The higher conductivities and the resulting higher flow rates near the soil surface were mainly due to preferential flowpaths. The tracer experiments and the model development process showed that the effect of preferential routes is, however, only partly included in the results of the soil analysis.

Tracer experiments implied, together with the model applications, that the real, large-scale hydraulic conductivities near and at saturation, and in particular in the upper 50 cm of the soil profile, are significantly higher than expected based on the soil analysis. In order to conceptualise and model field-scale phenomena, the soil hydraulic properties need to be determined on the corresponding scale. The inverse, one-dimensional groundwater model, using the water table data of the recession period of the ion tracer experiment, produced estimates of the saturated hydraulic conductivity that were compatible with the dual-permeability model for simulating the migration,

strengthening and dilution of the tracer plume. Assessment of the representativeness of the water retention data was not directly supported by the data available from the tracer experiments and the modelling process.

The dye tracer experiments visualized preferential flowpaths related to large voids around stone surfaces, to loose, heterogeneous soil material, and to structural variation caused by roots, fauna and chemical reactions in soil. The dyed flowpaths reached the same depth as roots, i.e. 40 cm from the top of the mineral soil profile and nearly 50 cm from the top of the organic layer. Changes in the water levels during the ion tracer experiment implied that the transitional zone at about 50 cm depth is critical in terms of the generation of subsurface stormflow, dominated by lateral preferential flow. Lateral flow increased non-linearly when the water table approached the uppermost soil horizon. The conductivity of the soil near the soil surface was so high that not even the heavy irrigation of the ion tracer experiment could produce infiltration or saturation excess overland flow. Subsurface stormflow, enabled by preferential flow paths, is therefore the dominating mechanism of runoff generation in the study slope.

The ion tracer experiment provided distinctive concentration data on the development and analysis of different versions of Richards' equation-based flow and solute transport models. The modelling process showed that a one pore domain model is as such inadequate in capturing the observed stormflow event, produced by the tracer experiment. Outcome of the one pore domain model improved by fine-tuning the initial moisture status and parameterisation, but in particular by restricting the model application to a fraction of the total pore space that contributes actively to runoff generation. However, water and solutes are transferred between the different pore spaces of soil, whereupon a parallel and coupled simulation of the soil matrix is necessary alongside the simulation of the active pore domain, which leads into the development of two pore domain models.

The modelling process clearly demonstrated the superiority of a two pore domain approach in simulating subsurface stormflow and conservative solute transport in the study slope. The dual-permeability model developed was able to capture the main mechanisms behind the observed event and was therefore considered a sufficient representation of runoff generation at the study slope. Richards' equation was considered suitable for describing flow in both pore domains, and shortcomings related to the model outcomes were considered to result from the parameter values, in particular from the saturated moisture content, rather than from structural inadequacy of the model. The study thereby supports the development of dual-permeability models to simulate

flow and solute transport in mineral forest soils in the boreal region in general. The development of dual-permeability models requires a variety of data for the model parameterisation and simulations, information on the representativeness and shortcomings of the data, a clear perception of the key mechanisms behind the modelled phenomenon, and the ability to adjust the model to meet the needs of the specific site and phenomenon in question. Considering the parameterisation, identification and testing of a dual-permeability model, this study emphasizes the importance of tracer data.

The presented parameterisation routine proved to be an applicable way to parameterise a dual-permeability model, and it provides an option for fixing, adjusting and calibrating parameters when utilising measured parameter values in combination with tracer data and inverse modelling. Values for the fractioning of the total pore space into the two pore domains, for the saturated hydraulic conductivity of the preferential flow domain, and for the water exchange coefficient between the domains could be identified based on the concentration data of the tracer experiment, when the water retention parameters and the saturated hydraulic conductivity of the soil matrix were fixed based on the soil analysis. The adjusted or calibrated parameters mainly controlled the model outcome, whereas the fixed parameters had a smaller influence on the key processes. According to the model applications, the most crucial parameter to be measured as reliably as possible is the soil pore space that saturates in natural conditions.

A combination of soil analysis, tracer experiments and detailed physics-based models gives valuable information on the hydraulic properties, on the subsurface flow and solute transport processes, and on the requirements and capabilities of model applications of forest soils. A tight interplay between experimental work and model development benefits both the measurements and the model development, as the data and models are evaluated against each other. The amount of data required for the development of detailed, physics-based models is, however, excessive, and the models are usually too heavy for wider operational use. This poses a challenge both to measurement techniques and to the development of simpler models for the various operational tasks in environmental assessments. Considering the main mechanism to be included in simpler models, the study emphasizes the role of preferential flow in a fraction of the total pore space, linked with a dynamic exchange of water and solutes with the soil matrix. As for the further development of the model of this study, evaluation against soil moisture data in dry conditions benefits the investigation of the water retention properties and the exchange coefficient.

References

Abbaspour, K. C., Johnson, C. A. and van Genuchten, M. Th. 2004. Estimating Uncertain Flow and Transport Parameters Using a Sequential Uncertainty Fitting Procedure. Vadose Zone Journal, vol. 3, pp. 1340-1352.

Airaksinen, J. 1978. Soil and groundwater hydrology. Kirjapaino Osakeyhtiö Kaleva. Oulu. In Finnish.

Allaire, S. E., Roulier, S. and Cessna, A. J. 2009. Quantifying preferential flow in soils: A review of different techniques. Journal of Hydrology, vol. 378, pp. 179-204.

Amoozegar, A. 2002. Chapter 3.4.3.5: Piezometer Method (Saturated Zone). Pp. 870-877 in Methods of Soil Analysis, Part 4, Physical Methods. Dane, J. H. and Topp, G. C. (ed.). Number 5 in the Soil Science Society of America Book Series. Published by the Soil Science Society of America, Inc., USA.

Aubertin, G. M. 1971. Nature and Extent of Macropores in Forest Soils and Their Influence on Subsurface Water Movement. U.S.D.A. Forest Service Research Paper NE-192.

Beldring, S. 2002. Runoff Generating Processes in Boreal Forest Environments with Glacial Tills. Nordic Hydrology, vol. 33 (5), pp. 347-372.

Beven, K. J. 1997. TOPMODEL: A CRITIQUE. Hydrological Processes, vol. 11, pp. 1069-1085.

Beven, K. J. 2004. Surface runoff at the Horton Hydrologic Laboratory (or not?). Journal of Hydrology, vol. 293, pp. 219-234.

Beven, K. J. 2006. Streamflow generation processes. Selection, Introduction and Commentary by Keith J. Beven. In the Series “Benchmark papers in Hydrology”, Series Editor Jeffrey J. McDonnell. International Association of Hydrological Sciences. Press: Wallingford, Oxfordshire.

Beven, K. J. 2008. On doing better hydrological science. Hydrological Processes, vol. 22, pp. 3549-3553.

Beven, K. J. and Binley, A. 1992. The future of distributed models: model calibration and uncertainty prediction. Hydrological Processes, vol. 6, pp. 279-298.

Beven, K. J. and Freer, J. 2001. A dynamic TOPMODEL. Hydrological Processes, vol. 15, pp. 1993-2011.

Beven, K. J. and Germann, P. 1982. Macropores and Water Flow in Soils. Water Resources Research, vol. 18 (5), pp. 1311-1325.

Bishop, K., Seibert, J., Köhler, S. and Laudon, H. 2004. Resolving the Double Paradox of rapidly mobilized old water with highly variable responses in runoff chemistry. Hydrological Processesses, vol. 18, pp. 185–189.

Blöschl, G. and Sivapalan, M. 1995. Scale Issues in Hydrological Modelling: A Review. In: Scale Issues in Hydrological Modelling, edited by Kalma, J. D. and Sivapalan, M. John Wiley & Sons.

Brassington, R. 1998. Field Hydrogeology. Second Edition. John Wiley & Sons Ltd, England.

Brewer, R. 1964. Fabric and mineral analysis of soils. Wiley, New York.

Bronstert, A. 1999. Capabilities and limitations of detailed hillslope hydrological modeling. Hydrological Processes, vol. 13, pp. 21-48.

Buckingham, E. 1907. Studies on the movement of soil moisture. Bulletin 38. USDA, Bureau of Soils, Washington D.C.

Burger, H. 1922. Physikalische Eigenschaften von Wald- und Freilandböden. Mitteilung der Schweizerischen Zentralanstalt für das forstliche Versuchswesen, vol. 13(1), pp. 1–221. In German.

Buttle, J. M. and House, D. A. 1997. Spatial variability of saturated hydraulic conductivity in shallow macroporous soils in a forested basin. Journal of Hydrology, vol. 203, pp. 127-142.

Buttle, J. M. and McDonald, D. J. 2002. Coupled vertical and lateral preferential flow on a forested slope. Water Resources Research, vol. 38 (5), pp. 18-1 – 18-15.

Buytaert, W., Reusser, D., Krause, S. and Renaud, J. P. 2008. Why can't we do better than TOPMODEL? Hydrological Processes, vol. 22, pp. 4175-4179.

Cajander, A. K. 1949. Forest types and their significance. Posthumous publication. Acta Forestalia Fennica, 56: 5. 71 pp.

Celia, M. A., Bouloutas, E. and Zarba, R. L. 1990. A general mass-conservative numerical solution for the unsaturated flow equation. Water Resources Research, vol. 26 (7), pp. 1483–1496.

Davis, S. N., Thompson, G. M., Bentley, H. W. and Stiles, G. 1980. Ground-water tracers – a short review. Ground Water, vol. 18, pp. 14-23.

Deeks, L. K., Bengough, A. G., Stutter, M. I., Young, I. M. and Zhang, X. X. 2008. Characterisation of flow paths and saturated conductivity in a soil block in relation to chloride breakthrough. Journal of Hydrology, vol. 348: 3-4, pp. 431-441.

Dressler, M. The website for SurGe gridding and mapping software. Last revised 21.12.2010. Available at: http://surgeweb.sweb.cz/

Dunn, S. M., McDonnell, J. J. and Vaché, K. B. 2007. Factors influencing the residence time of catchment waters: A virtual experiment approach. Water Resources Research, vol. 43, W06408. American Geophysical Union.

Dusek, J., Vogel, T., Lichner, L. and Cipakova, A. 2010. Short-term transport of cadmium during a heavy-rain event simulated by a dual-continuum approach. Journal of Plant Nutrition and Soil Science, vol. 173, pp. 536-547.

Dyck, S. and Peschke, G. 1995. Grundlagen der Hydrologie. 3. Auflage. Verlag für Bauwesen GmbH Berlin. In German.

Ebel, B. A. and Loague, K. 2006. Physics-based hydrologic-response simulation: Seeing through the fog of equifinality. Hydrological Processes, vol. 20, pp. 2887-2900.

Espeby, B. 1989. Water Flow in a Forested Till Slope – Field Studies and Physically Based Modelling. Dissertation. Royal Institute of Technology, Department of Land and Water Resources. Report Trita-Kut No. 1052. Stockholm, Sweden.

FAO. 1988. Soil Map of the World. FAO/UNESCO, Rome. World Resources Report 60.

Fetter, C. W. 2001. Applied Hydrogeology. 4th edition. Prentice-Hall Inc., Upper Saddle River, New Jersey.

Finér, L., Ahtiainen, M., Mannerkoski, H., Möttönen, V., Piirainen, S., Seuna, P. and Starr, M. 1997. Effects of harvesting and scarification on water and nutrient fluxes. A description of catchments and methods, and results from the pretreatment calibration periods. The Finnish Forest Research Institute, Research Papers 648.

Finnish Environment Institute. 2006. Hydrological overview 2005. A web-document, in Finnish. First published 29.3.2006, last revised 19.5.2010. Available at: http://www.miljo.fi/default.asp?node=16403&lan=fi

Flury, M. and Flühler, H. 1994. Brillant Blue FCF as a Dye Tracer for Solute Transport Studies – A Toxicological Overview. Journal of Environmental Quality, vol. 23, pp. 1108-1112.

Flury, M. and Wai, N. N. 2003. Dyes as tracers for vadose zone hydrology. Reviews of Geophysics, vol. 41, 1 / 1002.

Fowler, M. 2004. UML distilled: a brief guide to the standard object modeling language. Third edition. Addison-Wesley, Boston.

Gaiser, R. N. 1952. Root channels and roots in forest soils. Soil Science Society of America, Proc., vol. 16(1), pp. 62-65.

Gerke, H. H. 2006. Preferential flow descriptions for structured soils. Journal of Plant Nutrition and Soil Science, vol. 169, pp. 382-400.

Gerke, H. H. and van Genuchten, M. T. 1993a. A Dual-Porosity Model for Simulating the Preferential Movement of Water and Solutes in Structured Porous Media. Water Resources Research, vol. 20 (2), pp. 305-319.

Gerke, H. H. and van Genuchten, M. T. 1993b. Evaluation of a first-order water transfer term for variably saturated dual-porosity flow models. Water Resources Research, vol. 29, pp. 1225–1238.

Gerke, H. H. and van Genuchten, M. T. 1996. Macroscopic representation of structural geometry for simulating water and solute movement in dual-porosity media. Advances in Water Resources, vol. 19 (6), pp. 343-357.

Gerke, H. H., Dusek, J., Vogel, T. and Köhne, J. M. 2007. Two-Dimensional Dual-Permeability Analyses of a Bromide Tracer Experiment on a Tile-Drained Field. Vadose Zone Journal, vol. 6 (3), pp. 651-667.

Germann, P. and Beven, K. 1981. Water flow in soil macropores, 3, A statistical approach. The Journal of Soil Science, vol. 32, pp. 31-39.

Graham, C. B., Woods, R. A. and McDonnell, J. J. 2010a. Hillslope threshold response to rainfall: (1) A field based forensic approach. Journal of Hydrology, vol. 393, pp. 65-76.

Graham, C. B. and McDonnell, J. J. 2010b. Hillslope threshold response to rainfall: (2) Development and use of a macroscale model. Journal of Hydrology, vol. 393, pp. 77-93.

Grayson, R. and Blöschl, G. 2000. Spatial Modelling of Catchment Dynamics. In: Grayson, R. and Blöschl, G. (eds). 2000. Spatial Patterns in Catchment Hydrology: Observations and Modelling. Cambridge University Press.

Greenland, D. J. 1977. Soil damage by intensive arable cultivation: Temporary or permanent? Philos. Trans. R. Soc. London, Ser. B 281:193–208.

Gupta, H. V., Wagener, T. and Liu, Y. 2008. Reconciling theory with observations: elements of a diagnostic approach to model evaluation. Hydrological Processes, vol. 22, pp. 3802-3813.

Gärdenäs, A. I., Šimůnek, J., Jarvis, N. and van Genuchten, M. Th. 2006. Two-dimensional modelling of preferential water flow and pesticide transport from a tile-drained field. Journal of Hydrology, vol. 329, pp. 647-660.

Haldorsen, S. and Krüger, J. 1990. Till Genesis and Hydrogeological Properties. Nordic Hydrology, vol. 21, pp. 81-94.

Harr, R. D. 1977. Water Flux in Soil and Subsoil on a Steep Forested Slope. Journal of Hydrology, vol. 33, pp. 37-58.

Hewlett, J. D. and Hibbert, A. R. 1967. Factors affecting the response of small watersheds to precipitation in humid areas. In: International Symposium on Forest Hydrology. Sopper, W. E. and Lull, H. W. (ed.), pp. 275-290.

Hoover, M. D. and Hursh, C. R. 1943. Influence of topography and soil-depth on runoff from forest land. Transactions - American Geophysical Union, vol. 24, pp. 693-697.

Hopp, L. and McDonnell, J. J. 2009. Connectivity at the hillslope scale: Identifying interactions between storm size, bedrock permeability, slope angle and soil depth. Journal of Hydrology, vol. 376, pp. 378-391.

Horton, R. E. 1933. The role of infiltration in the hydrologic cycle. Transactions - American Geophysical Union, vol. 14, pp. 446-460.

Hubbart, J. (Lead Author), Kundell, J. (Topic Editor). 2007. History of hydrology. In: Encyclopedia of Earth. Ed. Cleveland, C. J. Washington, D.C.: Environmental Information Coalition, National Council for Science and the Environment. First published May 20, 2007. Last revised May 21, 2007. Retrieved October 3, 2007.
Available at: http://www.eoearth.org/article/History_of_hydrology

Hyvärinen, V. (ed.). 1994. Hydrological Yearbook 1994. Finnish Environment Institute. Oy Edita Ab, Helsinki.

Hyyppä, J., Niemelä, J., Nuotio, T. and Räisänen, M-L. 1992. Soil formation. Atlas of Finland. Section 123–126 (1990): Geology. Helsinki, National Board of Survey. Geographical Society of Finland, pp. 20–21. In Finnish.

Hänninen P. and Penttinen, S. 2006. Annual variation of water content, temperature, and electrical conductivity of groundwater in different types of forest soils in North Karelia in 2002-2005. Report of the Geological Survey of Finland, P31.4.050. In Finnish.

Hänninen, P., Laine-Kaulio, H. and Sutinen, R. 2010. Macropores and preferential flowpaths in the vadose zone. Vesitalous, vol. 3, pp. 33-37. In Finnish.

Hänninen, P., Sutinen, R., Lintinen, P. and Lojander, S. 2000. Computational water conductivity of the upper parts of soil in Finland. In: Pro Terra no 4. Extended abstracts of the national congress for Soil Sciences. Peltola, L. (ed.). Finnish Soil Science Society and University of Helsinki. In Finnish.

Hänninen, P., Sutinen, R., Suomi, T., Äikää, O., Penttinen, S. and Majaniemi, J. 2003. Soil monitoring stations of the Geological Survey of Finland in 2000-2002. Report of the Geological Survey of Finland, P31.4.035. In Finnish.

Ilvesniemi, H., Pumpanen, J., Duursma, R., Hari, P., Keronen, P., Kolari, P., Kulmala, M., Mammarella, I., Nikinmaa, E., Rannik, Ü., Pohja, T., Siivola, E. and Vesala, T. 2010. Water balance of a boreal Scots pine forest. Boreal Environment Research, vol. 15, pp. 375-396.

James, A. L., McDonnell, J. J., Tromp-van Meerveld, H. J. and Peters, N. E. 2010. Gypsies in the palace: experimentalist's view on the use of 3-D physics-based simulation of hillslope hydrological response. Hydrological Processes, vol. 24, pp. 3878-3893.

Jansson, C., Espeby, B. and Jansson, P. E. 2005. Preferential water flow in a glacial till soil. Nordic Hydrology, vol. 36 (1), pp. 1-11.

Jansson, P.-E. and Halldin, S. 1979. Model for the annual water and energy flow in a layered soil. In: Halldin, S. (ed.). Comparison of Forest and Energy Exchange Models. Society for Ecological Modellin, Copenhagen, pp. 145-163.

Jansson, P.-E. and Karlsberg, S. 2001. Coupled Heat and Mass Transfer Model for Soil-Plant-Atmosphere Systems. User's manual. Division of Land and Water Resources, KTH, Stockholm.

Jarvis, N. 1991. MACRO: a model of water movement and solute transport in macroporous soils. Reports and Dissertations 19, Swedish University of Agricultural Science, Department of Soil Science.

Jarvis, N. 2007. A review of non-equilibrium water flow and solute transport in soil macropores: principles, controlling factors and consequences for water quality. European Journal of Soil Science, vol. 58, pp. 523–546.

Jarvis, N., Larsbo, M., Roulier, S., Lindahl, A. and Persson, L. 2007. The role of soil properties in regulating non-equilibrium macropore flow and solute transport in agricultural topsoils. European Journal of Soil Science, vol. 58, pp. 282-292.

Jauhiainen, M. 2004. Relationships of particle size distribution curve, soil water retention curve and unsaturated hydraulic conductivity and their implications on water balance of forested and agricultural hillslopes. Doctoral dissertation. Helsinki University of Technology, Water resources publications, 165 p.

Jenssen, P. D. 1990. Methods for Measuring the Saturated Hydraulic Conductivity of Tills. Nordic Hydrology, vol. 21, pp. 95-106.

Johnson, M. S. and Lehmann, J. 2006. Double-funneling of trees: Stemflow and root-induced preferential flow. Ecoscience, vol. 13 (3), pp. 324-333.

Jongerius, A. 1957. Morphologic investigation of the soil structure. Meded. Stricht. Bodemkartering. Bodem Stud. Wageningen, the Netherlands.

Kareinen, T. and Ilvesniemi, H. 2002. Analysis of water fluxes in forest soils using multi-region models. In: Pro Terra no. 15. Extended abstracts of the national congress for Soil Sciences. Peltola, L. and Esala, M. (ed.). Finnish Soil Science Society and University of Helsinki. In Finnish.

Karvonen, T. 1988. A Model for Predicting the Effect of Drainage on Soil Moisture, Soil Temperature and Crop Yield. Doctoral thesis. Helsinki University of Technology, Finland.

Karvonen, T. 2003. Solute Transport in Soil and Groundwater. Web book, Helsinki University of Technology. Updated on November 20th 2003, cited on October 4, 2007. Available at:
http://www.water.tkk.fi/wr/kurssit/Yhd-12.126/oppimateriaali/paa_e.htm

Kettunen, J. 1993. Model-oriented data analysis with applications to lake and soil water simulation. Doctoral thesis, Helsinki University of Technology, Finland.

Kienzler, P. M. and Naef, F. 2008. Subsurface storm flow formation at different hillslopes and implications for the 'old water paradox'. Hydrological Processes, vol. 22, pp. 104-116.

Kirchner, J. W. 2003. A double paradox in catchment hydrology and geochemistry. Hydrological Processes, vol. 17, pp. 871–874.

Kirchner, J. W. 2006. Getting the right answers for the right reasons: linking measurements, analyses, and models to advance the science of hydrology. Water Resources Research, vol. 42, W03S04.

Klemeš, V. 1986. Operational testing of hydrological simulation models. Hydrological Sciences – Journal, vol. 31, pp. 13-24.

Klotz, D. and Seiler, K. P. 1980. Labor und Geländeversuche zur Ausbreitung konservativer Tracer in fluvioglazialen Kiesen von Oberbayern. GSF-Ber. R250, 74-89, München. In German.

Koivusalo, H. and Kokkonen, T. 2003. Modelling runoff generation in a forested catchment in southern Finland. Hydrological Processes, vol. 17, pp. 313-328.

Koivusalo, H., Karvonen, T. and Lepistö, A. 2000. A quasi-three-dimensional model for predicting rainfall-runoff processes in a forested catchment in southern Finland. Hydrology and Earth System Sciences, vol. 4, pp. 65-78.

Kämäri, J., Rankinen, K., Finér, L., Piirainen, S. and Posch, M. 1998. Modelling the response of soil and runoff chemistry to forest harvesting in a low deposition area (Kangasvaara, Eastern Finland). Hydrology and Earth System Sciences, vol. 2 (4), pp. 485-495.

Käss, W. 1998. Tracing Technique in Geohydrology. A. A. Balkema Publishers, Brookfield, USA.

Köhne, J. M., Mohanty, B. P. and Šimůnek, J. 2006. Inverse Dual-Permeability Modeling of Preferential Water Flow in a Soil Column and Implications for Field-Scale Solute Transport. Vadose Zone Journal, vol. 5, pp. 59-76.

Laine-Kaulio, H. 2008. Subsurface flow in a forested till slope: Soil analysis, tracer experiments and physics-based modelling. Licentiate's thesis, Helsinki University of Technology. 100 pp.

Larsbo, M. and Jarvis, N. J. 2003. MACRO5.0. A Model of Water Flow and Solute Transport in Macroporous Soil. Technical description. Emergo 2003:6, Studies in the Biogeophysical Environment, SLU. Department of Soil Science, Uppsala.

Larsbo, M., Roulier, S., Stenemo, F., Kasteel, R. and Jarvis, N. 2005. An Improved Dual-Permeability of Water Flow and Solute Transport in the Vadose zone. Vadose Zone Journal, vol. 4, pp. 398-406.

Laudon, H., Seibert, J., Köhler, S. and Bishop, K. 2004. Hydrological flow paths during snowmelt: Congruence between hydrometric measurements and oxygen 18 in meltwater, soil water, and runoff. Water Resources Research, vol. 40, W03102.

Laudon, H., Sjöblom, V., Buffam, I., Seibert, J. and Mörth, M. 2007. The role of catchment scale and landscape characteristics for runoff generation of boreal streams. Journal of Hydrology, vol. 344, pp. 198-209.

Laurén, A., Finér, L. Koivusalo, H., Kokkonen, T., Karvonen, T., Kellomäki, S., Mannerkoski, H. and Ahtiainen, M. 2005. Water and nitrogen processes along a typical water flowpath and streamwater exports from a forested catchment and changes after clear-cutting: a modelling study. Hydrology and Earth System Sciences, vol. 9 (6), pp. 657-674.

Lepistö, A. 1994. Areas contributing to generation of runoff and nitrate leaching as estimated by empirical isotope methods and TOPMODEL. Aqua Fennica, vol. 24, pp. 103-120.

Lepistö, A., Seuna, P., and Bengtsson, L. 1994. The environmental tracer approach in storm runoff studies in forested catchments. FRIEND: Flow Regimes from International Experimental and Network Data. Proceedings of the Braunschweig Conference, October 1993. IAHS Publications, no. 221.

Lind, B. B. and Lundin, L. 1990. Saturated hydraulic conductivity of Scandinavian tills. Nordic Hydrology, vol. 21, pp. 107-118.

Loague, K. and VanderKwaak, J. E. 2004. Physics-based hydrological response simulation: platinum bridge, 1958 Edsel, or useful tool. Hydrological Processes, vol. 18, pp. 2949-2956.

Luthin, J. N. and Kirkham, D. 1949. A piezometer method for measuring permeability of soil in situ below a water table. Soil Science, vol. 68 (5), pp. 349-358.

Luxmoore, R. J., Jardine, P. M., Wilson, G. V., Jones, J. R. and Zelazny, L. W. 1990. Physical and chemical controls of preferred path flow through a forested hillslope. Geoderma, vol. 46, pp. 139-154.

Mannerkoski, H., Finér, L., Piirainen, S. and Starr, M. 2005. Effect of clear-cutting and site preparation on the level and quality of groundwater in some headwater catchments in eastern Finland. Forest Ecology and Management, vol. 220, pp. 107-117.

McDonnell, J. J. 1990. A Rationale for Old Water Discharge Through Macropores in a Steep, Humid catchment. Water Resources Research, vol. 26 (11), pp. 2821-2832.

McDonnell, J. J. 2003. Where does water go when it rains? Moving beyond the variable source area concept of rainfall-runoff response. Hydrological Processes, vol. 17, pp. 1869-1875.

McDonnell, J. J. and Tanaka, T. 2001. On the future of forest hydrology and biogeochemistry. Hydrological Processes, vol. 15, pp. 2053-2055.

McDonnell, J. J. Benchmark Papers Anthology, the web page of the Oregon State University, course on Hillslope Hydrology. Retrieved October 3, 2007. Original year of publication unknown. Available at: http://www.cof.orst.edu/cof/fe/watershd/fe537/bpapers.html

McDonnell, J. J., Sivapalan, M., Vaché, K., Dunn, S., Grant, G., Haggerty, R., Hinz, C., Hooper, R., Kirchner, J., Roderick, M. L., Selker, J. and Weiler, M. 2007. Moving beyond heterogeneity and process complexity: A new vision for watershed hydrology. Water Resources Research, vol. 43, W07301.

McIntosh, J., McDonnell, J. J. and Peters, N. E. 1999. Tracer and hydrometric study of preferential flow in large undisturbed soil cores from the Georgia Piedmont, USA. Hydrological Processes, vol. 13, pp. 139-155.

McIntyre, D. S. 1974. Pore space and aeration determinations. In: Methods for analysis of irrigated Soils, pp. 67-74. Loveday, J. (ed.). Commonw. Agric. Bur. Farnham Royal, United Kingdom.

Mikola, P. 1982. Application of Vegetation Science to Forestry in Finland. In: Jahn, G. (ed.). Handbook of Vegetation Science, part 12, pp. 199-224. Dr. W. Junk Publishers, The Hague.

Miyazaki, T. ed. 2006. Water flow in soils. 2nd edition. CRC Press, Taylor & Francis Group.

Mohanthy, B., Kanwar, R. and Everts, C. 1994. Comparison of Saturated Hydraulic Conductivity Measurement Methods for a Glacial-Till Soil. Soil Science Society of America Journal, vol. 58 (3), pp. 672–677.

Mosley, M. P. 1979. Streamflow Generation in a Forested Watershed, New Zealand. Water Resources Research, vol. 15 (4), pp. 795-806.

Mulungu, D. M. M., Ichikawa, Y. and Shiiba, M. 2005. A physically based distributed subsurface–surface flow dynamics model for forested mountainous catchments. Hydrological Processes, vol. 19, pp. 3999-4022.

Mäkitalo, K. 2009. Soil hydraulic properties and conditions, site preparation, and the long-term performance of planted Scots pine (Pinus sylvestris L.) on upland forest sites in Finnish Lapland. Academic dissertation. Dissertationes Forestales 80.

Möttönen, V. 2000. Variation in the hydraulic properties of forest soil before and after felling. Licentiate thesis. University of Joensuu, Faculty of Forest Sciences, Management of Forest Ecosystems. In Finnish.

Neary, D. G., Ice, G. G. and Jackson, C. R. 2009. Linkages between forest soils and water quality and quantity. Forest Ecology and Management, vol. 258, pp. 2269-2281.

Nyberg, L. 1995. Water flow path interactions with soil hydraulic properties in till soil at Gårdsjön, Sweden. Journal of Hydrology, vol. 170, pp. 255-275.

Ogata, A. and Banks, R. B. 1961. A solution of the differential equation of longitudinal dispersion in porous media. U.S. Geological Survey Professional Paper 411-A.

Peel, M. C., Finlayson, B. L. and McMahon, T. A. 2007. Updated world map of the Köppen-Geiger climate classification. Hydrology and Earth System Sciences, vol. 11, pp. 1633-1644.

Penttinen, S. 2000. Electrical and hydraulic classification of forest till soils in central Lapland, Finland. Academic Dissertation. Published by the Geological Survey of Finland, Bulletin no. 398.

Perret, J., Prasher, S. O., Kantzas, A. and Langford, C. 1999. Three-Dimensional Quantification of Macropore Networks in Undisturbed Soil Cores. Soil Science Society of America, vol. 3, pp. 1530-1543.

Peters, N. E., Ratcliffe, E. B. and Tranter, M. 1998. Tracing solute mobility at the Panola Mountain Research Watershed, Georgia, USA: variations in Na^+, CI^-, and H_4SiO_4 concentrations. Hydrology, Water Resources and Ecology in Headwaters. Proceedings of the HeadWater'98 Conference held at Meran, Italy, April 1998. IAHS Publication no. 248.

Pickens, F. J., Grisak, E. G. 1980. Scale-dependent dispersion in a stratified granular aquifer. Water Resources Research, vol. 17, pp. 1191-1211.

Pierce, A. J., Stewart, M. K. and Sklash, M. G. 1986. Storm Runoff Generation in Humid Headwater Catchments. 1. Where Does the Water Come From? Water Resources Research, vol. 22, no. 8, pp. 1263-1272.

Piirainen, S. 2002. Nutrient fluxes through a boreal coniferous forest and the effects of clear-cutting. Doctoral thesis published in: The Finnish Forest Research Institute, Research Papers 859.

Piirainen, S., Finér, L., Mannerkoski, H. and Starr, M. 2007. Carbon, nitrogen and phosphorus leaching after site preparation at a boreal forest clear-cut area. Forest Ecology and Management, vol. 243, pp. 10-18.

Postila, H. 2006. Physical and hydraulic properties and dispersion for different podzolic horizons of the forested hillside till soil in Kangaspuro and Mustamäki. Master's thesis. University of Oulu. In Finnish.

Pruess, K. 2004. The TOUGH codes—a family of simulation tools for multiphase flow and transport processes in permeable media. Vadoze Zone Journal, vol. 3, pp. 738–746.

Rausch, R., Schäfer, W., Therrien, R. and Wagner, C. 2005. Solute Transport Modelling. An Introduction to Models and Solution Strategies. Gebr. Bornträger Verlagsbuchhandlung, Stuttgart.

Ray, C., Ellsworth, T. R., Valocchi, A. J. and Boast, C. W. 1997. An improved dual porosity model for chemical transport in macroporous soils. Journal of Hydrology, vol. 193, pp. 270-292.

Ray, C., Vogel, T. and Dusek, J. 2004. Modeling depth-variant and domain-specific sorption and biodegradation in dual-permeability media. Journal of Contaminant Hydrology, vol. 70, pp. 63-87.

Refsgaard, J. C. 2000. Towards a Formal Approach to Calibration and Validation of Models Using Spatial Data. In: Grayson, R. and Blöschl, G. (eds). 2000. Spatial Patterns in Catchment Hydrology: Observations and Modelling. Cambridge University Press, 423 pp.

Refsgaard, J. C. and Henriksen, H. J. 2004. Modelling guidelines – terminology and guiding principles. Advances in Water Resources, vol. 27, pp. 71-82.

Richards, L. A. 1931. Capillary conduction of liquids through porous medium. Physics, vol. 1 (5), pp. 318-333.

Rodhe, A. 1989. On the Generation of Stream Runoff in Till Soils. Nordic Hydrology, vol. 20, pp. 1-8.

Russell, E. W. 1973. Soil conditions and plant growth. 10th ed. Longmans, London, UK.

Saastamoinen, S. and Laine-Kaulio, H. 2007. Preferential flowpaths in the top, midslope and slope bottom sections of a forested hillslope. Unpublished data.

Saastamoinen, S., Laine-Kaulio, H, and Klöve, B. 2009. Phosphorus Speciation and Sorption Processes in Preferential flow paths and Soil Matrix in Forested Podzolic Till Soil. Geophysical Research Abstracts, vol. 11, EGU2009-13315-1. EGU General Assembly 2009.

Salonen, V-P., Eronen, M. and Saarnisto, M. 2002. Practical Soil Science. Kirja-Aurora, Turku. In Finnish.

Schlesinger, S., Crosbie, R. E., Gagné, R. E., Innis, G. S., Lalwani, C.S., Loch, J., Sylvester, J., Wright, R. D., Kheir, N. and Bartos, D. 1979. Terminology for model credibility. SCS Technical Committee on Model Credibility. Simulation, vol. 32 (3), pp. 103–104.

Schwartz R. C., Juo, A. S. R. and McInnes, K. J. 2000. Estimating parameters for a dual-porosity model to describe non-equilibrium, reactive transport in a fine-textured soil. Journal of Hydrology, vol. 229, pp. 149-167.

Seibert, J. 1999. Conceptual runoff models – fiction or representation of reality? Comprehensive Summaries of Uppsala Dissertations from the Faculty of Science and Technology, no. 436.

Seibert, J. and McDonnell, J. J. 2002. On the dialog between experimentalist and modeler in catchment hydrology: Use of soft data for multi-criteria model calibration. Water Resources Research, vol. 38 (11), 1241.

Shipitalo, M. J., Nuutinen, V., Butt, K. R. 2004. Interaction of earthworm burrows and cracks in a clayey, subsurface-drained, soil. Applied Soil Ecology, vol. 26, pp. 209-217.

Sidle, R. C., Noguchi, S., Tsuboyama, Y. and Laursen, K. 2001. A conceptual model of preferential flow systems in forested hillslopes: evidence of self-organization. Hydrological Processes, vol. 15, pp. 1675-1692.

Šimůnek, J. and van Genuchten, M. Th. 2008. Modeling Nonequilibrium Flow and Transport Processes Using HYDRUS. Vadose Zone Journal, vol. 7 (2), pp. 782-797.

Šimůnek, J., Jarvis, N. J., van Genuchten, M. Th. and Gärdenäs, A. 2003. Review and comparison of models for describing non-equilibrium and preferential flow and transport in the vadose zone. Journal of Hydrology, vol. 272, pp. 14-35.

Šimůnek, J., Šejna, M. and van Genuchten, M. Th. 1999. The HYDRUS-2D software package for simulating two-dimensional movement of water, heat, and multiple solutes in variably saturated media. Version 2.0, IGWMC – TPS – 53, International Ground Water Modeling Center, Colorado School of Mines, Golden, Colorado, 251 p.

Šimůnek, J., van Genuchten, M. Th. and Šejna, M. 2006. The HYDRUS Software Package for Simulating the Two- and Three-Dimensional Movement of Water, Heat, and Multiple Solutes in Variably-Saturated Media. Technical Manual, version 1.0. A web document, last revised 3.2.2011. Available at: http://www.pcprogress.com/

Sklash, M. G. and Farvolden, R. N. 1979. The role of groundwater in storm runoff. Journal of Hydrology, vol. 43, pp. 45-65.

Soilmoisture Equipment Corp. 1991. Operating instructions, Model 2800 K1 Guelph Permeameter. A web-document of Soilmoisture Equipment Corp., Santa Barbara, California. Published 10/1991, referred to 9/2005.
Available at: http://www.soilmoisture.com/PDF%20Files/82800k1.pdf

Spaaks, J. H., Bouten, W. and McDonnell, J. J. 2009. Iterative approach to modeling subsurface stormflow based on nonlinear, hillslope-scale physics. Hydrology and Earth System Sciences Discussion Papers, vol. 6, pp. 5205-5241.

Spitz, K. and Moreno, J. 1996. A Practical Guide to Groundwater and Solute Transport Modeling. John Wiley & Sons, Inc.

Stutter, M. I., Deeks, L. K. and Billet, M. F. 2005. Transport of conservative and reactive tracers through a naturally structured upland podzol field lysimeter. Journal of Hydrology, vol. 300, pp. 1-19.

Tracy, F. T. 1995. l-D, 2-D, and 3-D analytical solutions of unsaturated flow in groundwater. Journal of Hydrology, vol. 170, pp. 199-214.

Troch, P. A., Paniconi, C. and Emiel van Loon, E. 2003. Hillslope-storage Boussinesq model for subsurface flow and variable source areas along complex hillslopes: 1. Formulation and characteristic response. Water Resources Research, vol. 39 (11), 1316.

Tromp-van Meerveld, H. J., James, A. L., McDonnell, J. J. and Peters, N. E. 2008. A reference dataset of hillslope rainfall-runoff response, Panola Mountain Research Watershed, United States. Water Resources Research, vol. 44, W06502.

Tsuboyama, Y., Sidle, R., Shoji, N. and Hosoda, I. 1994. Flow and solute transport through the soil matrix and macropores of a hillslope segment. Water Resources Research, vol. 30 (4), pp. 879-890.

Uhlenbrook, S., McDonnell, J. J. and Leibundgut, C. 2001. Foreword to the special issue: Runoff generation and implications for river basin modeling. Freiburger Schriften zur Hydrologie, vol. 13, pp. 4-13.

Vakkilainen, P. 1982. On the estimation of evapotranspiration. Doctoral thesis, University of Oulu. Acta Universitatis Ouluensis C 20, Artes Construction 6.

Vakkilainen, P. 1986. Soil water. Chapter 6.1-6.3, pages 82-94 in: Applied Hydrology, edited by Mustonen, S. Vesiyhdistys ry, Helsinki. In Finnish.

van Dam, J. 2000. Field-scale water flow and solute transport. SWAP model concepts, parameter estimation, and case studies. Doctoral thesis. Wageningen University, The Netherlands.

van Genuchten, M. Th. 1980. A closed-form equation for predicting the hydraulic conductivity of unsaturated soils. Soil Science Society of America Journal, vol. 44, pp. 892–898.

van Genuchten, M. Th. and Gray, W. G. 1978. Analysis of Some Dispersion Corrected Numerical Schemes for Solution of the Transport equation. International Journal for Numerical Methods in Engineering, vol. 12, pp. 387-404.

Versteeg, H. K. and Malalasekera, W. 1995. An introduction to computational fluid dynamics. The finite volume method. Longman Group Ltd.

Vogel, T. 2004. Modeling flow and transport in natural porous media. Inaugural Professor lecture 7/2004. 30 pages. Czech Technical University in Prague.

Vogel, T., Gerke, H. H., Zhang, R. and van Genuchten, M. Th. 2000. Modeling flow and transport in a two-dimensional dual-permeability system with spatially variable hydraulic properties. Journal of Hydrology, vol. 238, pp. 78-89.

Vogel, T., Lichner, L., Dusek, J. and Cipakova, A. 2007. Dual-continuum analysis of a cadmium tracer field experiment. Journal of Contaminant Hydrology, vol. 92, pp. 50-65.

Vukovic, M. and Soro, A. 1992. Determination of hydraulic conductivity of porous media from grain-size composition. Water Resources Publications, Littleton, Colorado, USA, 83 p.

Wang, H. F. and Anderson, M. P. 1982. Introduction to Groundwater Modeling. Finite Difference and Finite Element Methods. W. H. Freeman and Company. San Francisco.

Warsta, L. 2007. Modelling overland and subsurface drainage runoffs at an agricultural field. Licentiate thesis. Helsinki University of Technology. 70 p.

Weiler, M. 2001. Mechanisms controlling macropore flow during infiltration. Dye tracer experiments and simulations. Dissertation. Swiss Federal Institute of Technology Zürich. Diss. ETHZ No. 14237.

Weiler, M. and Flühler, H. 2004. Inferring flow types from dye patterns in macroporous soils. Geoderma, vol. 120, pp. 137-153.

Weiler, M. and McDonnell, J. J. 2004. Virtual experiments: a new approach for improving process conceptualisation in hillslope hydrology. Journal of Hydrology, vol. 285, pp. 3-18.

Weiler, M. and Naef, F. 2000. Verification of flow processes in soils with combined sprinkling and dye tracer experiments. IAHS, Proceedings of the International Workshop on Runoff Generation and Implications for River Basin Modelling. Freiburg, Germany, pp. 345-355.

Weiler, M., Uchida, T. and McDonnell, J. 2003. Connectivity due to preferential flow controls water flow and solute transport at the hillslope scale. MODSIM 2003, Townsville, Australia.

Weyman, D. R. 1970. Throughflow on hillslopes and its relation to the stream hydrograph. Bulletin of the International Association of Scientific Hydrology, XV, 2, 6/1970.

Whipkey, R. Z. 1965. Subsurface stormflow from forested slopes. Bulletin of the International Association of Scientific Hydrology, X, pp. 74-85.

Whipkey, R. Z. 1967. Theory and Mechanics of subsurface stormflow. In Forest Hydrology. Sopper, W. E, Lull, H. W (ed.). Proc. NSF Advanced Science Seminar, pp. 255-260. Pergamon, New York, USA.

Woods, R. and Sivapalan, M. 1999. A synthesis of space-time variability in storm response: Rainfall, runoff generation, and routing. Water Resources Research, vol. 35 (8), pp. 2469-2485.

Youngs, E. G. 1968. Shape factors for Kirkham's piezometer method for determining the hydraulic conductivity of soil in situ for soils overlying an impermeable floor or infinitely permeable stratum. Soil Science, vol. 106, pp. 235-237.

Zaslavsky, D. and Kasiff, G. 1965. Theoretical formulation of piping mechanisms in cohesive soils. Geotechnique, vol. 15(3), pp. 305-316.

Aalto-DD 71/2011

ISBN 978-952-60-4245-9 (pdf)
ISBN 978-952-60-4244-2
ISSN-L 1799-4934
ISSN 1799-4942 (pdf)
ISSN 1799-4934

Aalto University
School of Engineering
Department of Civil and Environmental Engineering
www.aalto.fi

BUSINESS + ECONOMY

ART + DESIGN + ARCHITECTURE

SCIENCE + TECHNOLOGY

CROSSOVER

DOCTORAL DISSERTATIONS